IOWA STATE UNIVERSITY
Digital Repository

Retrospective Theses and Dissertations

Iowa State University Capstones, Theses and Dissertations

1991

The structure and energetics of gas phase Ni and Pd clusters

Mark Shawn Stave
Iowa State University

Follow this and additional works at: https://lib.dr.iastate.edu/rtd

 Part of the Physical Chemistry Commons

Recommended Citation
Stave, Mark Shawn, "The structure and energetics of gas phase Ni and Pd clusters " (1991). *Retrospective Theses and Dissertations*. 9620.
https://lib.dr.iastate.edu/rtd/9620

This Dissertation is brought to you for free and open access by the Iowa State University Capstones, Theses and Dissertations at Iowa State University Digital Repository. It has been accepted for inclusion in Retrospective Theses and Dissertations by an authorized administrator of Iowa State University Digital Repository. For more information, please contact digirep@iastate.edu.

www.manaraa.com

INFORMATION TO USERS

This manuscript has been reproduced from the microfilm master. UMI films the text directly from the original or copy submitted. Thus, some thesis and dissertation copies are in typewriter face, while others may be from any type of computer printer.

The quality of this reproduction is dependent upon the quality of the copy submitted. Broken or indistinct print, colored or poor quality illustrations and photographs, print bleedthrough, substandard margins, and improper alignment can adversely affect reproduction.

In the unlikely event that the author did not send UMI a complete manuscript and there are missing pages, these will be noted. Also, if unauthorized copyright material had to be removed, a note will indicate the deletion.

Oversize materials (e.g., maps, drawings, charts) are reproduced by sectioning the original, beginning at the upper left-hand corner and continuing from left to right in equal sections with small overlaps. Each original is also photographed in one exposure and is included in reduced form at the back of the book.

Photographs included in the original manuscript have been reproduced xerographically in this copy. Higher quality 6" x 9" black and white photographic prints are available for any photographs or illustrations appearing in this copy for an additional charge. Contact UMI directly to order.

U·M·I

University Microfilms International
A Bell & Howell Information Company
300 North Zeeb Road, Ann Arbor, MI 48106-1346 USA
313/761-4700 800/521-0600

Order Number 9207255

The structure and energetics of gas phase Ni and Pd clusters

Stave, Mark Shawn, Ph.D.

Iowa State University, 1991

U·M·I
300 N. Zeeb Rd.
Ann Arbor, MI 48106

The structure and energetics of gas phase Ni and Pd clusters

by

Mark Shawn Stave

A Dissertation Submitted to the

Graduate Faculty in Partial Fulfillment of the

Requirements for the Degree of

DOCTOR OF PHILOSOPHY

Department: Chemistry
Major: Physical Chemistry

Approved:

Signature was redacted for privacy.

In Charge of Major Work

Signature was redacted for privacy.

For the Major Department

Signature was redacted for privacy.

For the Graduate College

Iowa State University
Ames, Iowa

1991

TABLE OF CONTENTS

FORMAT OF THE DISSERTATION

This dissertation follows the alternative style format which permits the inclusion of papers submitted to scholarly journals. Three such papers have been included in this dissertation. The development of the MD/MC-CEM formalism as an approximation to the corrected effective medium (CEM) theory is contained in Paper I, entitled *"Corrected Effective Medium Method. V. Simplifications for Molecular Dynamics and Monte Carlo Simulations."* It has been accepted for publication in the Journal of Chemical Physics. The formulation of the analytic derivative of the CEM potential and its implementation on a hypercube is presented in Paper II, entitled *"Numerical Integration on a Hypercube Computer."* It has been submitted for publication in the Journal of Computational Physics. A detailed discussion of the structure and energetics of Ni_N and Pd_N clusters ($4 \leq N \leq 23$) appears in Paper III, entitled *"The Structure of Ni_N and Pd_N Clusters: $4 \leq N \leq 23$."* It has been submitted for publication in the Journal of Chemical Physics. In this dissertation, all three papers follow the style requirements as set forth by the Journal of Chemical Physics.

GENERAL INTRODUCTION

Clusters of transition metal atoms perform a number of technologically important functions. Their catalytic properties are used extensively in the petroleum refining and chemical manufacturing industries. They also facilitate the control of toxic gases such as carbon monoxide in automobile exhaust. Typically, these metal particles are < 100 Å in size and are dispersed throughout porous materials such as alumina or silica.[1] Their small size exposes most of the metal atoms to the gas phase environment about them. In comparison to the bulk metal, metal atoms in these clusters can have unique geometric arrangements and can be coordinatively unsaturated. This, in turn, affects the electronic structure of these metal clusters and contributes to their high reactivity. The specific relationships between the geometric and electronic structure of metal clusters and their catalytic activity are not thoroughly understood.

Fundamentally, experimental and theoretical investigations of metal clusters aim to increase our knowledge and understanding of their electronic and geometric structure as they evolve from a single atom to clusters of atoms and from clusters to the bulk phase. Model studies of catalytic systems have focused on gas phase clusters free of influence from the support. This research has uncovered a unique and rich diversity of physical and chemical properties for clusters of less than several hundred atoms. Often, these properties vary dramatically with the number and type of metal atoms in the cluster. Such discoveries have led to the suggestion that "small clusters are a novel state of matter, 'surfaces' in transition from molecules to bulk materials".[2a]

Gas phase, transition metal clusters are most commonly generated by means of laser vaporization of a metal sample in a flow tube.[2] Once vaporized the metal atoms are entrained in a stream of an inert carrier gas flowing through the tube. Collisions with the carrier gas atoms cool the metal vapor inducing nucleation and rapid growth of the metal clusters. The analysis of metal clusters is often facilitated by the addition of a chemically active reagent at some point into the stream. The metal clusters are allowed to react with the reagent for a predetermined amount of time before the stream passes through a nozzle expanding into a vacuum. After the expansion terminates the reaction, the products are photoionized and mass analyzed in a time-of-flight mass spectrometer. The rates of reaction and degree of saturation coverage of metal clusters of various size are evident in the mass spectra. Inferences are drawn from this data about the electronic and geometric structure of these metal clusters.

One such experimental investigation considered the steady state coverage of gas phase, transition metal clusters with deuterium.[2] Among their conclusions the investigators note the ability of very small clusters to chemisorb inordinate amounts of deuterium and the non-monotonic size dependence of the stoichiometry of the saturated product. In the range of 12 to 19 atoms, for instance, nickel cluster cations exhibit an odd/even alternation in their deuterium uptake capacity. Specifically, the saturated products appear to be $Ni_{12}D_{17}^+$, $Ni_{13}D_{16}^+$, $Ni_{14}D_{21}^+$, $Ni_{15}D_{16}^+$, $Ni_{16}D_{21}^+$, $Ni_{17}D_{17}^+$, $Ni_{18}D_{27}^+$ and $Ni_{19}D_{25}^+$. As suggested by the original investigators, this alternation may reflect an underlying variation of the hydrogen adsorption energy of these clusters. Undoubtedly, the structural stability of each

cluster influences its propensity to adsorb hydrogen.

The indirect information obtained in such experiments needs to be complemented by accurate computational models. Theoretical development of approaches such as the corrected effective medium (CEM) method[3] has been motivated by such a need. Based upon concepts developed within density functional theory, effective medium approaches[3e] approximately describe the atomic interactions determined by the delocalization of electrons in metal systems with more accuracy than simpler empirical potentials yet with less computational expense than self-consistent quantum chemical calculations. The CEM method enables studies that increase our knowledge of the structural and energetic properties of metal systems.

The computational intensity of CEM calculations currently limits its use for modeling large systems containing thousands of atoms. In Paper I, we present the conceptual and formal simplifications of the CEM theory that allow it to be used directly in molecular dynamics (MD) and Monte Carlo (MC) simulations of such systems, hence the acronym MD/MC-CEM. In order to demonstrate its potential, several brief applications of this method are also discussed.

The increased computational speed of the MD/MC-CEM method is achieved by assuming that effects due to the electron density of an arbitrary set of atoms can be approximated by similar effects within the homogeneous bulk phase of a metal. While this assumption may be valid for large, nearly homogeneous systems such as metal surfaces, it is often inaccurate for small and heteronuclear systems. In order to investigate the uptake of hydrogen by metal clusters, for example, atomic

interactions must be accurately modeled for the adsorbate both within and without the surface of the cluster. CEM calculations of the atomic hydrogen adsorption potential on the Ni (111) solid surface indicate that the simpler MD/MC-CEM interaction potential cannot consistently predict both the interaction energy of hydrogen adsorbed on the surface and absorbed within the metal. The effects on the interaction due to the electron density in each location are sufficiently different that the use of the MD/MC-CEM method is precluded.

The need for greater accuracy motivated additional development of the CEM method so that it could be used to model transition metal clusters and their reactions with adsorbates. In Paper II, we present two developments that have enabled not only the structural optimization of Ni_N and Pd_N clusters ($4 \leq N \leq 23$) using the CEM potential, but also the study of hydrogen uptake by these metal clusters. First, the analytic derivative of the kinetic, exchange and correlation energy functionals is described. Its formulation facilitates the evaluation of the interatomic forces determined by the CEM potential. It is essential for molecular dynamic simulations and efficient structural optimization calculations. Second, the computation of the CEM potential and forces would be almost prohibitive but for the recent implementation of the CEM code onto a hypercube computer. Details of the implementation and analysis of its performance are discussed in relation to the application of the CEM method to investigate metal clusters.

In Paper III, we discuss the predictions of CEM for stable structures of Ni_N and Pd_N clusters ($4 \leq N \leq 23$). Several unique structural properties of these clusters are described in contrast to the bulk and low Miller index surfaces of these metals.

Furthermore, the relationship between the geometrical structure and the nature of the atomic interactions within these transition metal clusters is developed by contrasting them with clusters of rare gas atoms. Significant differences are demonstrated between these two types of clusters. In relation to experimental investigations, the predictions of CEM are shown to be valuable in the interpretation of ammonia adsorption on Ni_N clusters.

In this paper, we also note several observations of relevance to the deuterium adsorption data discussed above. The even/odd alternation in the capacity to chemisorb deuterium correlates with two properties observed for Ni_N clusters in the range from 12 to 19 atoms. First, the clusters with even numbers of atoms are not as energetically stable as the clusters with odd numbers of atoms. Second, the Ni_{14}, Ni_{16}, and Ni_{18} clusters have stable isomers within approximately 100 meV of their most stable geometries. These isomers are not as compact as the most stable structures. Due to these characteristics, the clusters with even numbers of atoms may in fact bind the deuterium more strongly than the clusters with odd numbers of atoms. As a result, these clusters may adsorb more deuterium at saturation levels. Ongoing research is investigating such issues. Already, the variation of hydrogen binding energy to Ni_N clusters has been demonstrated as illustrated by Fig. 1. These studies will continue to provide a more detailed understanding of structure-reactivity relationships in transition metal clusters.

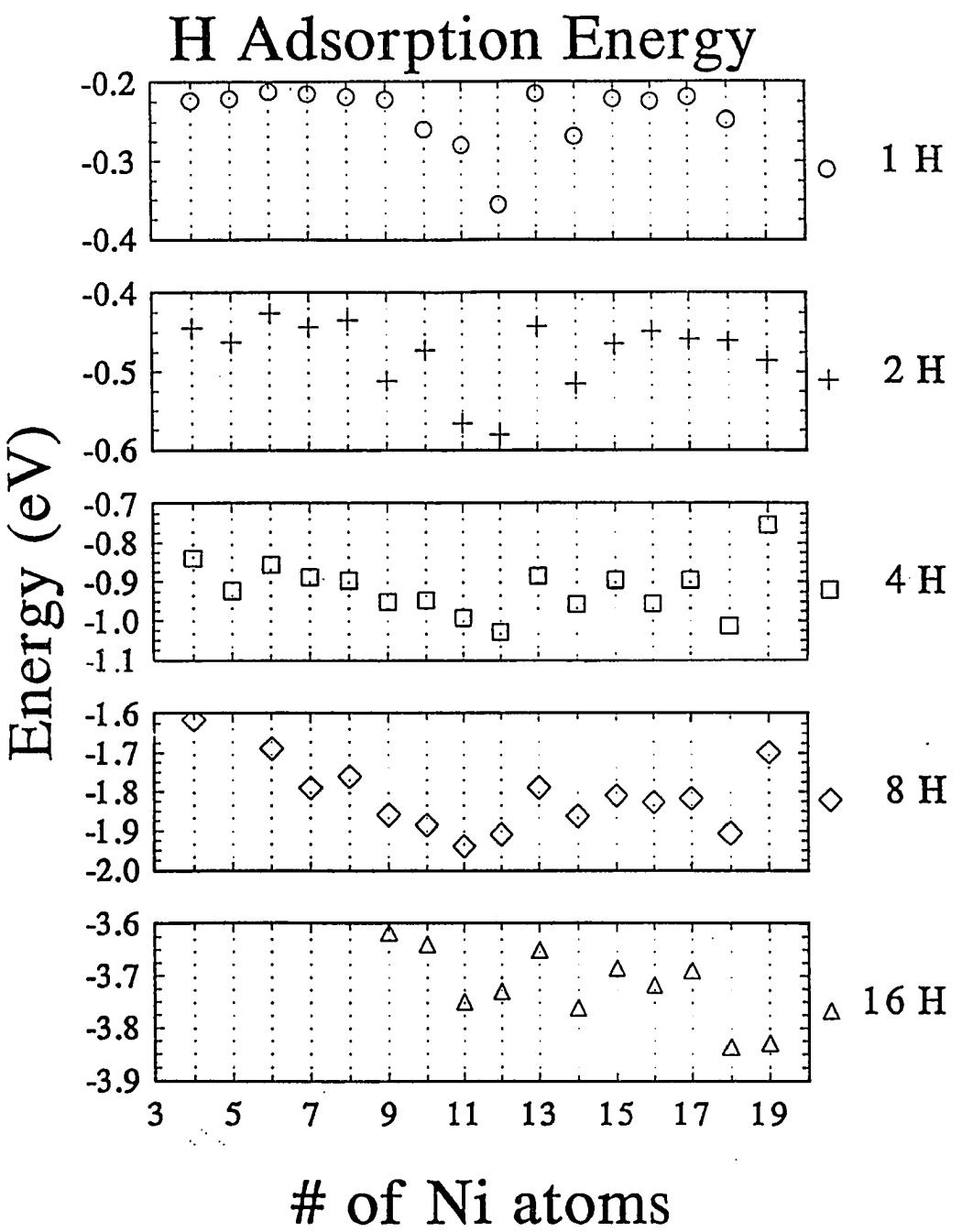

Fig. 1: Energy gained upon uptake of a given amount of hydrogen by Ni clusters of various size: $Ni_N + M\ ½\ H_2 \rightarrow Ni_NH_M$.

PAPER I.

CORRECTED EFFECTIVE MEDIUM METHOD: V. SIMPLIFICATIONS FOR MOLECULAR DYNAMICS AND MONTE CARLO SIMULATIONS

Corrected effective medium method: V. Simplifications for molecular dynamics and Monte Carlo simulations

Mark S. Stave
David E. Sanders[a]
Todd J. Raeker
and
Andrew E. DePristo

Ames Laboratory - USDOE
and
Department of Chemistry
Iowa State University
Ames, Iowa 50011

[a] IBM predoctoral Fellow

ABSTRACT

We present the conceptual and formal simplifications of the recently developed corrected effective medium (CEM) theory that enable this theory to be used directly in molecular dynamics (MD) and Monte Carlo (MC) simulations of large systems, hence the acronym MD/MC-CEM. The essential idea involves adjustment of the CEM embedding functions to include *approximately* the original explicit correction for kinetic-exchange-correlation energy differences between the real system and the many atom-jellium systems used as the zeroth order model. Examples of this construction are provided for the Ni, Pd, Ar and H/Pd(111) systems.

Finally, a few brief applications of this method to large systems are provided. These include relaxation of metal surfaces, structure of pure Ni and mixed NiCu clusters, sticking of Cu on Cu(100), and the scattering of Ar from H covered Pd(111).

I. INTRODUCTION

The potential energy surface (PES) and interatomic forces are central to treatments of equilibrium and non-equilibrium processes in chemistry and physics. Often an empirical procedure is used to obtain these: one assumes a convenient functional form with adjustable parameters and determines these parameters by fitting to some combination of calculated and experimental energies. Molecular mechanics methods form perhaps the most complete data base of parameters.[1,2]

There are two main conceptual and numerical problems with the above procedure. First, there is often little theoretical basis for the functional form which is generally chosen for convenience in differentiation and speed in computational evaluation; hence, the representation may not provide an accurate interpolation of the PES and extrapolation beyond the fitted points becomes problematic. Second, the parameters must be determined anew for each system which limits the predictive ability of the theory, not to mention making the entire application procedure extremely tedious. Indeed, one often needs to be quite sure that a system will display unusual behavior before spending the effort in constructing a PES.

For systems containing only a few atoms, these problems may not be particularly severe. The regions of configuration space important for the dynamics can be determined by inspection and (perhaps) intuition. Many calculated energies can be provided in this region by both accurate *ab initio* and first principle methods. Moreover, an exhaustive investigation of one particular system is often desirable, so that the fitting and parametrization of the PES is not an unduly tedious task relative to the amount of dynamical information gained.

For systems up to ten or twenty atoms, recent work of Car and Parrinello and coworkers[3] has demonstrated the feasibility of performing electronic structure calculations fast enough to evaluate the forces directly, at least within a SCF-LD framework. Approximate molecular structure techniques can also be used in an analogous manner as indicated by the work of Karplus and coworkers on protein dynamics.[2b]

For still larger systems, such direct calculations are not feasible and the determination of many interaction energies for fitting is also not possible. Furthermore, many different types of systems often need to be investigated in only slight detail (e.g., for the design of new materials). Hence, one does not wish to parametrize a functional form for each system (of which there will be a great variety). For large systems, moreover, one cannot simply choose any convenient functional form and expect adequate results. A good example is the use of the Lennard-Jones (12,6) form for the binding energy of monatomic metals;[4] the two parameters in the potential can be fixed by specification of the lattice constant and cohesive energy or the lattice constant and the Debye frequency. The former choice leads to an overestimate of the Debye frequency by a factor of about three while the latter leads to an underestimate of the cohesive energy by about a factor of five.[5-7] Replacement of the LJ(12,6) by a three parameter Morse potential (which can duplicate all three pieces of experimental data[8]) leads to unphysically large expansions of the surface layers.[7] One is thus led quite quickly to much more complex forms with many parameters. The situation for semiconductors is even worse.[9]

Progress has been made for metallic systems, however. The recently developed embedded atom method (EAM) provides a theoretically based form for metal-metal bonding with a limited number of parameters.[10] It has been applied successfully to a number of simulations in which many thousands of atoms evolve dynamically.[11] The effective medium (EM) method,[12] predating the EAM, has also been applied to large systems.[13]

In a number of recent articles,[14-19] we have derived, implemented and applied a new approach to the calculation of interaction energies based upon the explicit evaluation of corrections to the EM theory using density functionals. This corrected effective medium (CEM) theory allows the calculation of the interaction energy for any number (N) and type of atoms $\{A_i, i=1,...,N\}$. The basic idea of this theory is to model the interaction of each atom A_i with all other atoms $\{A_j, j=1,...,N, j\neq i\}$ by embedding atom A_i into a spin-unpolarized jellium of density n_i. The differences between the real and atom-jellium systems due to inhomogeneities of the electron density and the point charge of the nuclei are determined non-self-consistently and involve both Coulombic and kinetic-exchange-correlation energies. The fundamental theoretical development occurs in Ref. 16 with refinements and symmetry inclusions in Refs. 17-19.

For the present purposes, the important point is that the calculation of interaction energies with good accuracy at (relatively) low computational cost can be provided by this CEM theory. This has been illustrated for diatomic bond energies,[16] metal cluster binding energies,[17] surface free energies and relaxations,[18] and adsorbate-surface binding energies and structures.[19] However,

these energy evaluations are still orders of magnitude slower than simple empirical pair potentials, or even the EAM and EM methods. To gain this additional speed, one must give up some accuracy of course.

In this paper, we present the conceptual and formal simplifications of the CEM theory that allow the theory to be used directly in MD and MC simulations of large systems, hence the acronym MD/MC-CEM. The essential idea involves adjustment of the CEM embedding functions to include *approximately* the original explicit correction for kinetic-exchange-correlation energy differences between the real system and the many atom-jellium systems used as the zeroth order model. Examples of this construction are provided for the Ni, Pd, Ar and H/Pd(111) systems.

The remainder of this paper is divided into three sections. Section II briefly reviews the CEM theory and discusses the simplifications needed to use CEM in large scale simulations. Section III presents illustrative applications of the MD/MC-CEM method. Finally, a brief summary and conclusions are presented in Section IV.

II. MD/MC-CEM THEORY

Consider a system of N atoms $\{A_i, i=1, ..., N\}$ where each A_i can be any type of atom. The nuclei are located at $\{\underset{\sim}{R}\}=(\vec{R}_1, \vec{R}_2, ..., \vec{R}_N)$ while the vectors locating a position relative to the nuclei are $\{\underset{\sim}{r}\}=(\vec{r}_1, \vec{r}_2, ..., \vec{r}_N)$. The interaction energy can be written in the exact form[16]

$$\Delta E(\{A_i\}) = \sum_{i=1}^{N} \Delta E_J(A_i; n_i) + \Delta V_C + \Delta G(\{A_i\}) \ . \tag{1}$$

The first term is the sum of the embedding energies for each atom A_i embedded into jellium of density n_i, $\Delta E_J(A_i; n_i)$. The second is the difference in the Coulombic energy between the real system and every atom embedded in jellium, ΔV_C. The third is the difference in the sum of the kinetic, exchange, and correlation energies between the real system and every atom embedded in jellium, $\Delta G(\{A_i\})$. This term is given by

$$\Delta G = G(\{A_i\}) - \sum_{i=1}^{N} [G(A_i+n_i) - G(n_i)] \ , \tag{2}$$

where G(S) is the kinetic-exchange-correlation energy of the system S.

In Eq.(1) the summation of atom-jellium systems is the zeroth order model for the real N-atom system. The corrections to this zeroth order model include Coulombic and kinetic-exchange-correlation energies. Both arise from the difference in electron density homogeneity between the real and atom-jellium systems, with the latter depending explicitly on the gradient of the electron density. These corrections are not calculated self-consistently.

In the CEM approach the approximation of *superposition of atomic electron densities* is utilized. Thus, the system electron density is simply expressed as

$$n(\vec{r}) = \sum_{i=1}^{N} n(A_i; \vec{r}_i) \ , \tag{3a}$$

where the atomic electron density is the sum of both up- and down-spin densities

$$n(A_i; \vec{r}_i) = n^+(A_i; \vec{r}_i) + n^-(A_i; \vec{r}_i) \ . \tag{3b}$$

As a result the Coulombic energy difference is simply the summation of atom-atom Coulomb integrals,

$$\Delta V_C = \sum_{i=1}^{N} \sum_{j \neq i}^{N} V_C(i,j) \ , \tag{4}$$

and is independent of the jellium densities, $\{n_i\}$. In order to determine the jellium densities, a quadratic functional approximation to ΔG is minimized with respect to the $\{n_i\}$, yielding the expression:

$$n_i = \sum_{j \neq i}^{N} \int \left[n^+(A_i; \vec{r}_i)\, n^+(A_j; \vec{r}_j) + n^-(A_i; \vec{r}_i)\, n^-(A_j; \vec{r}_j) \right] d\vec{r} / Z_i \ , \tag{5a}$$

which reduces for unpolarized densities to

$$n_i = \frac{1}{2} \sum_{j \neq i}^{N} \int n(A_i; \vec{r}_i)\, n(A_j; \vec{r}_j)\, d\vec{r} / Z_i \ , \tag{5b}$$

where Z_i is the atomic number. The integrals in Eqs.(5) are over all space with $\vec{r}_i = \vec{r} - \vec{R}_i$ and $\vec{r}_j = \vec{r} - \vec{R}_j$.

The embedding energies are known quantities. In one case, they have been calculated by Puska *et al.* for nearly all the atoms through Cu as a function of jellium density using the SCF-LSD approach.[20] These values are denoted as $\Delta E_P(A_i; n_i)$. In another case, they can be constructed from the binding potentials for the homonuclear diatomic and homogeneous bulk systems, as discussed in detail in Refs. 17-19, and as illustrated below. These values are denoted as $\Delta E_C(A_i; n_i)$. In these papers, the distinction between these two energy functions was discussed and it was shown that they are two special cases of a more general embedding function that is a function of both the jellium density and the work function of the jellium. Thus, the subscript "C" indicates that these embedding values are determined from essentially "covalent" binding interactions, in contrast to the SCF-LSD results that have a large contribution from ionic binding. Both functions can be evaluated via interpolation.

Eqs.(1-5) define the CEM interaction energy. These expressions can be evaluated after specifying the following:

1) the embedding function for each atom in the system;

2) the atomic densities and gradients;

3) the kinetic, exchange and correlation energy density functionals.

The reader interested in a more detailed derivation and justification of the theory is referred to Refs. 16-19, and an upcoming review.[14] The problem of interest here involves the evaluation of the terms in Eq.(1), and eventually the modification of

this equation.

To begin, note that evaluation of the atom-atom Coulomb energies and the electron density overlaps can be accomplished with relatively little computational work even for non-spherical atomic densities. The subsequent densities can then be used to evaluate the embedding energy functions. (Details of the evaluation of these terms can be found in Ref. 21 for spherical densities and Ref. 14 for the general case.)

The time-consuming part involves the correction term, $\Delta G(\{A_i\})$. The term $G(A_i+n_i)$ involves a three dimensional quadrature over one center, but does not depend upon the geometry of the N-atom system (except via the specification of the jellium density n_i). It can be evaluated for a number of jellium densities, tabulated and then evaluated by interpolation much like the embedding functions. The general term $G(\Sigma A_i)$, however, involves a three dimensional quadrature over many centers, and varies explicitly with each geometrical change in the coordinates $\{\underset{\sim}{R}\}$. This integration is performed efficiently using Becke's fuzzy cell integration method[22] with one cell per atomic center. The integration within each cell utilizes Gauss-Laguerre radial, Gauss-Legendre and Gauss-Chebyshev angular quadratures,[23] and requires 5,000-10,000 integration points per cell for an accuracy of 0.001 eV. At each of these points, the electron density and gradient from every atom must be evaluated. Although the radial densities and derivatives for each atom are stored in a large table, and the required values determined by linear interpolation, there are so many points in a large system (i.e., > 5000N) that evaluation of $G(\Sigma A_i)$ is by far the most time consuming part of the calculation.

The *direct* use of CEM in MD or MC simulations of large systems is prohibitive computationally due to this multicenter integration. However, this problem may be eliminated in the following way. The *ansatz* may be made that the effect of ΔG on the interaction energy can be incorporated by redefinition of the embedding energies:

$$\sum \Delta F_J(A_i; n_i) \approx \sum \Delta E_J(A_i; n_i) + \Delta G(\{A_i\}) \; . \tag{6}$$

Here ΔF_J is a new function of the jellium density. At first Eq.(6) may not appear sensible since the left side is an explicit function of the jellium densities while the right side is an explicit function of the jellium densities and coordinates via ΔG. However, since the jellium densities depend explicitly on the coordinates via Eq.(5), Eq.(6) is meaningful. This leads to the much simpler MD/MC-CEM form of the interaction energy:

$$\Delta E(\{A_i\}) = \sum \Delta F_J(A_i; n_i) + \Delta V_C \; . \tag{7}$$

This equation, while an approximation, can always be tested by performing full CEM calculations for selected configurations of the system. However, the approximation in Eq.(6) can also be tested directly at least in a semi-quantitative manner.

In principle, the corrections of the full CEM theory enable accurate predictions of interaction energies for diverse systems. For example, the atoms in a homonuclear diatomic or bulk system could conceivably have the same jellium density yet the correction energies would be significantly different for the two systems. Both interaction energies can be predicted by CEM since the corrections

can account for the vast differences in the electron density environments.[16-18]

Now consider the qualitative conditions under which one might expect Eq.(6) to hold. A formal justification of Eq.(6) requires

$$\Delta G(\{A_i\}) \sim \sum f(A_i; n_i) , \tag{8}$$

where each f is an arbitrary function of the jellium density. In regard to the approximation in Eq.(8), one should note that a *functional* of the total electron density and its gradient for a particular system is approximated by a sum of *functions*. Each of these functions pertains to a particular atom in the system and is supposedly universal in the sense of being independent of the particular system under study. If the electron density environment does not change too drastically, this will be an adequate approximation. In contrast to CEM, MD/MC-CEM obviously cannot be expected to predict the interaction energies of both a diatomic and bulk system at a given jellium density due to the vast difference in electron density environment. In fact, Eq.(8) can only be exact for any one system in which there is just one independent distance and one independent jellium density. In any other case, it is not possible to enforce the $f(A_i; n_i)$ to be single valued. This will be clear shortly when we show explicit tests of such a replacement.

A more quantitative analysis can be provided by illustrating a construction method for the $\Delta F_J(A_i; n_i)$. Consider two systems: a homonuclear diatomic and a monatomic bulk solid. Since in both systems all atoms are the same type and are in identical environments, the functions for all atoms are the same and Eq.(6) becomes for a homonuclear diatomic and

for a monatomic bulk solid, where WS(1) indicates that the integration extends only

$$\Delta F_J(A_1; n_1) = \Delta E_J(A_1; n_1) + \frac{1}{2}\Delta G(A_1, A_2) \tag{9a}$$

$$\Delta F_J(A_1; n) = \Delta E_J(A_1; n_1) + \Delta G(\{A_j\})_{WS(1)} \tag{9b}$$

over the Wigner-Seitz cell of A_1. Eqs.(9) provide a simple way to determine the new embedding functions for homonuclear systems.

As examples, consider the Ni and Pd systems. Since ΔG must be evaluated, we note the density functionals. The kinetic energy functional is an accurate Padé approximation[24] in $|\nabla n| / n^{4/3}$ that approximately sums the full series in the gradients of the electron density. The local Dirac exchange functional[25] and the local Gunnarsson-Lundqvist (GL) correlation functional[26] are used. Fig. 1 shows the contribution of the ΔG term in Eqs.(9a) and (9b), respectively. Clearly, ΔG is not a universal function of the jellium density since the diatomic and bulk portions do not match. In particular, note that for any given jellium density different values of ΔG for the diatomic and bulk systems lead to a double valued relationship in Eq.(8). This is due to the difference in the electron density environments of the two systems.

The situation is not as bad as it appears, however, since the range of jellium densities near equilibrium for the diatomic system does not overlap that for the bulk system. Only a very contracted diatomic and very expanded bulk overlap, where energy errors of $\approx$ 0.2 - 0.6 eV are not particularly significant with respect to the large interaction energy. Additionally, only the effect of ΔG on the interaction energy of the system is directly of interest, not the actual value of ΔG. To investigate these

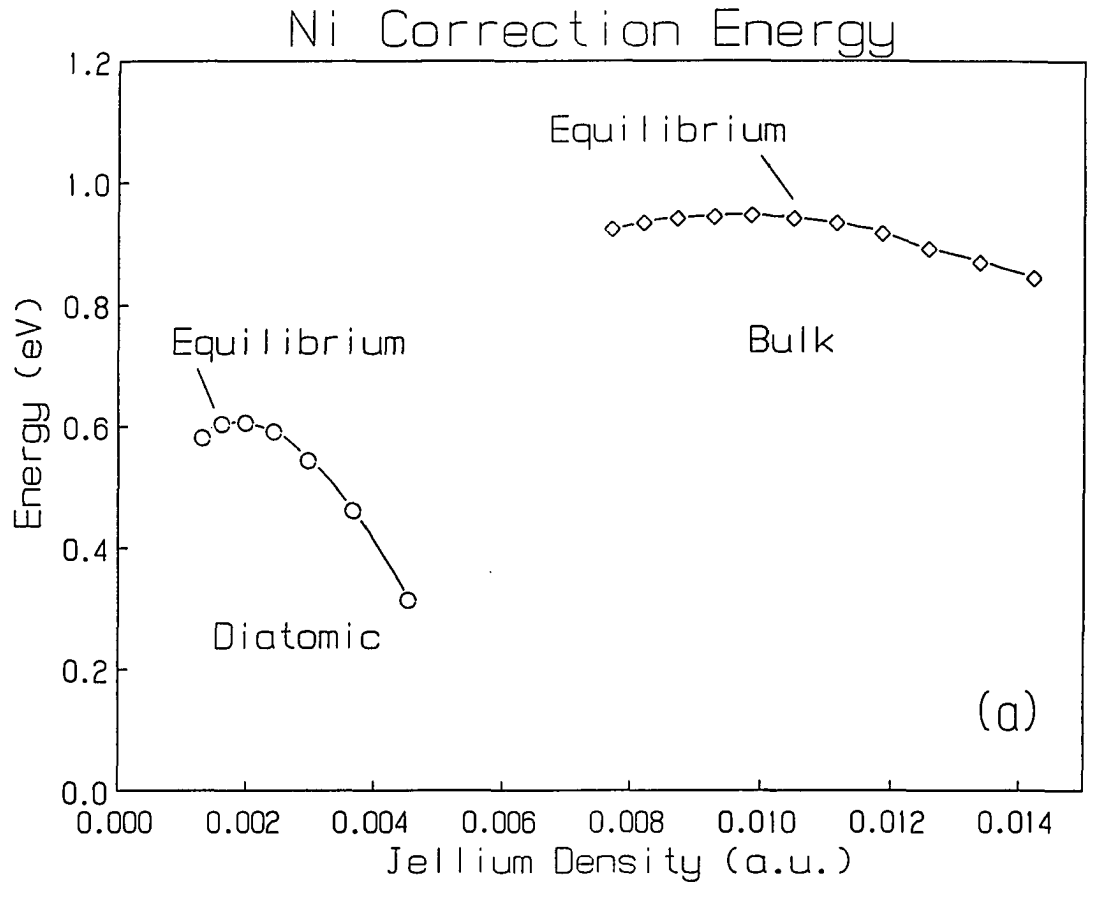

Fig. 1: The correction energy contribution in Eqs.(9), for the a) Ni and b) Pd systems. The values labeled diatomic (o) are ½ΔG, calculated as the bond length varies. The values labeled bulk (◇) are ΔG, calculated as the lattice constant varies.

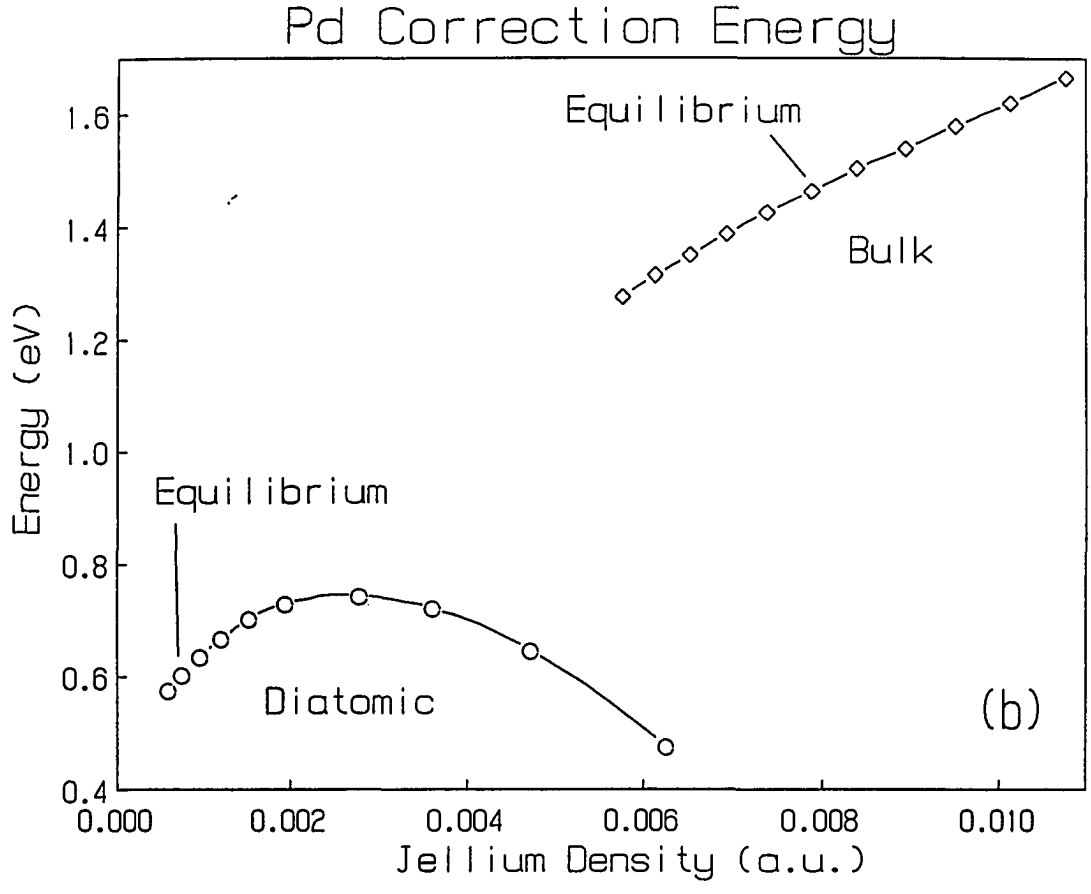

Fig. 1: **(continued)**

energies, note that the full CEM covalent embedding function ΔE_C is determined[16-18] by inverting the homonuclear diatomic binding curve and the monatomic bulk cohesive energy curve:

$$\Delta E_C(A_1; n_1) = \{\Delta E(A_1, A_2) - V_C(1,2) - \Delta G(A_1, A_2)\}/2 \ , \tag{10a}$$

$$\Delta E_C(A_1; n_1) = \Delta E_{coh}(A_1) - \frac{1}{2}\sum_{j\neq 1}^{N} V_C(1,j) - \Delta G(\{A_j\})_{WS(1)} \ . \tag{10b}$$

Combining Eqs.(9) and (10) yields

$$\Delta F_C(A_1; n_1) = \{\Delta E(A_1, A_2) - V_C(1,2)\}/2 \ , \tag{11a}$$

$$\Delta F_C(A_1; n_1) = \Delta E_{coh}(A_1) - \frac{1}{2}\sum_{j\neq 1}^{N} V_C(1,j) \ . \tag{11b}$$

Hence, the new covalent functions are determined in an analogous way to the old functions. Since the density in Eqs.(10) and (11) will be the same and since the diatomic and bulk densities are quite separate, the validity of Eqs.(11) can be determined by the smoothness of ΔF_C as a function of density. This is the criterion used in Refs. 17 and 18 to indicate the universality of the function ΔE_C. However, one should not lose sight of the fact that the approximation in Eq.(6) underlies Eqs.(11). *Hence, the accuracy and validity of the MD/MC-CEM formalism must be lower than those of the CEM formalism.*

The analogous functions ΔE_C and ΔF_C have been constructed for Ni and Pd. The diatomic binding curve used in Eqs.(10a) and (11a) is a Morse potential with

parameters determined by fitting to the binding energy, vibrational frequency and bond length. This yields (D_e, α_e, R_e) of (2.092 eV, 1.017 Bohr^{-1}, 4.157 Bohr) and (1.04 eV, 0.6825 Bohr^{-1}, 5.008 Bohr) for Ni and Pd, respectively.[27] The points are evaluated at 1.00-1.05R_e in steps of 0.01R_e. The bulk cohesive energy used the universal binding energy curve[28] in the form of a Morse curve in the lattice constant, $\Delta E_{coh}(a) = D\,[\exp(-2\alpha(a-a_0))-2\exp(-\alpha(a-a_0))]$. The values of (D, α, a_0) are (-4.44 eV, 0.538464 Bohr^{-1}, 6.65 Bohr) and (-3.89 eV, 0.592743 Bohr^{-1}, 7.35 Bohr) for Ni and Pd, respectively.[29] The value of α was determined from the bulk modulus of 1.86×10^{11} J/m^3 and 1.808×10^{11} J/m^3 for Ni and Pd, respectively. The points are evaluated at 0.95-1.05a_0 in steps of 0.01a_0. This Morse form should be more accurate than a simple harmonic expansion. In contrast to the mismatch of ΔG in Fig. 1, the function ΔF_C in Fig. 2 is rather smooth in appearance. This situation occurs because ΔG is generally a rather small fraction of the embedding energy in the compressed diatomic and bulk limits. However, we must caution that when small energies are needed the errors in neglecting ΔG can be unacceptable. In that case, no methods presently available are sufficiently fast to use CEM directly in MD or MC studies of systems with many degrees of freedom.

As an illustration of the accuracy that can be expected for energies, a few surface energies are listed in Table I for the perfectly terminated surfaces of the Ni and Pd systems. (The surface energies vary only slightly as a function of the relaxation of the layers as can be seen in Table II and Ref. 18.) The more approximate MD/MC-CEM theory is still quite good, a substantial improvement over the computationally and formalistically similar EAM. Of course, CEM is more

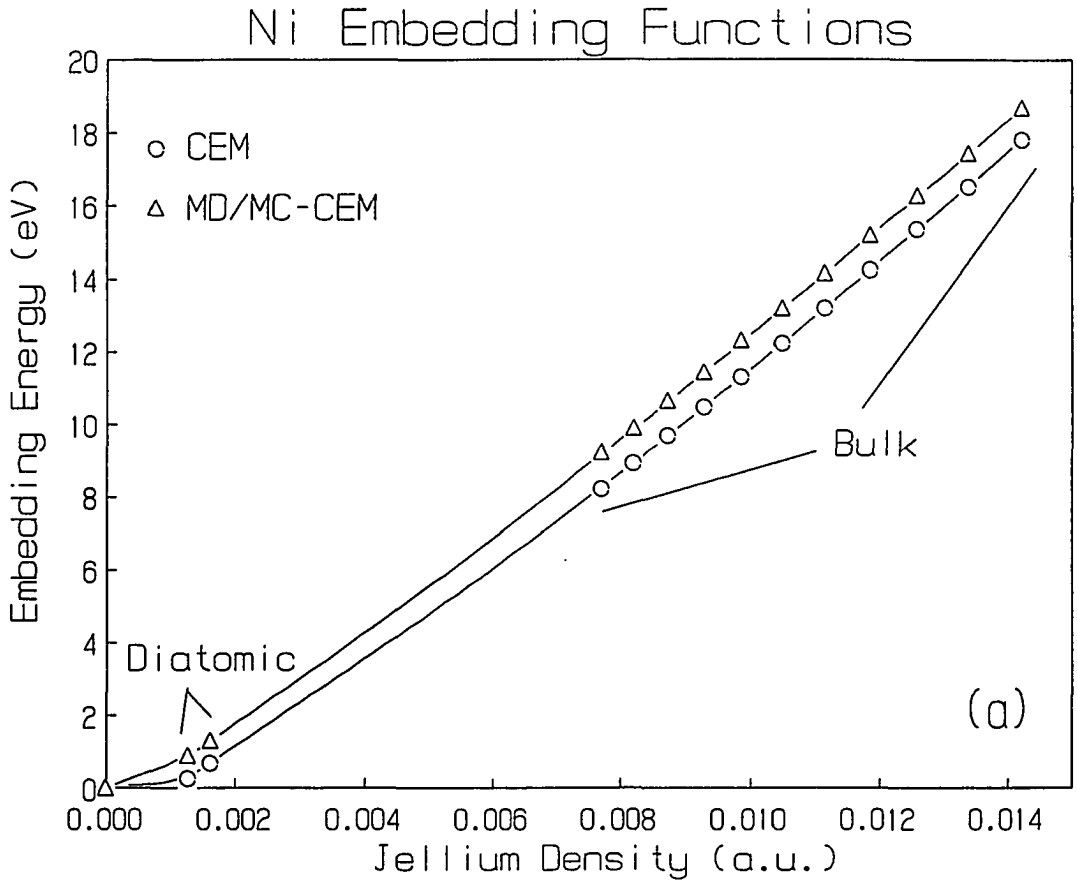

Fig. 2: **The covalent embedding functions for CEM (o) and MD/MC-CEM (Δ) for the a) Ni and b) Pd systems. The values labeled diatomic are calculated as the bond length varies, with only the $1.00R_e$ and $1.05R_e$ results shown for clarity. The values labeled bulk are calculated from the monatomic metal as the lattice constant varies.**

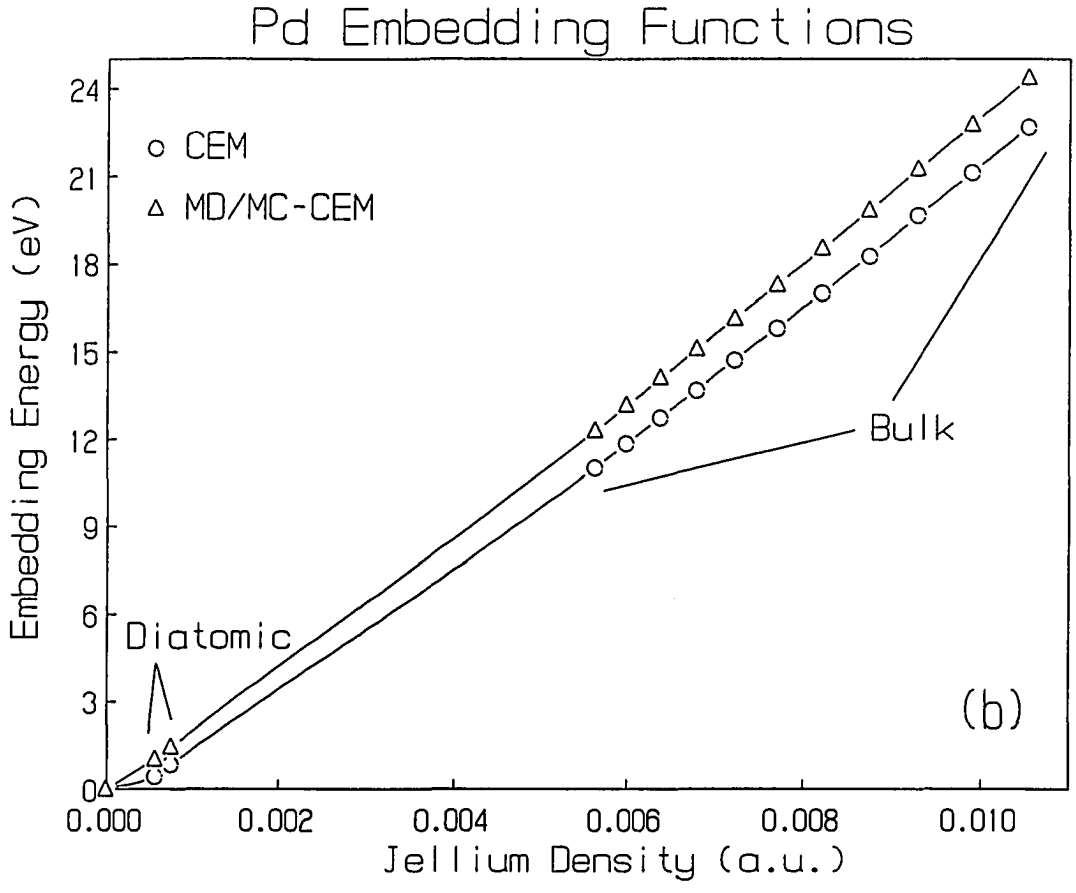

Fig. 2: **(continued)**

Table I. Surface energies of the low Miller index surfaces of Ni and Pd.

		Surface Energies σ_S (J/m^2)			
atom	face	CEM	MD/MC-CEM	EAM	Expt.[b]
Ni	100	2.08	2.48	1.54	
	110	2.27	2.70	1.73	2.38
	111	1.98	2.36	1.28	
Pd	100	1.77	2.02	1.25	
	110	1.93	2.20	1.37	2.00
	111	1.67	1.91	1.05	

[a]EAM values from Ref. 10(c).
[b]Average of a polycrystalline surface from Ref. 30.

accurate than MD/MC-CEM, but we would suggest that the accuracy of the latter is acceptable for many purposes. Nonetheless, if energies an order of magnitude smaller are required, as occur for reconstructions and perhaps for relaxations, then such inaccuracy would not be acceptable. This will be discussed more in the first application in Section IV.

Complications may arise for heteronuclear systems. If the interactions are expected to be similar to the homonuclear case, then the ΔF_C determined for the homonuclear systems can be used. This predictive ability is a major advantage of the CEM method. If the bonding is expected to be ionic, then the results of Eqs.(9-11) with ΔE_P on the right-hand side may be used. The question of the appropriateness of the embedding function ΔF_J for any system is no different than for ΔE_J. Thus, the same caution concerning strong electronegative and

electropositive elements must be used as for the full CEM calculations. Indeed, full CEM calculations can be performed for the system under consideration to determine the adequacy of the type of embedding function chosen. This information, in turn, can be used to determine ΔF_J.

For example, ΔF_P can be constructed for a single H atom interacting with Pd(111). For Pd the covalent embedding functions, ΔE_C and ΔF_C in Fig. 2, can be used. For H the binding interaction will be largely ionic, implying that the Puska *et al.* embedding function can be used.† The CEM interaction energy of the H-Pd(111) system is then

$$\Delta E(H, \{Pd_i\}) = \Delta E_P(H; n_H) + \sum \Delta E_C(Pd_i; n_i) + \Delta V_C(H, \{Pd_i\}) + \Delta G(H, \{Pd_i\}) , \quad \textbf{(12a)}$$

while the energy of the Pd(111) system without the H is

---

†Since $\Delta E_P(H; n)$ was not known at sufficiently large densities for the system of interest here, it was supplemented with two high density binding energies for H in bulk Pd. These values are the experimental heat of solution at infinite dilution (ΔH_H=-0.10 eV[31a], along with the vibrational frequency of a H atom in its bulk octahedral site of 0.066 eV[31b]) and the estimated tetrahedral minus octahedral energy of ≈0.2 eV.[32] This difference cannot change by more than 0.2 eV and still have the more stable site be octahedral. The embedding function region of importance for H on Pd(111) is insensitive to such a small change. The added complication has nothing to do with MD/MC-CEM and is only mentioned since the reader may wonder about the origin of the high density points for $\Delta E_P(H)$ in Fig.3. Alternatively, one could do further SCF-LD calculations of ΔE_P.

$$\Delta E(\{Pd_i\})^0 = \sum \Delta E_C\left(Pd_i; n_i^0\right) + \Delta V_C(\{Pd_i\}) + \Delta G(\{Pd_i\}) \ . \qquad \textbf{(12b)}$$

The superscript "0" indicates that the density is only due to the Pd atoms. The analogous equations within the MD/MC-CEM formalism are

$$\Delta E(H, \{Pd_i\}) = \Delta F_P(H; n_H) + \sum \Delta F_C(Pd_i; n_i) + \Delta V_C(H, \{Pd_i\}) \ , \qquad \textbf{(13a)}$$

$$\Delta E(\{Pd_i\})^0 = \sum \Delta F_C\left(Pd_i; n_i^0\right) + \Delta V_C(\{Pd_i\}) \ . \qquad \textbf{(13b)}$$

Now it is the additional interaction of H with Pd(111), $\Delta E(H,\{Pd_i\})-\Delta E(\{Pd_i\})^0$, that is required to be similarly reproduced by the two functions, $\Delta E_P(H;n)$ and $\Delta F_P(H;n)$, not the interaction energies, $\Delta E(H,\{Pd_i\})$. The latter include the surface free energy of the Pd(111) that will not be the same in both forms. In other words, $\Delta E(\{Pd_i\})^0$, differs slightly between Eqs.(12b) and (13b) because the function $\Delta F_C(Pd_i;n_i^0)$ is guaranteed to duplicate the binding energy of Pd_2 and Pd(bulk), but not necessarily the surface energy (as is apparent from the data presented in Table I). This slight inaccuracy should not be included in the new H-atom embedding function.

Setting the difference, $\Delta E(H,\{Pd_i\}) - \Delta E(\{Pd_i\})^0$, equal between the two forms yields

$$\Delta F_P(H; n_H) = \Delta E_P(H; n_H) + \Delta G(H,\{Pd_i\}) - \Delta G(\{Pd_i\}) +$$

$$\sum \left[\left\{\Delta E_C(Pd_i; n_i) - \Delta E_C\left(Pd_i; n_i^0\right)\right\} - \right. \qquad \textbf{(14)}$$

$$\left.\left\{\Delta F_C(Pd_i; n_i) - \Delta F_C\left(Pd_i; n_i^0\right)\right\}\right] .$$

This expression defines the new embedding function for the H-atom in terms of quantities calculable by the full CEM form. In Fig. 3, the functions $\Delta E_P(H;n)$ and $\Delta F_P(H;n)$ are shown. The latter is again quite smooth, implying that it could be used for other faces of Pd and other metals with acceptable accuracy.

It is worthwhile to describe an alternative interpretation of the MD/MC-CEM theory. MD/MC-CEM is simply a convenient parametrization of CEM providing lower accuracy over a range of systems and/or configurations. Instead of determining ΔF_c from experimental data as in Eq.(11), it is also feasible to find ΔF_c (or ΔF_p) by requiring MD/MC-CEM results to agree with CEM values over a restricted range of system configurations. Then, the MD/MC-CEM results would be as accurate as the CEM values but would apply over a much smaller range of systems. The choice of construction will depend upon the need for accuracy vs. generality. The important point is that ΔF_J are not universal in the same sense as ΔE_J. This point will require further study.

Before presenting several applications of the MD/MC-CEM theory, we should mention that the efficiency of the EM and EAM methods in numerical simulations has provided strong impetus for the present simplifications of the CEM procedure. While it is no surprise that the MD/MC-CEM, EAM and EM formalisms are similar, they are not identical. In particular, although the EAM interaction energy is a sum of embedding and two body functions just as in Eq.(7), all the EAM functions are chosen empirically. In contrast, only the embedding functions ΔF_C are semi-empirical in MD/MC-CEM since the original, semi-empirical ΔE_C are used to generate ΔF_C via Eq.(6). Moreover, the pairwise additive Coulomb energies are

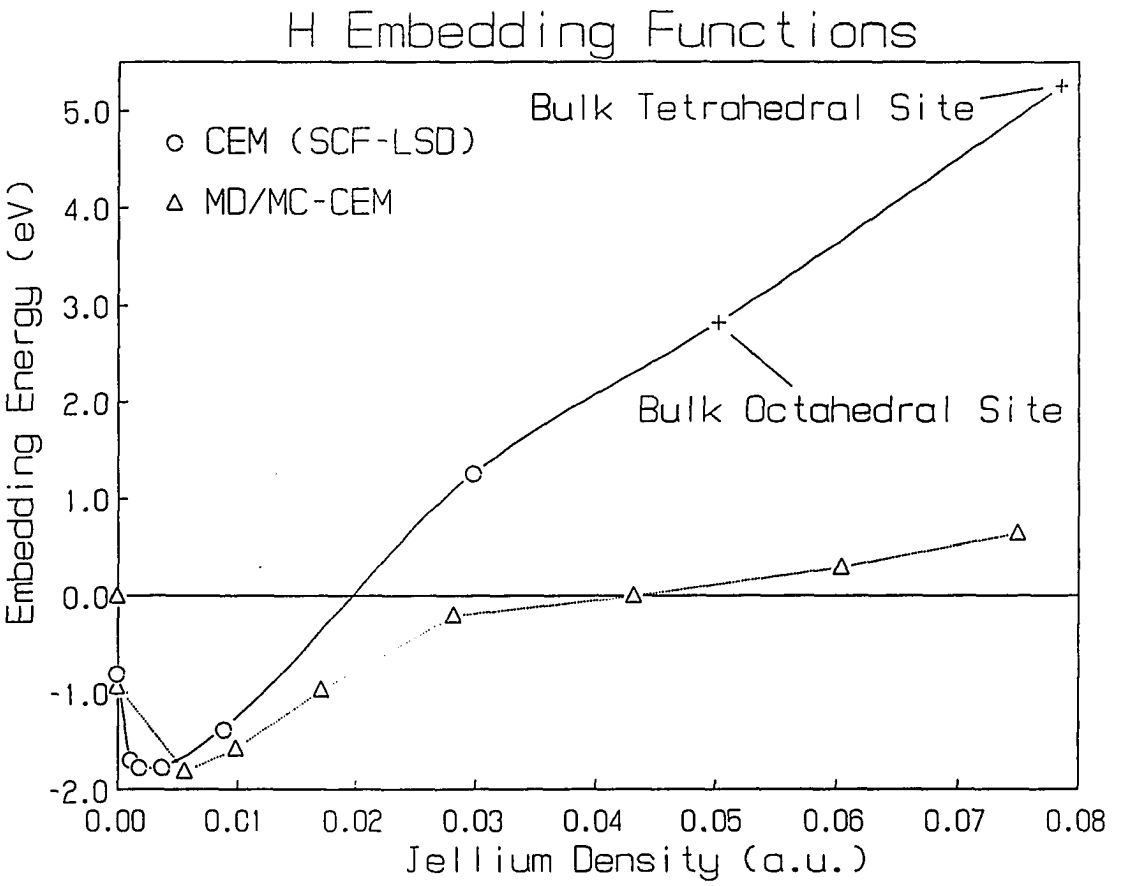

Fig. 3: The Puska *et al.* embedding function for CEM (o) supplemented by two high density points (+) (see text) and the transformed function for MD/MC-CEM (Δ) using CEM results for the H-Pd(111) interaction.

attractive and the non-additive embedding energies are generally repulsive in MD/MC-CEM. This is exactly the opposite of the EAM form. Although the renormalization of the repulsions is certainly possible by subtracting out any linear function of density and putting it into the Coulomb energy, this is unsatisfactory since it will make the repulsions very complex in form. The MD/MC-CEM form is actually more closely related to the original EM method. The EM approach utilizes an approximate evaluation of the Coulomb integrals and a simpler prescription for the jellium densities both of which are valid in the limit of slowly varying electron density.[12d] An upcoming review[14] will provide more detailed comparisons of these methods. The advantages of MD/MC-CEM include generality and accuracy.

III. EXAMPLES

A number of problems can now be treated with relative ease. A few brief illustrations will be considered here: surface relaxation, structure of metal clusters, sticking of Cu atoms to a Cu(100) surface, and scattering of Ar from Pd(111) and H(1x1)/Pd(111). All of these will be considered in much more detail in separate publications dealing in depth with each topic. These examples are chosen to illustrate both the power and limitations of the MD/MC-CEM approach, especially with regard to the full CEM theory. *It is especially important to describe the latter since theories like MD/MC-CEM can be utilized so easily in a great variety of situations, even when they are not applicable.*

As a first test case, we consider the relaxation of the Ni and Pd surfaces using the functions ΔF_C given in Fig. 2. Results are shown in Table II for the relaxation of a few low index surfaces of Ni and Pd and are compared to full CEM, EAM and experimental results. The MD/MC-CEM and CEM values were obtained by MC simulated annealing with 400 energy evaluations per temperature with six temperatures. Note the accuracy of the CEM calculations relative to either the MD/MC-CEM or EAM values. The relative inaccuracy of MD/MC-CEM is quite surprising in comparison to the very good values for the surface energy in Table I. To see why this arises, consider the variation of the relaxation energy with the change in the first interlayer spacing for the Ni(110) system as shown in Fig. 4. Within the CEM method it is immediately apparent that the contribution from ΔG drives the contraction, while the variation due solely to the homogeneous embedding plus Coulomb contributions would lead to a much smaller contraction. Thus, the

Table II. Relaxation of the low Miller index surfaces of Ni and Pd.

Atom	Face	$\%\Delta_{12}$	$\%\Delta_{23}$	$\%\Delta_{34}$	$\%\Delta_{45}$	$\Delta\sigma_S$[a]	Method
Ni	100	+1.1				-0.003	MD/MC-CEM[b]
		-3.2±1.0				-0.020	CEM[b,c]
		-3.04	-0.35	-0.02	-0.02		EAM[d]
		-3.2					Expt.[e]
	110	-1.1				-0.002	MD/MC-CEM[b]
		-7.7±1.3				-0.041	CEM[b,c]
		-7.01	+1.84	-0.98	+0.34		EAM[d]
		-8.7	+3.0	-0.5			Expt.[f]
Pd	110	-3.5				-0.009	MD/MC-CEM[b]
		-7.4±1.9				-0.039	CEM[b,c]
		-11.20	+2.49	-1.18	+0.40		EAM[d]
		-6	+1				Expt.[g]

[a]Surface relaxation energy in units of J/m^2.
[b]CEM and MD/MC-CEM calculations for one layer relaxation only.
[c]The listed uncertainties of $\%\Delta d_{12}$ for the CEM method are due to the finite precision of the numerical integration of ΔG in combination with the flatness of the variation of the relaxation energy vs. $\%\Delta d_{12}$ as evident in Fig. 4.
[d]Ref. 10(c).
[e]Ref. 33.
[f]Ref. 34.
[g]Ref. 35.

smoothing of the electron density environment due to the contraction lowers ΔG which in turn drives the contraction. This is a classic mechanism for surface relaxation.

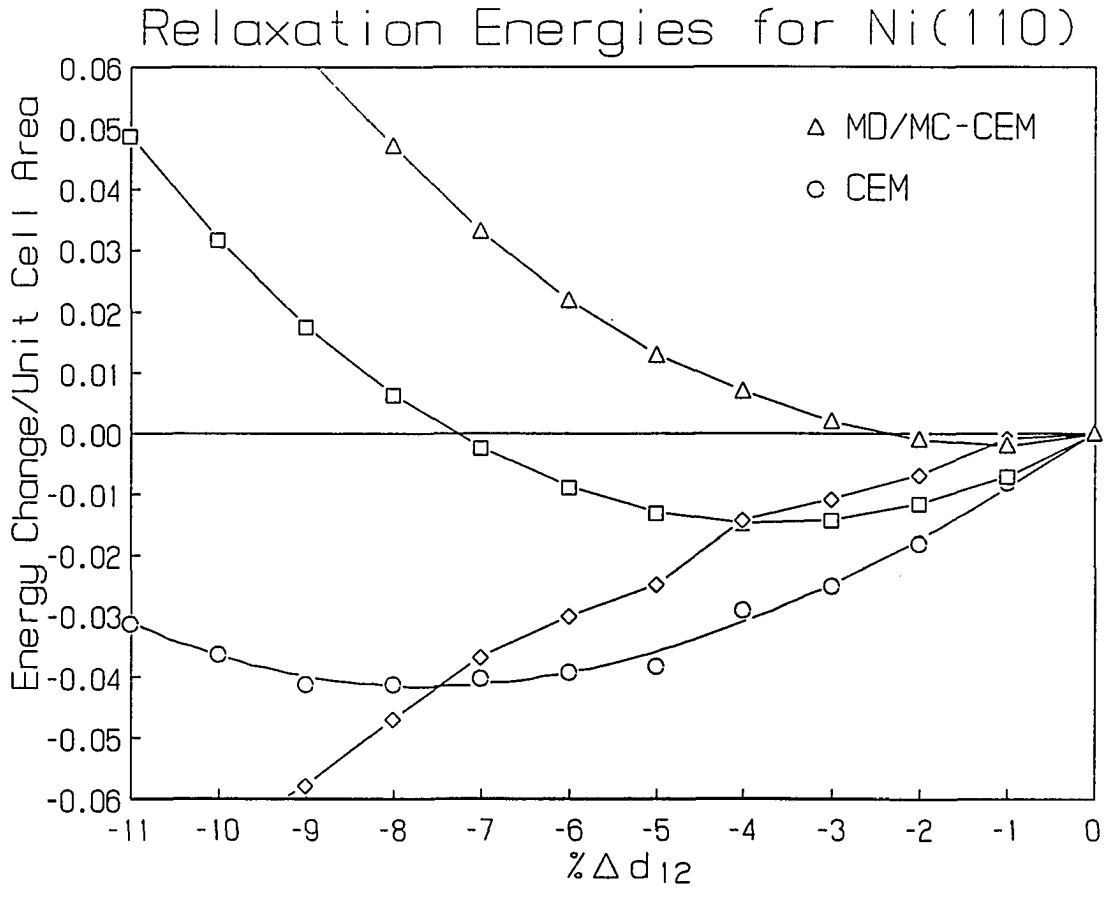

Fig. 4: The relaxation energy (J/m^2) for the Ni(110) system within the CEM (○) and MD/MC-CEM (△) methods plotted as a function of the contraction of the spacing between the surface and first sub-surface layer relative to this spacing in a non-relaxed surface. The contributions to the CEM relaxation energy due to the embedding plus Coulomb energies (□) and to ΔG (◇) are also shown.

The MD/MC-CEM relaxation energy variation in Fig. 4 predicts an even smaller contraction than that predicted by simply neglecting the ΔG contribution within the CEM method. This occurs because the inclusion of ΔG into ΔE_C for a bulk system has the opposite effect as compared to the surface: expansion of the bulk lowers the density and the ΔG term (c.f., Fig. 1a) while contraction of the surface increases the density but lowers the ΔG term. These regions overlap in density but have different ΔG.

From the above analysis, it is clear that the prediction of surface relaxation is generally not possible using MD/MC-CEM theory. Furthermore, this suggests that relaxations can only be treated accurately upon inclusion of gradients of the electron density in the kinetic-exchange-correlation functional (i.e., kinetic energy lowering).[36] The only puzzling feature is the reasonable accuracy of the EAM calculations in Table II, at least for Ni(100) and Ni(110). Since the EAM surface energies in Table I are not even as good as the MD/MC-CEM values and since the EAM predicted relaxation in Pd(110) is poor compared to that in Ni(110), we suspect that the prediction of surface relaxation by the EAM method is simply fortuitous. We would strongly suggest that this example provides an illustration of the importance of understanding the physical and chemical basis for a particular phenomena and not just focusing on the "accuracy" of the results.

It is also important to note that the energy change upon relaxation is quite small. Hence, if one does not require knowledge of the geometry to an accuracy of a few percent, the MD/MC-CEM results are perfectly acceptable. The method certainly provides very good values for the energies.

As a second illustration, we consider the structure and energetics of small Ni clusters and a $Ni_{13}Cu_6$ cluster using the functions ΔF_C given in Fig. 2 for Ni and constructed analogously for Cu. Clusters of rare gas atoms have been studied extensively both experimentally[37] and theoretically[38]. Theoretical studies, often employing a two body Lennard-Jones potential, have focused on the identification of very stable structures (i.e., local minima on the PES) and, hopefully, even the most stable structure (i.e., the global minimum of the PES). This work has demonstrated the predominance of local fivefold symmetry sites in the structure and growth of these clusters. For example, for LJ particles between the very stable icosahedron (N=13) and double icosahedron (N=19) clusters, the progression of most stable structures reportedly involves the formation of a pentagon centered about one of the icosahedral fivefold axes followed by capping this new pentagonal face. (The only exception to this progression known by us was obtained in a quantum Monte Carlo study for N=17.[38b])

In order to discover stable cluster configurations within the MD/MC-CEM model, simulated melting and annealing of Ni clusters was performed using a Langevin molecular dynamics approach.[2a,6,39,40] The melting of a cluster was simulated at approximately 2500 K for 20 ps. Subsequent annealing started at a temperature near 2000 K and was reduced by a factor of 0.95 until a threshold temperature was reached. 500 K, 200 K and 100 K thresholds were used with 10 ps, 20 ps and 40 ps time intervals spent at each temperature in the respective annealing schedules. This led to cooling rates of 5.4 K/ps, 2.0 K/ps and 0.80 K/ps for the simulated annealing in a given job. The time step for all simulations was 0.01

ps. At the end of both the melting and the annealing, the simulations were interrupted so that the cluster could be rapidly quenched to a point where the maximum force on any atom was less than $1x10^{-5}$ eV/Bohr. Finally, this sequence of melting then annealing was repeated four times in a given job. This procedure should have a reasonable probability of determining the global minimum and various local minima in the PES for a cluster of N atoms.

Table III lists the minima determined by the above procedure. Only the lowest energy configuration and those within several hundred meV of this most stable geometry for a N atom cluster are shown.† For temperatures less than 1000 K those structures higher in energy have a very low Boltzmann probability of existing in thermodynamic equilibrium with the selected geometries. Ball and stick diagrams are shown in Fig. 5 for some of the geometries in Table III. The total energy difference between two N atom clusters in the lowest energy configuration and a N-1 atom cluster with a N+1 atom cluster in their respective minimum energy configurations is plotted in Fig. 6. This quantity indicates the stability of the lowest energy configuration of N atoms relative to the lowest energy structures of the neighboring N-1 and N+1 atom clusters. Note the great relative stability of the icosahedron (13.1), the double icosahedron (19.1) and the triple icosahedron (23.1). On the other hand, note the large tendency of the 14 and 18 atom clusters toward decomposition into their neighboring cluster sizes.

---

†The structures 16.3 and 17.4 were not found using the melting then annealing procedure but were obtained by simple quenches of clusters with the same initial symmetry. They are included since they are the most stable configurations for LJ clusters.

Table III. Geometries and MD/MC-CEM binding energies for small Ni clusters.

Index[a]	Description[b]	B.E. (eV/atom)
4.1	T_d tetrahedron	-1.873
5.1	D_{3h} trigonal bipyramid	-2.071
6.1	O_h octahedron	-2.268
7.1	D_{5h} pentagonal bipyramid	-2.369
8.1	D_{2d} trigonal dodecahedron	-2.450
9.1	C_{2v} bicapped pent. bipyr.	-2.518
9.2	D_{3h} tricapped trigonal prism	-2.512
10.1	C_{3v} tricapped pent. bipyr.	-2.590
11.1	C_{2v} quadcapped pent. bipyr.	-2.647
12.1	C_{5v} quintcapped pent. bipyr.	-2.729
13.1	I_h icosahedron	-2.837
14.1	C_{3v} capped (face) icosahedron	-2.837
14.2	C_{2v} capped (edge) icosahedron	-2.836
15.1	D_{6d} l.s. 1-6-1-6-1	-2.882
15.2	C_{2v} bicapped icosahedron	-2.869
16.1	D_{3h} l.s. 3-3-4-3-3	-2.903
16.2	C_s l.s. 2-6-1-6-1	-2.899
16.3	C_s tricapped icosahedron	-2.893
17.1	T_d l.s. 1-6-1-6-3	-2.925
17.2	C_{2v}	-2.921
17.3	C_1	-2.920
17.4	C_s quadcapped icosahedron	-2.910

[a]The index N.M signifies the M^{th} configuration of a N atom cluster. For a given value of N the configurations are listed in decreasing stability. See Fig. 5 for ball and stick diagrams for most of these clusters.

[b]The description includes the symmetry point group of the configuration and usually either a descriptive name or the layer structure (l.s.) of the cluster. The layer structure is specified in terms of the number of atoms in a given layer. Generally the layers are perpendicular to the principal axis of symmetry and the atoms contained within a layer are nearly coplanar. For example, the structure 15.1 has three atoms lying on the C_6 axis separated by two hexagonal arrangements of atoms (c.f., Fig. 5). Thus, its layer structure is 1-6-1-6-1.

Table III. (continued)

Index[a]	Description[b]	B.E. (eV/atom)
18.1	C_{5v} quintcapped icosahedron	-2.944
18.2	C_s l.s. 1-4-1-5-1-5-1	-2.944
18.3	C_{2v} l.s. 4-6-1-6-1	-2.940
19.1	D_{5h} double icosahedron	-3.007
20.1	C_{2v} capped double icosahedron	-3.018
20.2	D_{3d} l.s. 3-3-1-3-3-1-3-3	-3.012
21.1	C_s l.s. 1-6-1-6-1-5-1	-3.034
22.1	D_{6h} l.s. 1-6-1-6-1-6-1	-3.055
22.2	C_1 l.s. 2-6-1-6-1-5-1	-3.048
23.1	D_{3h} triple icosahedron	-3.088
24.1	C_1	-3.094
25.1	C_1	-3.115

As for the LJ particles the most stable configurations of clusters of 7 to 12 atoms are derived largely from the pentagonal bipyramid (7.1). The structure 8.1 replaces one of the pentagonal atoms of structure 7.1 with 2 atoms. This structure is only a slight distortion of a capped pentagonal bipyramid which is reported to be the LJ global minimum.[38] The lowest energy structures for clusters of 9 to 12 atoms are all derived by capping structure 7.1 and are exactly the same as the reported global minima found for the LJ potential.[38] Thus, clusters of 7 to 12 atoms are dominated by the pentagonal symmetry of structure 7.1. For the 13 and 19 atom clusters, the icosahedral and double icosahedral configurations, respectively, are again characterized by points of fivefold symmetry. In contrast to the LJ clusters, however, several stable structures for clusters of 14 to 18 atoms were discovered that are not dominated by points of fivefold symmetry. Fig. 7 contrasts

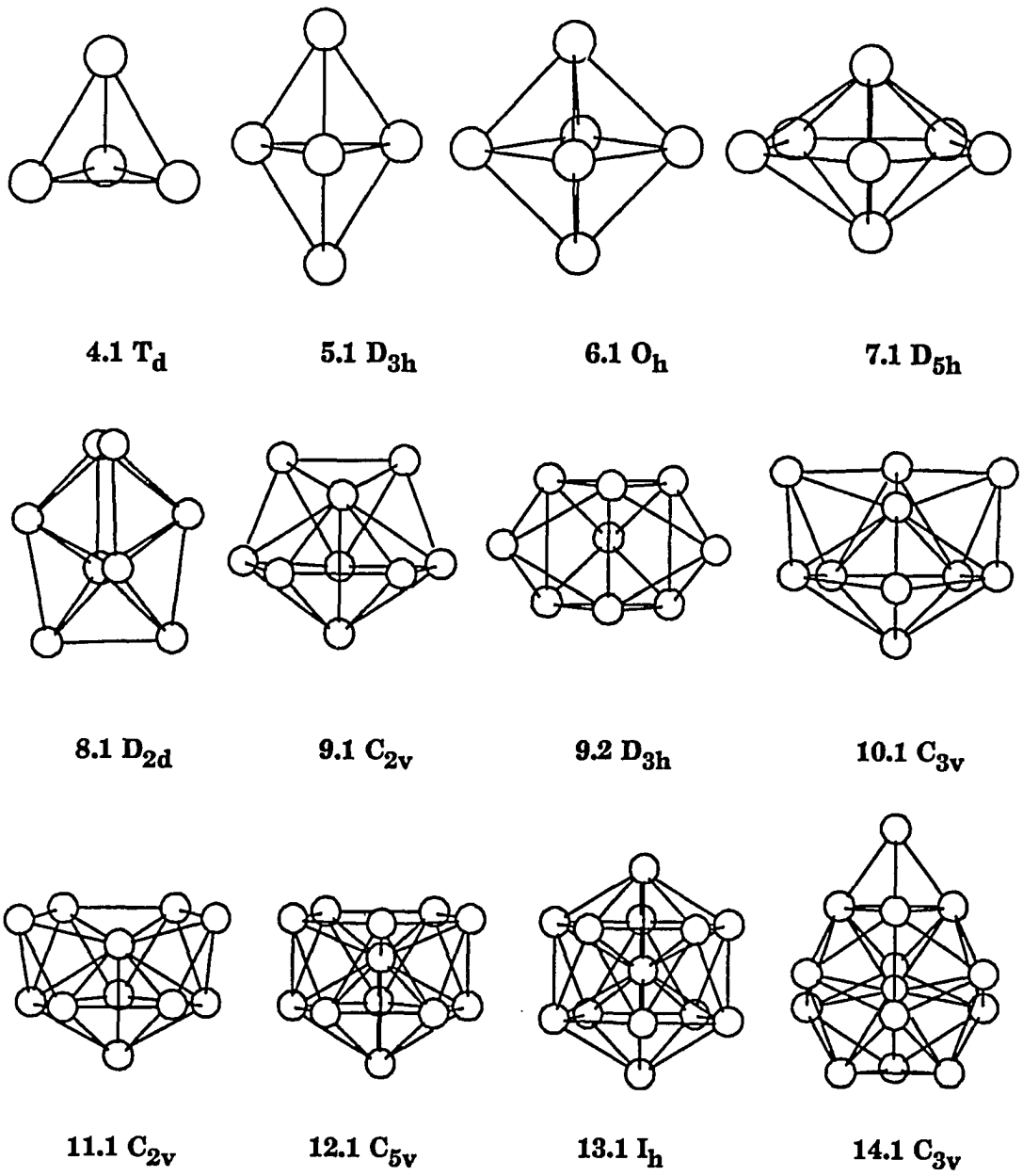

Fig. 5: Ball and stick diagrams for stable geometries of small Ni clusters obtained by a process of simulated melting and annealing. Usually the principal axis of symmetry lies along the length of the page.

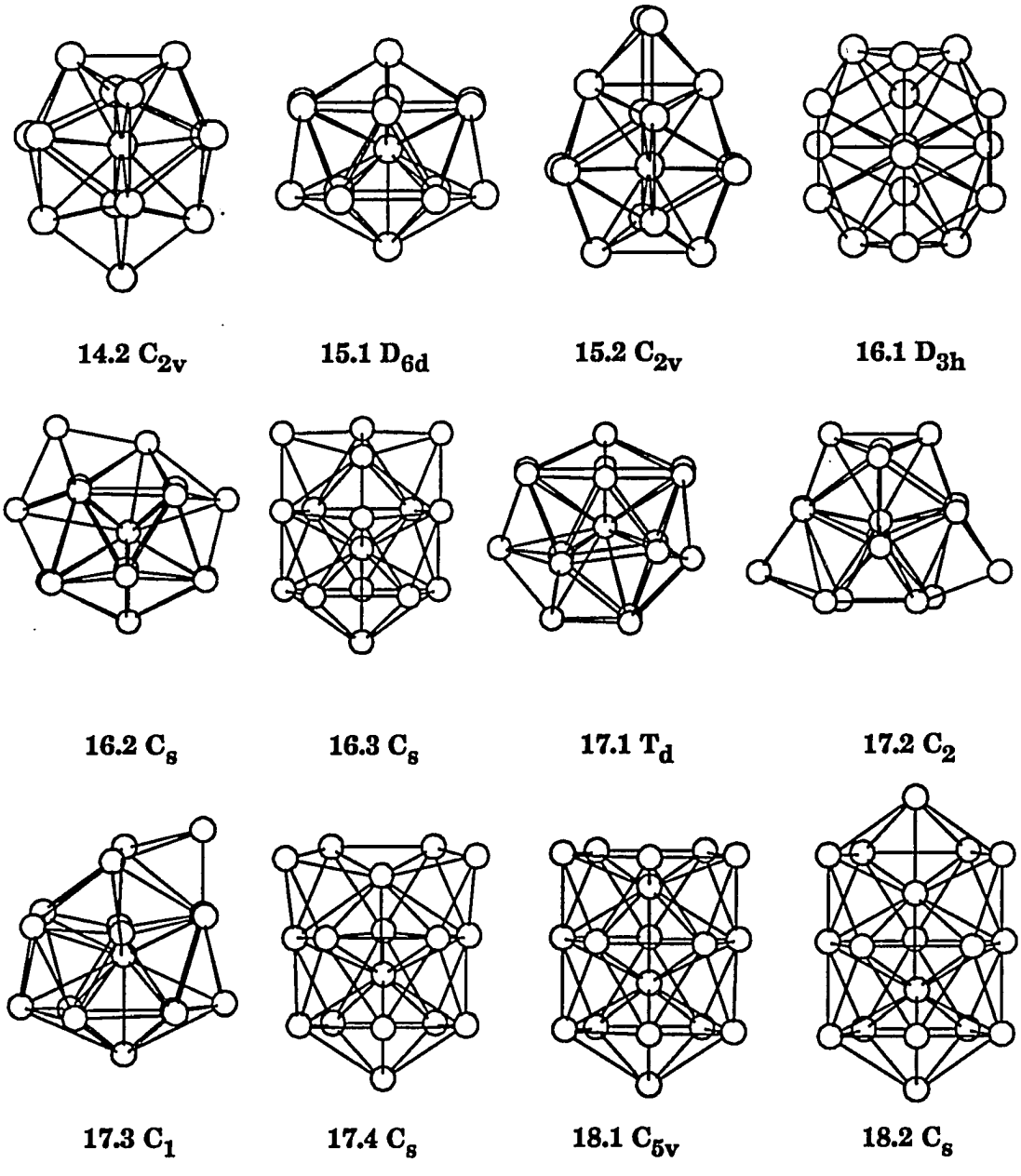

Fig. 5: (continued)

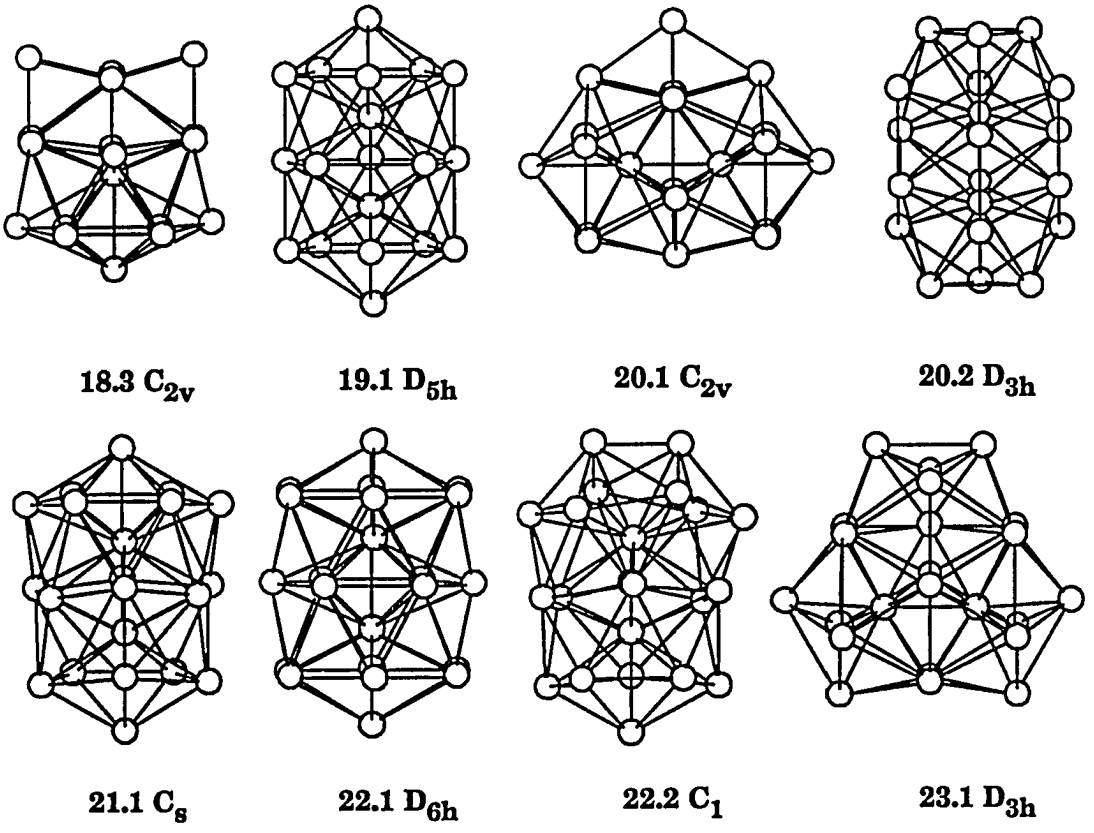

Fig. 5: (continued)

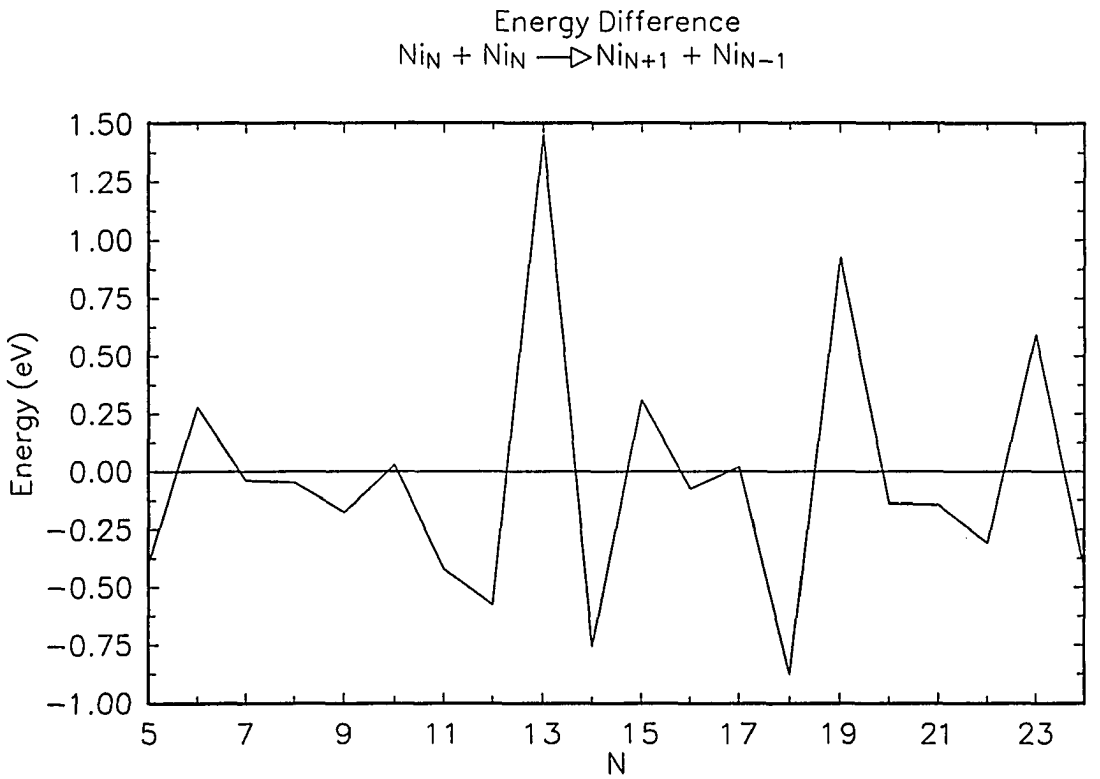

Fig. 6: The total energy difference between the most stable configurations of neighboring Ni_N, Ni_{N+1} and Ni_{N-1} clusters. See text for a complete explanation of this difference.

the LJ minima, dominated by the symmetry of the icosahedron, with stable structures that are dominated by points of threefold and sixfold symmetries. In particular, note the perfect sixfold rotation axis in the structure 15.1. As shown in the bottom row of Fig. 7, this axis also dominates the structure of 16.1, 17.1 and 18.3. Energetically, the structures 15.1, 16.1 and 17.1 are all more than a 100 meV more stable than their LJ counterparts in the top row. In fact, there is a peak in Fig. 6 for the structure 15.1. Although the 14 and 18 atom structures in the bottom row are not global minima, they are only tens of meV less stable than those in the top row. Thus, the structure of clusters of 14 to 18 Ni atoms is not dominated by points of fivefold symmetry using the MD/MC-CEM potential.

In order to test the accuracy of this prediction, an extensive MC simulated annealing of Ni_{15} using the full CEM potential was performed. This resulted in a structure with the exact same symmetry as structure 15.1. Its binding energy was -3.051 eV/atom. In addition, the MD/MC-CEM structure 15.2 was used as the initial geometry in a CEM annealing simulation in which the initial temperature was sufficiently low so that it would be unlikely for the cluster to climb out of this local minima. This simulation resulted in a structure with the same symmetry as 15.2 whose binding energy was -3.027 eV/atom. The cluster energy difference between these two CEM minima was 366 meV, indicating even greater stability for the structure with a sixfold axis and corroborating the MD/MC-CEM results.

Due to the substantial increase in stability of 15.1 over 15.2 in CEM vs. MD/MC-CEM, we decided to investigate clusters 18.1 and 18.3 which are nearly equal in energy using MD/MC-CEM. The relative stabilities of these structures

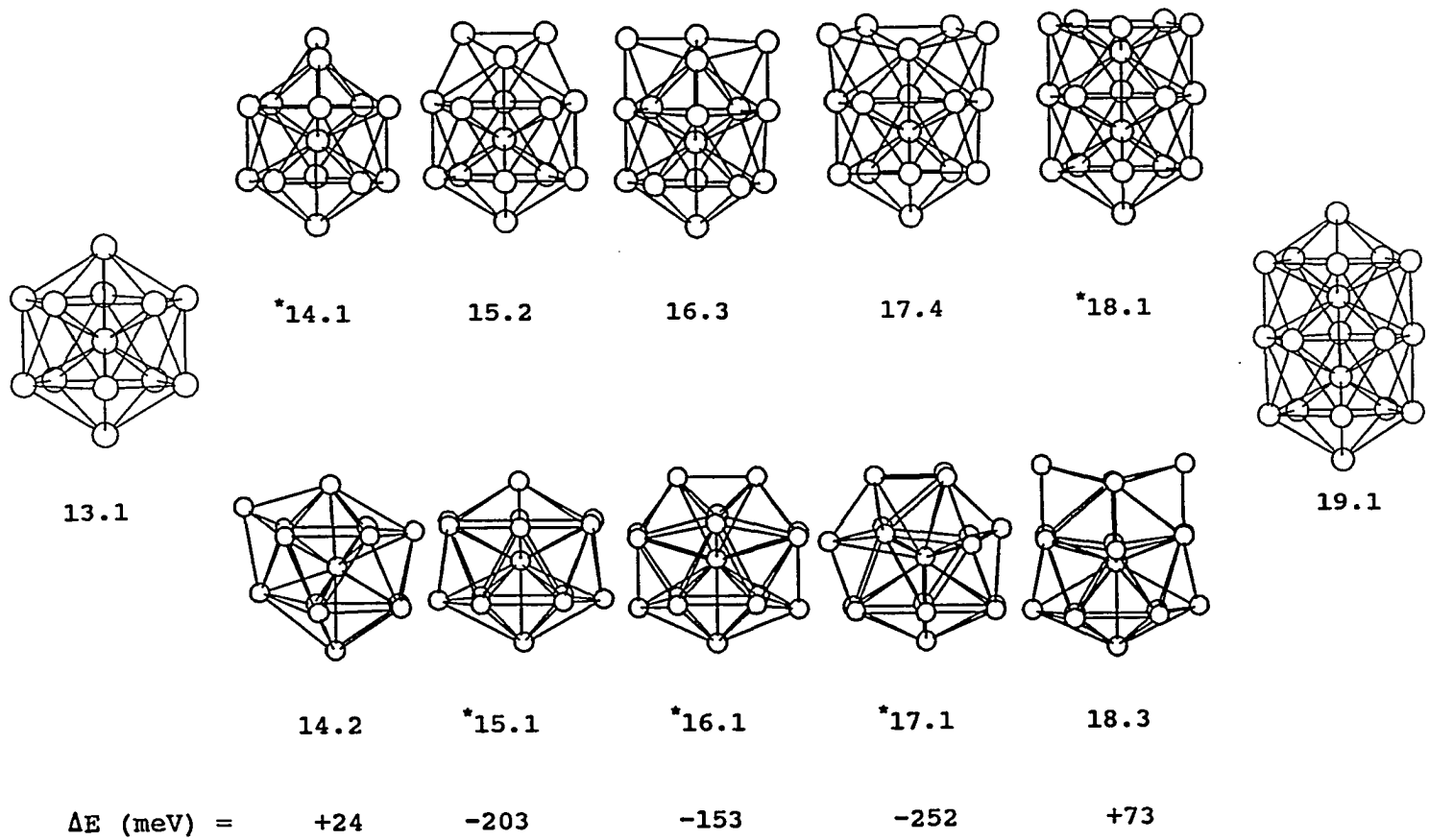

Fig. 7: A comparison of two different structural progressions from the icosahedron to the double icosahedron. The geometries of the top row are the reported lowest energy structures for the LJ pair potential.[38] The structures marked by an asterisk are the most stable geometries for the MD/MC-CEM potential. ΔE is the total energy difference between the bottom and top row structures.

within the full CEM potential was checked by simply scaling the coordinates by some factor. Both structures relaxed within CEM so that their equilibrium size was 97.0% of their size within the MD/MC-CEM potential. Interestingly, the structure 18.3 was more stable than structure 18.1 for all scaling factors between 95% and 105%. At the minimum, the CEM total energy for structures 18.1 and 18.3 was -55.838 eV and -56.020 eV, respectively, or increased stability of 18.3 by 182 meV. This change in the relative stability of the two structures would likely be confirmed by performing an unrestricted MC simulated annealing of the Ni_{18} cluster using the CEM potential. Such minimizations are very expensive now, but future improvements of the computational efficiency of CEM may allow a more complete comparison between the MD/MC-CEM and CEM predictions.

The important point is that metallic clusters modeled within either the MD/MC-CEM or the CEM formalism display significantly different structural characteristics than rare gas clusters modeled by pairwise Lennard-Jones potentials. These differences are due to the delocalized electronic nature of the bonding in metallic clusters. Such delocalization is more accurately accounted for within the CEM theory than within the MD/MC-CEM theory, and thus the former predicts even larger differences from Lennard-Jones type structures.

Bimetallic clusters play a significant role in catalysis.[41] Segregation of the constituent atom types leads to marked effects upon the catalytic selectivity of these clusters. Fig. 8a shows a Cu_6Ni_{13} cluster that was obtained from the melting-annealing process mentioned previously. The overall structure of the cluster is a double icosahedron, as might be expected. The top and bottom axial atoms and

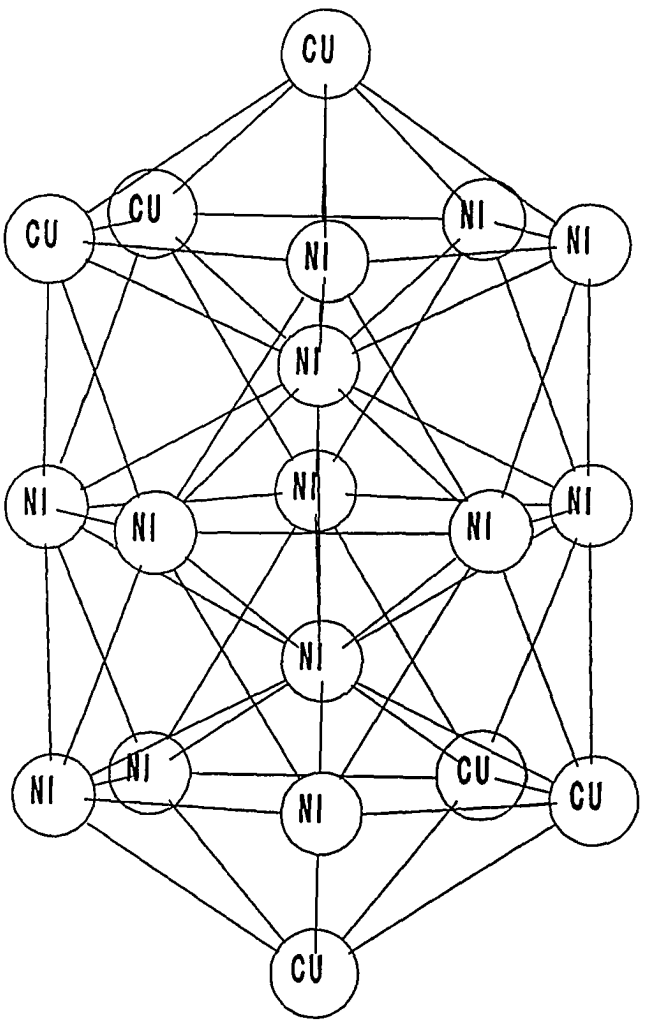

(A)

Fig. 8: Several structures for a Cu_6Ni_{13} cluster obtained by a process of simulated melting and annealing.

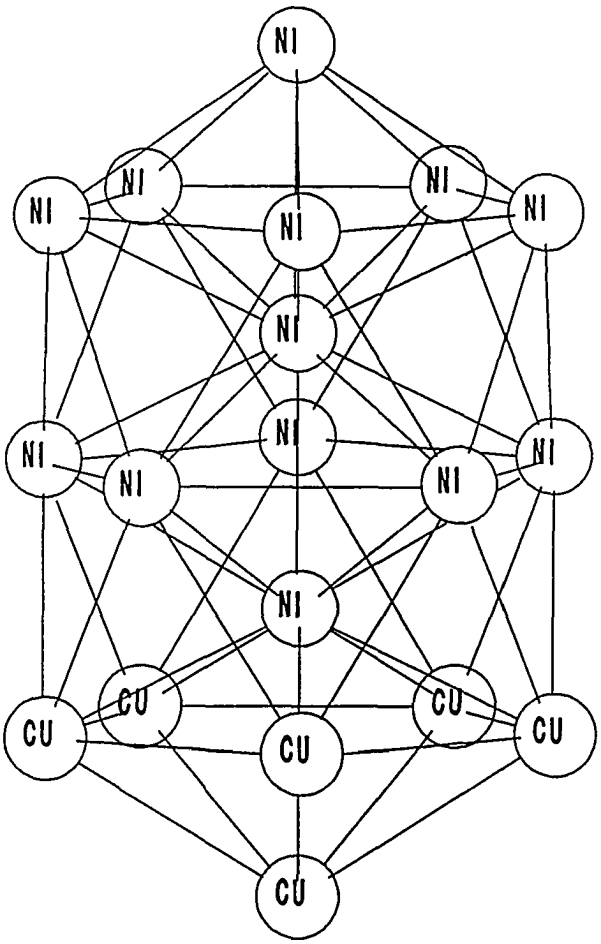

(B)

Fig. 8: (continued)

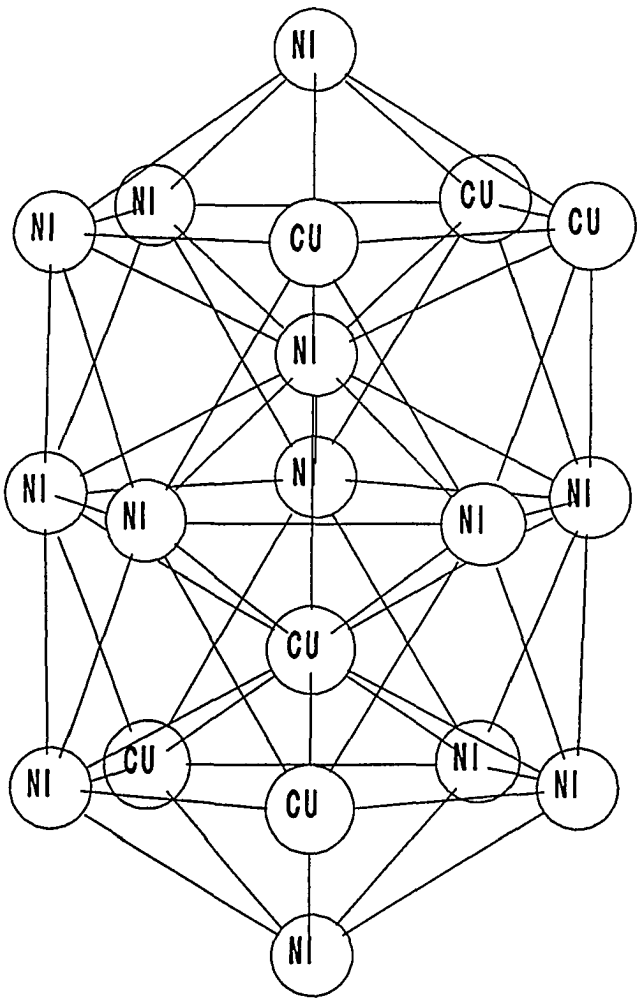

(c)

Fig. 8: (continued)

those atoms in the top and bottom pentagonal planes have a coordination of 6; those in the middle pentagonal plane have a coordination of 8; and, the two inner Ni atoms have a coordination of 12. The average coordination is 6.00 for Cu and 7.69 for Ni. The separation of the Cu atoms into two groups in Fig. 8a has little significance upon the energy of the cluster. In fact, a similar structure in Fig. 8b with all the Cu atoms grouped together in the lower sixfold coordinated sites is 0.05 eV more stable than the cluster shown in Fig. 8a. In contrast, the structure in Fig. 8c with one interior Cu atom is 0.54 eV less stable than the cluster in Fig. 8a. Thus, segregation to the "surface" is exhibited even by this small bimetallic cluster.

It would be difficult to predict such segregation based upon the dimer binding energies[27] of D_0=2.08±.25, 2.01±.08 and 2.068±.01 eV for NiCu, Cu_2 and Ni_2, respectively. The surface free energies[30] of 1.79 and 2.38 J/m^2 for Cu and Ni would allow such a prediction, but one could not be sure that such a quantity is applicable to a 19 atom cluster. MD/MC-CEM calculations provide the theoretical basis for determining the effects at any cluster size.

As a third illustration and first example of a dynamical process, we consider the sticking of Cu atoms on the Cu(100) surface using the functions ΔF_C for Cu. The MD-LE technique[2a,6,40] was used to keep the surface at 77 K. Our intent was to determine the extent of transformation of the large energy released by formation of the Cu-Cu(100) bond (2.7 eV) into translational energy of the Cu atom on the surface. Since the diffusion barrier is only about 0.4 eV[42] (and is 0.47 eV using MD/MC-CEM theory), this transformation had been postulated as leading to epitaxial films[43] and had even been found in simulations using LJ models.[44] In

Fig. 9, we show time frames in the collision of Cu with a small part of the Cu(100) surface which clearly indicates that the Cu is adsorbed directly into a four-fold site without any ballistic motion. (The simulation used a much larger number of moving Cu atoms, nearly 250, but only a few are shown for clarity.) These snapshots are representative of all trajectories which demonstrated no motion of the incident Cu atom out of the original unit cell.

The difficult part of the above prediction is the balance between two features: the transformation of the binding energy into translational energy of the adatom vs. dissipation of the binding energy into the lattice. It is not possible to guess which one will dominate. In fact, we have performed a similar simulation using a LJ potential fit to the Debye frequency and the lattice constant of Cu.[5] It resulted in considerably greater transformation of the released energy into translational energy of the Cu adatom. Using a LJ potential fitted to the cohesive energy and the lattice constant of Cu,[4] or a Morse potential fitted to all three pieces of data,[8] resulted in much better agreement with the MD/MC-CEM predictions. Thus, the LJ(12,6) form can be too stiff for a metal[5-7] and can thus yield the wrong answer. (A stiffer material acts like a rigid surface which leads to large mobility.) The MD/MC-CEM theory gets the important features right: diffusion barrier of 0.47 eV, Debye frequency and surface energy. (Note that relaxation of the initial Cu surface plays no role in this problem.)

As the fourth and final illustration, we consider the scattering of Ar from clean and H(1x1) covered Pd(111) surfaces. The incident atom, adsorbates and substrate were all described by the MD/MC-CEM interaction energies and forces,

Cu-Cu(100)

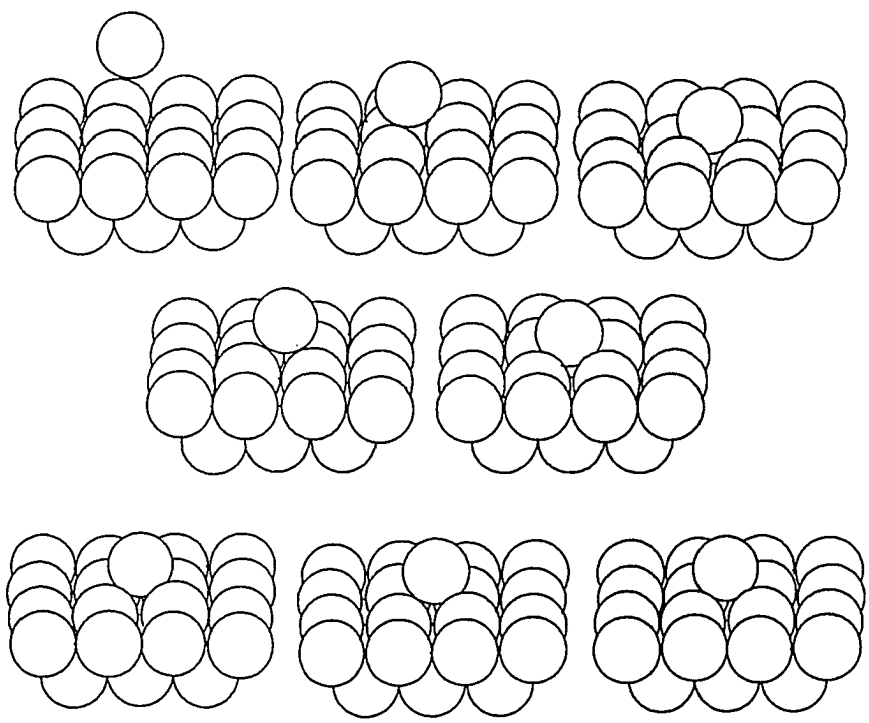

INITIAL KINETIC ENERGY OF GAS = 0.25 eV
INCIDENT ANGLE = 0°
SURFACE TEMPERATURE = 77 K
TIME INCREMENT = 0.20 ps

Fig. 9: A typical trajectory of a Cu atom incident on Cu(100).

with Ar and Pd using ΔF_C and H using ΔF_P. ΔF_C(Ar) is shown in Fig. 10 as determined from the diatomic[45a] and bulk binding curves. The particular values for the bulk modulus, lattice constant and cohesive energy are 2.86 x 10^9 J/m^3 [45b], 5.31 Å[45c] and 0.0800 eV,[45d] respectively. For the rare gas atoms the bulk determines the low density points and the diatomic repulsive potential determines the high density points, a reversal of all the other systems. Adjustable parameters are absent from all these calculations. Approximately 1000 trajectories were completed with an initial kinetic energy of 1.0 eV and initial incidence angle of 30^0 for the Ar atom. Fig. 11 shows the angular distributions. The distribution maximum occurs at 34^0 for both the scattering from clean and H(1x1) covered surfaces. The average final kinetic energy of the scattered Ar at the distribution maxima is 0.70 eV for the clean surface and 0.56 eV for the H(1x1) covered surface. The scattering from adsorbate covered surfaces, considered so difficult, is rather simple using the MD/MC-CEM forces in conjunction with a new scattering code.[21]

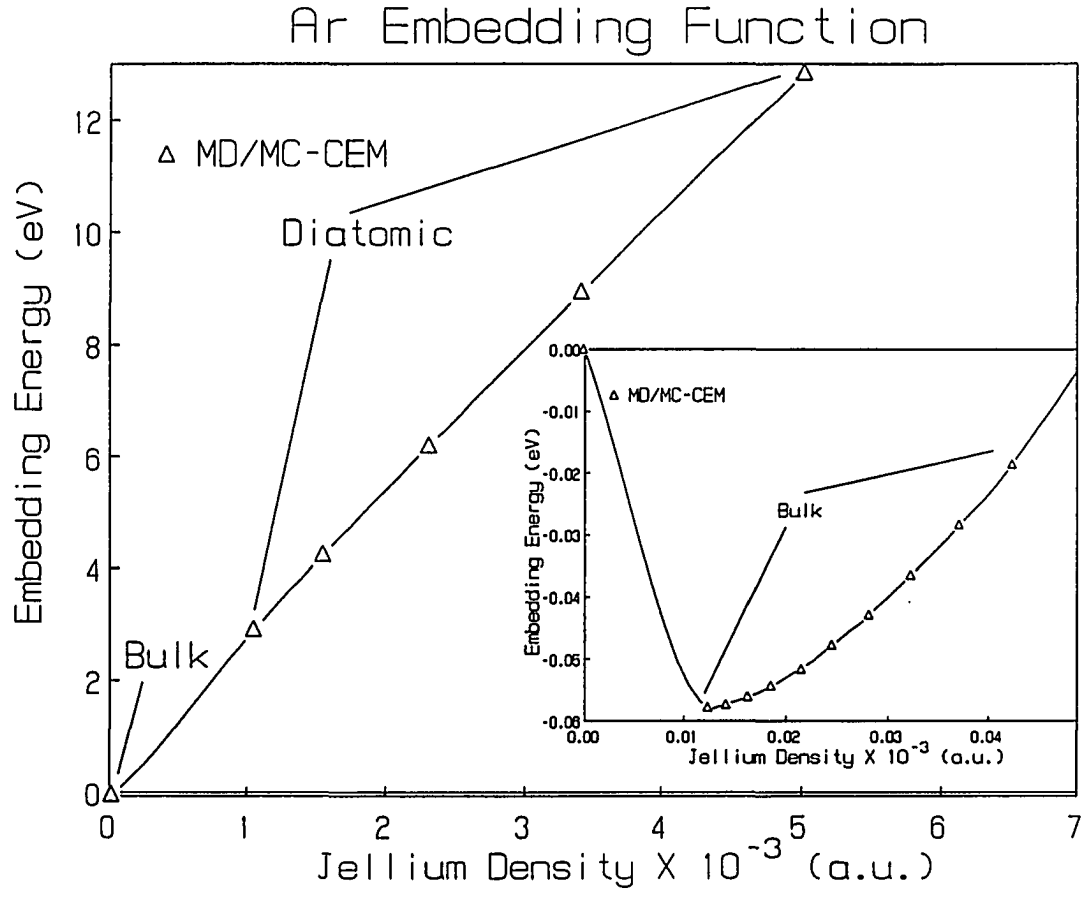

Fig. 10: **The MD/MC-CEM covalent embedding function for Ar. The inset shows the bulk region in detail.**

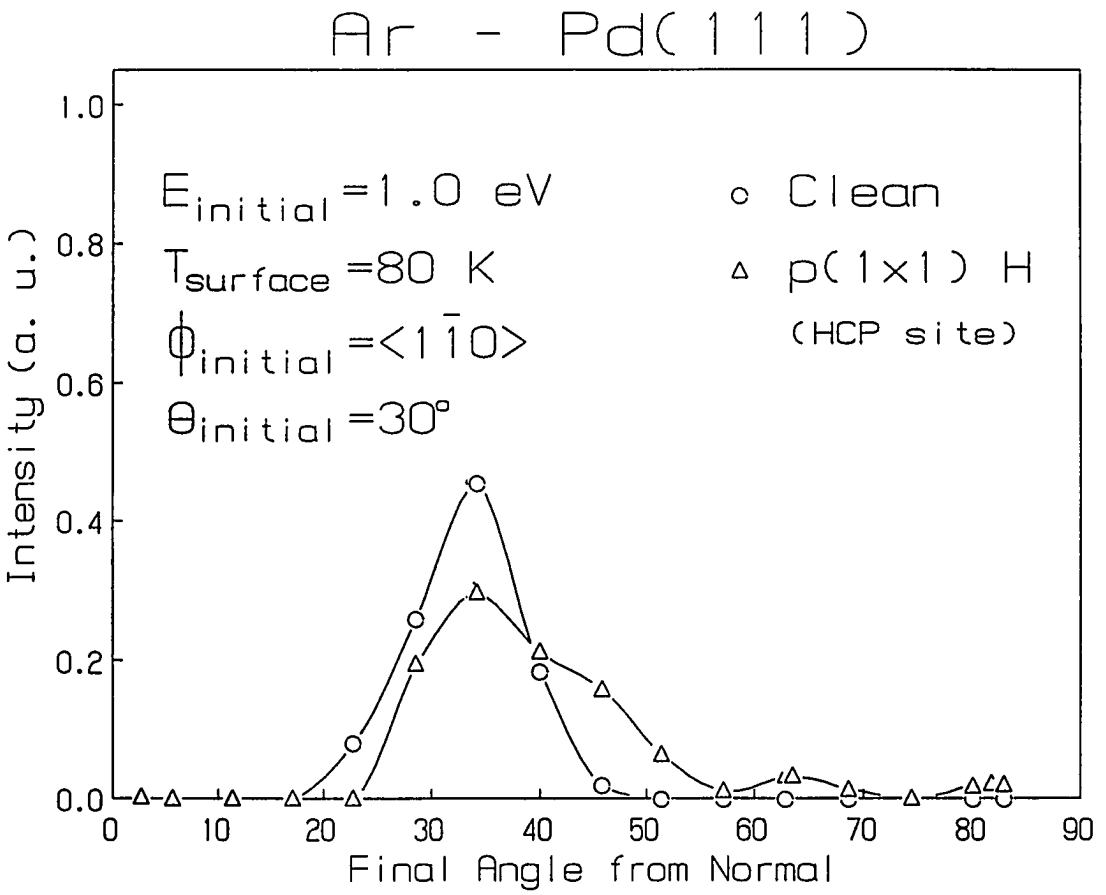

Fig. 11: Angular distributions of Ar atoms with 1.0 eV of initial kinetic energy scattered from clean and H covered Pd(111). The azimuthal angle is denoted as ϕ and the angle from the surface normal is denoted as θ.

IV. SUMMARY AND CONCLUSIONS

We have presented the MD/MC-CEM theory, a conceptual and formal simplification of the CEM method, that can be used directly in large scale MD and MC simulations. This theory incorporated, via an approximate new embedding function, the original correction for kinetic-exchange-correlation energy differences between the real system and the many atom-jellium systems. As a result of this approach, a sophisticated, accurate many-body potential in the MD/MC-CEM method can be evaluated at about one-half the speed (per pair of atoms) of a simple LJ(12,6) pairwise additive form. Examples were provided for the Ni, Pd and Ar/H/metal systems.

Several brief illustrations of the application of this method to large systems were presented. These included relaxation of metal surfaces, structure of pure Ni and mixed NiCu clusters, sticking of Cu on Cu(100), and the scattering of Ar from H covered Pd(111).

It is worthwhile to emphasize that the embedding functions in the MD/MC-CEM method do not have to be redetermined for each new system. For example, once the functions are known for Ni and Cu, the full Ni_MCu_N system can be treated for any number of Ni and Cu atoms. Once they are known for Ar, H and Pd, scattering of Ar from H/Pd(111) can be done at any coverage, as can the scattering of Ar from Ar covered Pd(111); any other face can be used for the Pd also. With the previous embedding functions for Ni and Cu, one can scatter Ar from these surfaces also. There is no refinement and adjustment of parameters to experimental data for any one system, a tedious "art".

There will be systems and observables for which the new MD/MC-CEM method is not sufficiently accurate. Indeed, the illustration of surface relaxations demonstrated precisely this feature. Our limited experience at present would indicate that processes and effects that are dependent upon energy differences of less than about 0.1 eV have to be treated with caution using MD/MC-CEM. The basic problem is that incorporation of the kinetic-exchange-correlation energy difference into the embedding function is unlikely to be so accurate. In these cases, one must resort to more accurate and computationally intensive approaches. Possibly, these approaches could simply be used to check some of the MD/MC-CEM predictions; the full CEM formalism is one method capable of such a role. On the other hand, more direct approximations of ΔG could be implemented than the one currently employed in the MD/MC-CEM formalism. These improved approximations would more accurately account for variations in electron density environments.

For many situations such small energies are not critical. Three cases were illustrated herein: structure of (a number of) pure Ni and mixed NiCu clusters, sticking of Cu on Cu(100), and the scattering of Ar from H covered Pd(111). For such problems, the capabilities provided by the accuracy of the MD/MC-CEM PES along with the very fast force evaluations should open new horizons in the treatment of the structure and dynamics of complicated many-body systems.

ACKNOWLEDGEMENTS

The authors thank S. Sinnott for supplying the surface energy and relaxation results prior to publication. This article was supported by the Division of Chemical Sciences, Office of Basic Energy Sciences of the U.S. Department of Energy through the Ames Laboratory, which is operated for the U.S. DOE by Iowa State University under Contract No. W-7405-Eng-82. Partial support was also received from NSF Grant CHE-8609832. Some of the calculations were performed on the Pittsburgh Supercomputer Center's CRAY YMP. One of the authors (M.S.S.) also acknowledges the support of the Alworth Memorial Foundation.

REFERENCES

1. U. Burkert and N. L. Allinger, *Molecular Mechanics* (American Chemical Society, Washington, D. C., 1982).

2. (a) C. L. Brooks, III, M. Karplus and B. M. Pettitt, Adv. Chem. Phys. **71**, 1 (1988).
   (b) P. A. Bash, M. J. Field and M. Karplus, J.A.C.S. **109**, 8092 (1987).

3. (a) R. Car and M. Parrinello, Phys. Rev. Lett. **55**, 2471 (1985);
   (b) D. Hohl, R. O. Jones, R. Car and M. Parrinello, Chem. Phys. Lett. **139**, 540 (1987);
   (c) D. Hohl, R. O. Jones, R. Car and M. Parrinello, J. Chem. Phys. **89**, 6823 (1988);
   (d) P. Ballone, W. Andreoni, R. Car and M. Parrinello, Phys. Rev. Lett. **60**, 271 (1988);
   (e) G. Galli, R. M. Martin, R. Car and M. Parrinello, Phys. Rev. Lett. **62**, 555 (1989).

4. T. Halicioglu and G. M. Pound, Phys. Stat. Solidi A **30**, 619 (1975).

5. A. E. DePristo, Surf. Sci. **141**, 40 (1984);

6. A. E. DePristo and H. Metiu, J. Chem. Phys. **90**, 1229 (1989).

7. H. Metiu and A. E. DePristo, J. Chem. Phys. **91**, 2735 (1989).

8. L. A. Girifalco and V. G. Weizer, Phys. Rev. **114**, 687 (1959).

9. (a) F. Stillinger and T. Weber, Phys. Rev. B **31**, 5262 (1985);
   (b) R. Biswas and D. R. Hamann, Phys. Rev. B **36**, 6434 (1987);
   (c) K. Ding and H. C. Andersen, Phys. Rev. B **34**, 6987 (1986);
   (d) D. W. Brenner and B. J. Garrison, Phys. Rev. B **34**, 1304 (1986);
   (e) M. I. Baskes, Phys. Rev. Lett. **59** 2666, (1987);
   (f) J. Tersoff, Phys. Rev. B **37** 6991, (1988).

10. (a) M. S. Daw and M. I. Baskes, Phys. Rev. B **29**, 6443 (1984);
    (b) S. M. Foiles, M. I. Baskes and M. S. Daw, Phys. Rev. B **33**, 7983 (1986);
    (c) N. Ting, Y. Qingliang, and Y. Yiying, Surf. Sci. **206**, L857 (1988);
    (d) M. S. Daw, Phys. Rev. B **39**, 7441 (1989).

11. (a) B. J. Garrison, N. Winograd, D. M. Deaven, and C. T. Reimann, Phys. Rev. B **37**, 7197 (1988);
    (b) M. Lundberg, Phys. Rev. B **36**, 4692 (1987);
    (c) A. F. Voter, Proc. SPIE-Int. Soc. Opt. Eng. **821**, 214 (1988);
    (d) M. I. Baskes, S. M. Foiles, and C. F. Melius, J. Nucl. Mater. **145**, 339 (1987).

12. (a) J. K. Norskov and N. D. Lang, Phys. Rev. B **21**, 2136 (1980);
(b) M. J. Stott and E. Zaremba, Phys. Rev. B **22**, 1564 (1980);
(c) K. N. Jacobsen, J. K. Norskov, and M. J. Puska, Phys. Rev. B **35**, 7423 (1987), and references therein;
(d) J. K. Norskov, J. Chem. Phys. **90**, 7461 (1989).

13. (a) K. W. Jacobsen, Comments Condens. Matter Phys. **14**, 129 (1988);
(b) T. McMullen, M. J. Stott, and E. Zaremba, Philos. Mag. A **59**, 161 (1989);
(c) P. Stoltze, J. K. Norskov, and U. Landman, Phys. Rev. Lett. **61**, 440 (1988).

14. T. J. Raeker and A. E. DePristo, Int. Rev. Phys. Chem. (to be published).

15. J. D. Kress and A. E. DePristo, J. Chem. Phys. **87**, 4700 (1987).

16. J. D. Kress and A. E. DePristo, J. Chem. Phys. **88**, 2596 (1988).

17. J. D. Kress, M. S. Stave and A. E. DePristo, J. Phys. Chem. **93**, 1556 (1989).

18. T. J. Raeker and A. E. DePristo, Phys. Rev. B **39**, 9967 (1989).

19. T. J. Raeker and A. E. DePristo, Corrected Effective Medium Calculations of the Chemisorption of H and N on Fe(100),(110) and W(110). Surf. Sci. (submitted September 1989).

20. (a) M. J. Puska, R. M. Nieminen and M. Manninen, Phys. Rev. B **24**, 3037 (1981);
(b) M. J. Puska, (private communication).

21. D. E. Sanders, M. S. Stave and A. E. DePristo, "SCT89: a computer code for atomic and molecular scattering from clean and adsorbate covered surfaces", J. Comp. Phys. (to be submitted).

22. A. D. Becke, J. Chem. Phys. **88**, 2547 (1988).

23. M. Abramowitz and I. A. Stegun, *Handbook of Mathematical Functions* (Dover, New York, 1972).

24. A. E. DePristo and J. D. Kress, Phys. Rev A **35**, 438 (1987).

25. P. A. M. Dirac, Proc. Camb. Philos. Soc. **26**, 376 (1930).

26. O. Gunnarsson and B. I. Lundqvist, Phys. Rev. B **13**, 4274 (1976).

27. M. D. Morse, Chem. Rev. **86**, 1049 (1986).

28. (a) J. R. Smith, J. H. Rose, J. Ferrante, and F. Guinea, in *Many-body*

Phenomena at Surfaces, edited by D. Langreth and H. Suhl (Academic Press, New York, 1984);
(b) J. H. Rose, J. Ferrante and J. R. Smith, Phys. Rev. Lett. **47**, 675 (1981).

29. C. Kittel, *Introduction to Solid State Physics*, 4th ed. (John Wiley, New York, 1971).

30. W. R. Tyson and W. A. Miller, Surf. Sci. **62**, 267 (1977).

31. (a) P. T. Gallagher and W. A. Oates, Metall. Trans. **245**, 179 (1969);
(b) J. Volkl and G. Alefeld, in *Hydrogen in Metals I, Topics in Applied Physics*, edited by G. Alefeld and J. Volkl (Springer-Verlag, New York, 1978), Vol. 28, p. 325.

32. N. A. Baykara, J. Andzelm and D. R. Salahub, Int. J. Quant. Chem. **29**, 1025 (1986).

33. J. W. Frenken, R. G. Smeek and J. F. Van der Veen, Surf. Sci. **135**, 147 (1983).

34. D. L. Adams, L. E. Petersen and C. S. Sorensen, J. Phys. C **18**, 1753 (1985).

35. C. L. Barnes, M. Q. Ding, M. Lindrous, R. D. Diehl and D. A. King, Surf. Sci. **162**, 59 (1985).

36. T. J. Raeker, S. B. Sinnott and A. E. DePristo, Surf. Sci. Lett. (to be submitted).

37. (a) J. Farges, M. F. de Feraudy, B. Raoult, and G. Torchet, J. Chem. Phys. **78**, 5067 (1983);
(b) J. Farges, M. F. de Feraudy, B. Raoult, and G. Torchet, J. Chem. Phys. **84**, 3491 (1986);
(c) J. Farges, M. F. de Feraudy, B. Raoult, and G. Torchet, Adv. Chem. Phys. **70**, Part 2, 45 (1988).

38. (a) M. R. Hoare and P. Pal, Adv. Phys. **20**, 161 (1971);
(b) D. L. Freeman and J. D. Doll, J. Chem. Phys. **82**, 462 (1985);
(c) L. T. Wille, Chem. Phys. Let. **133**, 405 (1987).

39. R. Biswas and D. R. Hamann, Phys. Rev. B **34**, 895 (1986).

40. (a) M. Berkowitz and J. A. McCammon, Chem. Phys. Lett. **90**, 215 (1982);
(b) C. L. Brooks III and M. Karplus, J. Chem. Phys. **79**, 6312 (1983);
(c) R. Lucchese and J. C. Tully, Surf. Sci. **137**, 1570 (1983); J. Chem. Phys. **80**, 3451 (1984).

41. (a) J. H. Sinfelt, Acc. Chem. Res. **20**, 134 (1987);

(b) G. Meitzner, G. H. Via, F. W. Lytle and J. H. Sinfelt, J. Chem. Phys. **87**, 6354 (1987);
(c) S. Mukherjee and J. L. Moran-Lopez, Surf. Sci. **189/190**, 1135 (1987);
(d) J. K. Strohl and T. S. King, J. Catal. **116**, 540 (1989).

42. J. J. de Miguel, *et al.*, J. Cryst. Growth **88**, 442 (1988).

43. W. F. Egelhoff and I. Jacob, Phys. Rev. Lett. **62**, 921 (1989).

44. M. Schneider, A. Rahman and I. K. Schuller, Phys. Rev. Lett. **55**, 604 (1985).

45. (a) R. A. Aziz and M. J. Slaman, Mol. Phys. **58**, 679 (1986);
(b) M. S. Anderson and C. A. Swenson, J. Phys. Chem. Sol. **36**, 145 (1975);
(c) O. G. Peterson, D. N. Batchelder, and R. O. Simmons, Phys. Rev. **150**, 703 (1966);
(d) L. A. Schwalbe, R. K. Crawford, H. H. Chen, and R. A. Aziz, J. Chem. Phys. **66**, 4493 (1977).

PAPER II.

NUMERICAL INTEGRATION ON A HYPERCUBE COMPUTER

Numerical integration on a hypercube computer

Mark S. Stave
and
Andrew E. DePristo

Ames Laboratory - USDOE
and
Department of Chemistry
Iowa State University
Ames, Iowa 50011

ABSTRACT

The numerical evaluation of integrals in three spatial dimensions is a computationally intensive operation that assumes a significant role in many scientific computer programs. This operation is readily parallelizable on a variety of computer architectures. In particular, we demonstrate that it can be efficiently performed on a hypercube computer using a simple algorithm. The observed speedup is nearly linear with increasing numbers of processing elements. The hypercube performance is competitive with a shared memory, multiprocessing supercomputer. Details of the implementation and analysis of its performance are discussed in relation to an application within a computational chemistry code based on a corrected effective medium theory.

I. INTRODUCTION

Pioneering studies have demonstrated the speedup available for scientific calculations by means of massively parallel computing[1,2]. Multicomputers consist of large numbers of processors plus local memory connected by high speed interprocessor communication networks. These are now capable of Gflops (i.e., 10^9 floating point operations per second) performance and will undoubtedly soon be capable of Tflops (i.e., 10^{12} flops) performance. Since their memory is distributed, these new supercomputers can be scaled to many thousands of processors. However, the distributed memory and interprocessor control can require development of new carefully crafted algorithms.

For more conventional supercomputers, current peak performance rates are on the order of several Gflops. These rates are attained by coupling ten or fewer very fast processors together with a shared, global memory. The number of processors on such shared memory architectures is limited since memory contention will eventually degrade performance[3,4].

In this paper, we consider the numerical evaluation of integrals by means of quadrature rules. This is a critical component of many scientific calculations. In particular, quantum chemical calculations based on density functional theory approximate the exchange and correlation energies of a many electron system by three dimensional integrals of the system electron density[5]. These integrals cannot be computed analytically since their integrands involve non-integer powers of the electron density. As a result, much research[6-9] has focused on optimal numerical algorithms for the evaluation of these integrals. This research has anticipated the

significant advances of massively parallel computing technology.

As a more concrete example of the kinds of theoretical problems, consider the structure and energies of metal clusters in the size range from 5-25 atoms. These are too large and complex to determine the structures directly from experiment. Thus, chemical reactions such as hydrogen and ammonia adsorption[10,11] are used experimentally to probe the structure of these metal clusters. This provides indirect information which needs to be complemented by accurate computational models. Modeling such systems, however, requires sophisticated interaction potentials. Using a corrected effective medium (CEM) method[12,15] based on density functional theory, we have predicted the structures of metal clusters for Ni and Pd[16]. To make such predictions, we had to perform unconstrained optimization of the cluster geometries within the CEM method, a procedure which was made possible only by the use of a hypercube computer. In light of the predictions of CEM, the experimental data can be rationalized, and a new type of growth sequence for metal vs. rare gas clusters could be detailed. Ongoing research involves the study of uptake of hydrogen by these metal clusters, a project that would not have even been initiated without the availability of the hypercube. Similar advances in modeling capabilities should be realized as physical scientists learn to use multicomputers.

The central development of this paper is a simple and efficient implementation of a numerical integration algorithm on a distributed memory computer. This multicomputer has a hypercube network of processing elements. The issues of partitioning the problem among the processors and of efficient interprocessor communication are discussed. To help the reader understand the

chemical context of this problem, a review of the use of density functionals in the CEM theory is presented in Section II. The quadrature scheme implementation on both a hypercube and two shared memory computers is discussed in Section III, while its performance on the various architectures is analyzed in Section IV. Throughout these sections our emphasis will be on the hypercube implementation. Concluding remarks are given in Section V. Details of our implementation on a hypercube computer are included in several appendices.

II. THEORETICAL AND COMPUTATIONAL DETAILS

Consider a system of N atoms $\{A_i, i=1,...,N\}$. The vectors $\{\vec{R}_i, i=1,...,N\}$ specify the positions of the nuclei, while the vectors $\{\vec{r}_i, i=1,...N\}$ specify a point in space relative to the nuclei. Within effective medium type theories[17] the interaction energy of this set of atoms is approximated initially as a sum of the N interaction energies between each atom and a medium that models the effect of the remaining N-1 atoms. This approximation reduces the problem from determining the interaction energy of an N-body system to determining the interaction energy of N one-body systems. The effective medium interacting with atom A_i is defined as an electron gas of uniform density along with a compensating uniform positive charge density. Usually, this effective medium is referred to as jellium and its interaction energy with an atom as an embedding energy. The intent of this approximation is to capture a significant portion of the interaction between an atom and a delocalized distribution of electrons.

Several corrections are added to this initial approximation to obtain the complete expression of the CEM interaction energy:

$$\Delta E(\{A_i\}) = \sum_{i=1}^{N} \Delta E_J(A_i; n_i) + \Delta V_C + \Delta G(\{A_i\}) \; . \qquad (1)$$

As explained above, the first term is the sum of embedding energies for each atom A_i embedded into jellium of density n_i, $\Delta E_J(A_i; n_i)$. The second corrects for the difference in Coulomb interaction energies between the N-atom system and the atom-in-jellium systems, ΔV_C. The third corrects for the difference in kinetic, exchange and correlation interaction energies between the N-atom system and the

atom-in-jellium systems, ΔG. These energy corrections arise due to differences in the electron and positive charge distributions between the N-atom and the N atom-in-jellium systems. These corrections have been shown to be important in the prediction of structures of metal clusters[16]. We do want to emphasize that CEM provides a non-self-consistent but rather accurate description of many aspects of metallic bonding, in contrast to simple empirical interaction potentials which are incapable of treating metallic bonding. A general review of the CEM method can be found in ref. [17] for the reader interested in the theoretical basis, relationship to other density functional based methods, and further applications.

Within CEM the correction energies are calculated via energy functionals of the total electron density of a system. The electron densities are approximated as a superposition of the spherical electron densities of isolated atoms and the jellium electron density. For the N-atom system the electron density is given by

$$\rho(\vec{r}) = \sum_{i=1}^{N} \rho_i(\vec{r} - \vec{R}_i) \ , \qquad (2)$$

where $\rho_i(\vec{r} - \vec{R}_i)$ is the spherical electron density of atom A_i. (The electron density of atom A_i is referred to as $n_i(A_i; \vec{r} - \vec{R}_i)$ in previous papers. The necessity for shorthand notation in subsequent equations precludes this earlier notation here.)

By far the most computationally intensive part of Eq. (1) is the evaluation of the kinetic, exchange and correlation interaction energies. The difference of these energies between the N-atom system and the N atom-in-jellium systems is written as

where n_i is the electron density of the jellium into which atom A_i is embedded. For

$$\Delta G = G(\{A_i\}) - \sum_{i=1}^{N} [G(A_i+n_i) - G(n_i)] , \quad (3)$$

each system these energies are expressed in terms of functionals as

$$G = c\int f(\rho, |\nabla_r \rho|^2)d\vec{r} , \quad (4)$$

where c is a constant and the integrand is an explicit function of both the system electron density, $\rho = \rho(\vec{r})$, and its gradient. While local density functionals depend only on the density (e.g., the local kinetic energy functional is proportional to $\rho^{5/3}$), more accurate, non-local density functionals also depend on the gradient of the density. As indicated in Eq. (4), the non-local functionals in our work depend explicitly on the squared magnitude of the total electron density gradient[18,19]. Due to the additive density approximation in Eq. (2), this variable is simply determined by summing the atomic electron density gradients,

$$|\nabla_r \rho|^2 = \left(\sum_{i=1}^{N} \frac{\partial \rho_i}{\partial x_i}\right)^2 + \left(\sum_{i=1}^{N} \frac{\partial \rho_i}{\partial y_i}\right)^2 + \left(\sum_{i=1}^{N} \frac{\partial \rho_i}{\partial z_i}\right)^2 , \quad (5)$$

where the subscripted variables are with respect to the atom A_i (e.g., $x_i = x - X_i$ where X_i is the x-coordinate of atom A_i).

Each of the N atom-in-jellium systems, $G(A_i + n_i)$, depends on the atomic coordinates only indirectly through the jellium electron density, which is proportional to the overlap of the electron densities of atom A_i with all other atoms. The jellium electron density into which an atom is embedded measures the average electron density about the atom due to all other atoms. It explicitly depends on the atomic coordinates. $G(A_i + n_i)$ can be evaluated once the jellium density has been

determined. The computational effort involved is minimal since the integration is about a single center with spherical symmetry. Adding the uniform electron density of jellium to the spherical electron density of an atom maintains the atom's spherical symmetry in the total electron density of an atom-in-jellium system. Furthermore, since the integral is not directly dependent on the atomic coordinates, it can be tabulated for a range of jellium densities and then evaluated with even less computational effort via piecewise cubic interpolation.

The kinetic, exchange and correlation energy of the N-atom system, $G(\{A_i\})$, poses the central computational challenge. Its evaluation entails a multi-center, three-dimensional integral over all space that varies explicitly with any change of the atomic coordinates. Four orders of magnitude more time are needed for this calculation than the combined total for all other terms in the CEM interaction energy. Thus, in the remainder of this paper, our emphasis will be on the efficient evaluation of this term.

Much of our research requires evaluation of the interatomic forces determined by the CEM potential. Their evaluation is again overwhelmingly dominated by the computation of the derivative of $G(\{A_i\})$. The analytic derivative of Eq. (4) with respect to the coordinates of atom A_j is given by

$$\nabla_{\vec{R}_j} G(\{A_i\}) = c\int \left(\nabla_{\vec{R}_j}\rho\right)\frac{\partial f}{\partial \rho} + \left(\nabla_{\vec{R}_j}|\nabla_{\vec{r}}\rho|^2\right)\frac{\partial f}{\partial |\nabla_{\vec{r}}\rho|^2}\,d\vec{r}\,, \qquad (6)$$

where the partial derivatives of f can easily be determined for any specific functional. When Eqs. (2) and (5) are differentiated with respect to the coordinates of atom A_j, many of the terms vanish. The remaining terms only require radial derivatives of the atomic electron densities since these densities are spherical. Specifically, the derivatives of Eqs. (2) and (5) are expressed as

$$\nabla_{\vec{R}_j}\rho = -\frac{\partial \rho_j}{\partial r_j}\hat{r}_j \tag{7}$$

and

$$\nabla_{\vec{R}_j}|\nabla_{\vec{r}}\rho|^2 = -2\left\{(\nabla_{\vec{r}}\rho)\frac{1}{r_j}\frac{\partial \rho_j}{\partial r_j} + \left(\frac{x_j}{r_j}\frac{\partial \rho}{\partial x} + \frac{y_j}{r_j}\frac{\partial \rho}{\partial y} + \frac{z_j}{r_j}\frac{\partial \rho}{\partial z}\right)\left(\frac{\partial^2 \rho_j}{\partial r_j^2} - \frac{1}{r_j}\frac{\partial \rho_j}{\partial r_j}\right)\right\}\hat{r}_j\,, \tag{8}$$

where $\hat{r}_j$ is the unit vector parallel to $\vec{r} - \vec{R}_j$. In addition to the atomic electron densities and gradients needed to evaluate the potential, second radial derivatives of the atomic electron densities are needed to evaluate the interatomic forces. The same grid of quadrature points can be used to evaluate the force on atom A_j as to evaluate the force on any other atom. Thus, most of the work can be overlapped in order to evaluate the 3N integrals determining the interatomic forces in a N-atom system. This calculation requires about twice as much time as the evaluation of the potential. In contrast, a central difference evaluation of the forces would require 6N times as much work.

The multi-center integrands for the N-atom system are dominated by the multiple cusps of the system electron density located at the atomic nuclei. A multi-center integral can be efficiently evaluated by decomposing it into a set of single center integrals, $\{g_i(\vec{r}), i=1,...,N\}$[5,6]. For any particular multi-center integrand, f, a

weight function can be assigned to each center (i.e., atom) so that

$$\int f(\vec{r})d\vec{r} = \sum_{i=1}^{N} \int g_i(\vec{r})d\vec{r}, \tag{9}$$

where $g_i(\vec{r}) = w_i(\vec{r})\, f(\vec{r})$ and the sum of all weights at any point in space is unity. Each weight function is approximately unity near its center and vanishes near any other center. In effect, this procedure partitions the three dimensional space of the system into "fuzzy" cells about each center. Sufficient accuracy for our applications can be attained by defining the space partitioning weights as

$$w_i(\vec{r}) = \rho_i(\vec{r}-\vec{R}_i)^2 \;/\; \sum_{j=1}^{N} \rho_j(\vec{r}-\vec{R}_j)^2 \,. \tag{10}$$

This weight requires little additional computation since it depends on the atomic electron densities that must be evaluated anyway. (The use of ρ_i^2 was found empirically to give better accuracy for any number of integration points compared to either ρ_i or ρ_i^3, but there is nothing fundamental about this fact.)

Since it is dominated by only one cusp, each single center integral can be straightforwardly evaluated by a product of Gaussian quadrature schemes. We use Gauss-Laguerre radial along with Gauss-Legendre and Gauss-Chebyshev angular quadratures. Many other single center quadrature schemes have been presented for similar applications[6-9]. Such quadrature rules approximate an integral by the discrete sum,

$$\int g_i(\vec{r})d\vec{r} \sim \sum_{k} Q_k g_i(\vec{q}_k), \tag{11}$$

where $\vec{q}_k$ and Q_k are the quadrature points and weights, respectively. Typically, on the order of 10^3 to 10^4 quadrature points per center are needed in order to attain precision commensurate with the accuracy of the CEM method (i.e., 0.005 eV/atom).

To summarize the computational problem, we note that the electron density for each atom, its gradient and, in the case of force evaluations, its second derivative must be evaluated at every quadrature point. This is accomplished efficiently by interpolation of evenly spaced tabulated values and thus is not a computational bottleneck. Even with this efficiency, the evaluation of the integrands such as $f(\rho,\nabla\rho)$ in Eq. (4) at each quadrature point still requires a large number of floating point operations. We have determined an approximate number based on the weights shown in Table I for specific operations. In order to compute $G(\{A_i\})$, there are 69 + 34 N floating point operations per quadrature point during potential evaluations and 104 + 64 N floating point operations per quadrature point during force evaluations. If 10^4 quadrature points per integration center (i.e., atom) are used to calculate forces in a 10 atom system, then more than 70×10^6 floating point operations must be performed in order to compute the analytic derivative of $G(\{A_i\})$. An appreciation of the magnitude of our computations is gained when one recognizes that on the order of 10^2 force evaluations are needed for the structural optimization of a cluster of metal atoms while on the order of 10^4 evaluations are needed for a molecular dynamic simulation of H uptake by a metal cluster. Thus, as a rule of thumb, $(10^2 - 10^4)\ N^2$ million floating point operations are required for each structural optimization or simulation. At a rate of 100 Mflops, the CPU time

Table I. Floating-point operation counts[a].

OPERATION	WEIGHT
Plus, Minus, Times	1
Comparison	1
Real-Integer Conversion	1
Reciprocal	3
Divide	4
Square Root	4
Sine, Cosine, Tangent, Arctangent	8
Exponential, Logarithm	8

[a]Based on the system used at Lawrence Livermore National Laboratories.

required for such calculations is $(1\text{-}10^2)\ N^2$ sec. Calculations for systems of up to N $\approx$ 100 are feasible.

In short, one of the chief computational challenges posed by the CEM method involves the numerical integration of the density functionals. The integration algorithm implemented requires thousands of quadrature points per atom. The computation associated with each point is substantial and scales linearly with the number of atoms, but is largely independent of the other points.

III. PARALLEL QUADRATURE SCHEME

Code structures that iterate over a sequence of data elements often are readily parallelizable. Fig. 1 illustrates the significant amount of data parallelism within the quadrature scheme. In the figure, loop D is only necessary for the evaluation of the derivative of $G(\{A_i\})$. Loops C and D are nested within loop B which is nested within loop A. In principle, each of the 10^5 to 10^6 points specified by the loops A and B could be distributed to a separate processor since they are all independent of each other. On each processor the value of the integrand could be computed at the given quadrature point and then multiplied by the quadrature weight. The results on the individual processors would be accumulated to yield the final result. Currently, we have not gone to this extreme since the number of processors is 8-1024 for the computers used in our research, which is significantly smaller than the total number of quadrature points. Because of the large variation in the number of processors on these machines, we have implemented the code in a variety of ways dependent on the architecture of specific machines. The goal is of course to exploit the parallelism within this algorithm.

A. Distributed Memory Architectures

This work has been greatly facilitated by the implementation of the quadrature scheme shown in Fig. 1 onto a nCUBE 2 hypercube. A hypercube network of dimension M has 2^M processing elements. Each processing element or node is connected to M neighboring nodes. In a hypercube of dimension of 4, for instance, node 0 can communicate directly with nodes 1, 2, 4 and 8. Development work was largely completed on the hypercube at the Scalable Computing Laboratory

General Code Structure

Loop A) over the integration centers

* **~ 10 to 100 iterations**
* **each iteration independent of others**

Loop B) over the quadrature points

* **> 10,000 iterations**
* **each iteration independent of others**

Loop C) over the atoms

* **~ 10 to 100 iterations**

Loop D) over the atoms (derivative only)

* **~ 10 to 100 iterations**
* **accumulate force on each atom**

Fig. 1: Diagram of the code structure of the numerical quadrature algorithm.

of Ames Laboratory, Ames. Currently, this machine has 128 nodes with 16 Mbytes of memory on node 0, 4 Mbytes on nodes 1 through 64 and 1 Mbyte on nodes 65 through 127. For large scale simulations we have also used the 1024 node hypercube at the Massively Parallel Computing Research Laboratory of Sandia National Laboratories, Albuquerque. Each node on this larger hypercube has more than 4 Mbytes of memory. For the nCUBE 2 the theoretical peak processing rate[20] of each node is 2.3 Mflops for double precision arithmetic. An ensemble of large numbers of these nodes makes the hypercube competitive with shared memory supercomputers provided a significant fraction of the peak speed is attained. A workstation connected to the nCUBE 2 hypercube provides users with a convenient interface. All program modifications, compilations, loading and debugging are performed on the host workstation.

The results presented herein, including the timings in the subsequent section, were obtained using release 2.2 of nCUBE 2 software. Internode communication is accomplished using the *nwrite* and *nread* nCUBE 2 library routines. Appendix A presents an example of their use in our code. The CEM code itself is written in standard FORTRAN 77.

The relatively small amount of memory per node is one of the first obstacles encountered when implementing a large code on a distributed memory machine. Currently, CEM requires more than 2 Mbytes of memory. If the code was implemented as one single node program, nodes with less than this amount of memory would be unusable for our application. In order to overcome this limitation, the CEM code was divided into two node programs. Additionally, a program on the

host workstation opens a subcube of dimension specified by the user and, then, loads the node programs onto it. On this subcube, the primary node program is loaded onto node 0 only. Everything except for the numerical integration is executed by this program. It reads an input file, prepares and sends to the secondary program any data needed for subsequent calculations. The secondary node program only evaluates the integrals and is small enough so that it can be loaded onto nodes with only 1 Mbyte of memory. After the secondary program has received the preliminary data, it waits to receive atomic coordinates from the primary program. Once the secondary program has received this data and evaluated the integrals, it sends the results to the primary program. The primary program on node 0 sends messages to the secondary program on all nodes using the broadcast mode of the *nwrite* routine. It receives messages from the secondary program on node 0. It is not necessary for the secondary program on the other nodes to send messages to the primary program. Although more programming and more message passing are required than would be the case for a single node program[21], this approach efficiently uses the available memory. In our application, the additional communication overhead is negligible.

The number of atoms is usually less than the number of available nodes since the computational intensity of each single center integral limits the system size to less than two hundred atoms with most computations involving systems of less than 50 atoms. Thus, the numerical integration is not processed concurrently by distributing the centers of integration across the nodes of a subcube since this would not allow scaling up to large numbers of processors.

Instead, the quadrature points for each center are distributed across the

nodes since the number of the former generally exceed the latter by a factor greater than ten. The computational work associated with each point varies only slightly depending on its radial distance from the center. Each single center integral is evaluated efficiently by assigning a subset of the total number of quadrature points to each node. The points are distributed so that the subsets differ in number of points by at most one. Each subset includes points of various radial distances from the center. Appendix B details the coding necessary for this distribution. This approach balances the computational work any node performs in comparison to the others. The observed speedup scales almost linearly with the number of processors as long as the number of quadrature points is significantly greater than the number of processors. When the number of processors increases in future machines, single center integrals could be evaluated by small subcubes of a larger cube. In this way, ensembles of subcubes could evaluate several of these single center integrals at once.

In view of Eq. (11), each node is given a subset of quadrature points for which it computes a partial sum of the integrand values multiplied by the quadrature weights. As specified in Section II, the evaluation of the integrand at each point requires a significant amount of computational work. Once all nodes have completed this stage, they must communicate with each other. Every step in this communication process requires an exchange of the partial sums between neighboring nodes followed by the addition of the two numbers to yield a new sum on every node. For a cube of dimension M the value on each node after M steps is a global sum of the original partial sums. Fig. 2 illustrates this process for a cube of dimension 2. The segment of code given in Appendix A performs this

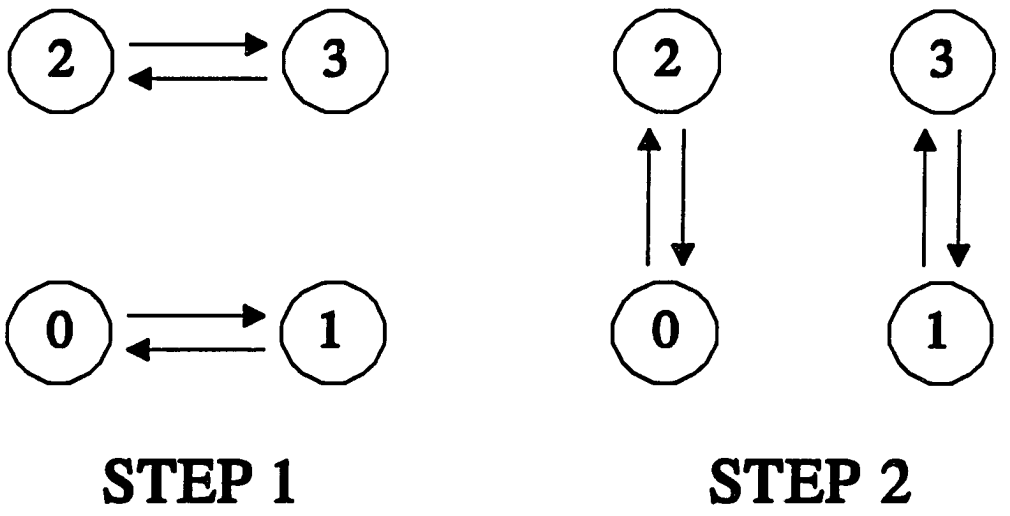

Fig. 2: Internode communication scheme illustrated for a hypercube of dimension 2.

communication. This internode communication scales logarithmically with the number of processors and requires very few floating point operations. Therefore, its execution time is negligible in comparison to that required for the evaluation of the integrand.

Fig. 3 summarizes the implementation of the quadrature scheme onto the hypercube computer. The algorithm is divided into sections of computational work and of internode communication. Each node computes a partial sum independent of all others. Once all the computational work is completed, the nodes must communicate in order to accumulate the partial sums into a single global sum. This communication synchronizes the nodes. The node that does the least amount of computational work reaches the communication section and then waits for the other nodes to complete their work. This idle time can be a significant source of overhead involved in parallel processing. Therefore, it is important to reduce this idle time by evenly distributing the work to the processors. As mentioned previously, the load balance is enhanced by distributing to each node quadrature points that have a range of radial distances to the integration center.

B. Shared Memory Architectures

In Section IV comparisons of the potential and force evaluation times are made between the nCUBE 2 computer and two shared memory multiprocessors. One of these multiprocessors is a 8 processor Silicon Graphics 4D/380S computer. Each of these processors has a theoretical peak processing rate[20] of 13.2 Mflops. The other multiprocessor is an 8 processor Cray 2 supercomputer. The theoretical peak processing rate[20] for each of these processors is 488 Mflops.

Hypercube Code Structure

Begin computation on each of 2^M nodes

Loop A) as in Fig. 1

Loop B) over a subset of quadrature points

*** > 10,000 / 2^M iterations per node**

Loop C) as in Fig. 1

Loop D) as in Fig. 1

Begin internode communication

*** accumulate partial sums across the nodes**

*** overhead $\propto$ M**

Fig. 3: Diagram of the code structure of the numerical quadrature algorithm as implemented on a hypercube computer.

For such a small number of processors on the shared memory machines, parallelization of the algorithm shown in Fig. 1 is implemented by distributing the centers of integrations to separate processors. Compiler preprocessors on these machines automatically insert parallel processing code as instructed by the programmer using compiler directives. A balanced workload on all processors is maintained by dynamically distributing the single center integrals one at a time to available processors.

To take better advantage of the smaller number of very powerful vector processors available on the Cray computer, the angular coordinates of the quadrature points are specified within loops C and D in Fig. 1. This modification ensures that all inner loops vectorize with more than 64 iterations even for systems of a small number of atoms.

On a different note, we mention that this algorithm for a shared memory computer would also allow concurrent processing on a network of workstations. It is unlikely that a workstation network would approach the number of processors on the nCUBE 2.

IV. COMPUTATIONAL PERFORMANCE

The peak theoretical performance for an nCUBE 2 processor is 2.3 Mflops. Using the weights in Table I, the measured rates for our implementation of the quadrature algorithm are 1.1 and 1.2 Mflops for potential and force evaluations, respectively. These rates have been observed for systems ranging from 16 to 128 atoms. Little extra effort beyond compiling the FORTRAN source code is needed to attain this level of performance on each node. Note, these rates are averages over the inner loops of the quadrature scheme shown in Fig. 1. Since a significant number of memory references are required within these loops, the observed rates are reasonable. More floating point intensive loops should demonstrate faster rates. In fact, a rate of 1.65 Mflops is observed for loop D of the analytic derivative.

The estimated ratings per processor for force evaluations on the Silicon Graphics and Cray 2 computers are 4 Mflops and 80 Mflops, respectively. The observed Mflops as a fraction of the theoretical peak rate for the nCUBE 2 hypercube, Silicon Graphics and Cray 2 processors is 0.52, 0.30 and 0.16, respectively. The memory references inside the inner loops degrade the performance of the more powerful processors significantly more than the nCUBE 2 processor.

Massively parallel computing can suffer from large interprocessor communication overhead. Table II lists the ratio of the hypercube communication to computation time in the quadrature scheme in units of *parts per thousand.* Each entry includes a range of values. The node that does the most work has the minimum communication overhead, while the node that does the least work has the maximum. Increasing the number of nodes decreases the computational work per

Table II. Ratio of the hypercube communication to computation time in the quadrature algorithm expressed in units of *parts per thousand.*[a]

# of nodes	# of atoms 16	32	64	128
16	0.1 - 1.0	0.0 - 3.0	0.0 - 4.5	0.0 - 2.9
32	0.3 - 2.1	0.1 - 4.1	0.0 - 5.0	0.0 - 3.3
64	0.7 - 3.6	0.3 - 6.5	0.1 - 5.6	0.1 - 3.5
128	1.8 - 5.9	0.6 - 9.2	0.3 - 6.9	0.1 - 4.5

[a]These values were determined during the evaluation of forces for Ni_N clusters.

node and increases the amount of message passing. As a result, the communication overhead should increase. Conversely, increasing the number of atoms increases the computational work more than the internode communication and the overhead should diminish. The minimum values listed in Table II clearly reflect these trends. However, the maximum values do not decrease with increasing numbers of integration centers (i.e., atoms). The evaluation of many single center integrals accentuates any work load imbalance due to the distribution of quadrature points. Further optimization might reduce the spread of values shown in Table II by a more even distribution of work. Nevertheless, the overhead of this communication between nodes is never more than several percent of the computational work even if extrapolated to very large hypercubes.

The advantage of massively parallel computing depends critically on whether the efficiency of an algorithm scales linearly with increasing numbers of processors. Table III lists the time required to evaluate the interatomic forces in Ni_N clusters of various size. More than 99% of this time is needed to evaluate the analytic

Table III. Force evaluation time (sec.) for Ni_N clusters on the nCUBE 2 computer.[a]

# of	# of atoms			
nodes	16	32	64	128
16	11.89	39.72	137.98	482.31
32	5.95 (1.000)	19.90 (0.999)	69.06 (1.000)	241.39 (1.000)
64	2.99 (0.999)	9.98 (0.999)	34.60 (0.999)	120.91 (0.999)
128	1.50 (0.998)	5.02 (0.998)	17.37 (0.999)	60.67 (0.999)
256	0.79 (0.989)	2.63 (0.990)	8.96 (0.993)	30.81 (0.996)
512	0.40 (0.988)	1.34 (0.988)	4.55 (0.991)	15.62 (0.994)

[a]The numbers in parentheses are values of the scaling parameter, p, defined Eq. (12).

derivative of $G(\{A_i\})$. The time required to evaluate other terms in the potential is practically negligible. As the number of nodes is increased by factors of two, the speedup in the evaluation time is always greater than 1.9. The scalability of an algorithm can be analyzed in terms of the formula,

$$t_M = 2^4 t_4 (2^{-M})^p \ , \qquad (12)$$

where t_M is the evaluation time using a cube of dimension M. In this definition the evaluation time on a four dimensional hypercube is used as a reference to examine how the efficiency of the algorithm scales with increasing hypercube size. For perfect linear scaling the exponent, p, would be one. Values for this parameter are listed in parentheses in Table III. As evident in the table, the value of this exponent is slightly less than one for every entry. The scalability would be improved by using one node program instead of two and by parallel processing the other terms

of the CEM potential also. In spite of these additional sources of overhead, the algorithm currently implemented scales almost linearly with increasing number of nodes.

The performance of the hypercube is competitive with more conventional shared memory supercomputers. Fig. 4 shows the time needed to evaluate the interatomic forces in a Ni_{64} cluster. For the Silicon Graphics and Cray 2 multiprocessors, timings for 2, 4 and 8 processors are shown. For the nCUBE 2 computer, timings for 32, 128 and 512 processors are shown. As the number of processors is increased, the nCUBE 2 performance eventually equals the Cray 2 performance. For our application 64 nCUBE 2 nodes are approximately equivalent to a CRAY 2 processor.

The data for the Cray 2 computer was obtained in a multi-user environment, while the data for the Silicon Graphics and nCUBE 2 computers were obtained in a dedicated, single user environment. Note that the two shared memory computers scale slightly less than linearly with the number of processors: the exponents "p" in Eq. (12), scaled to the two processor (M=1) values, are (0.96, 0.94) and (0.96, 0.84) for (4, 8) processors on the Silicon Graphics and Cray machines, respectively. The value of 0.84 for the 8 processor Cray likely reflects memory contention in the multi-user environment. There is nothing else in the comparisons that would favor the nCUBE 2 over either of the shared memory machines.

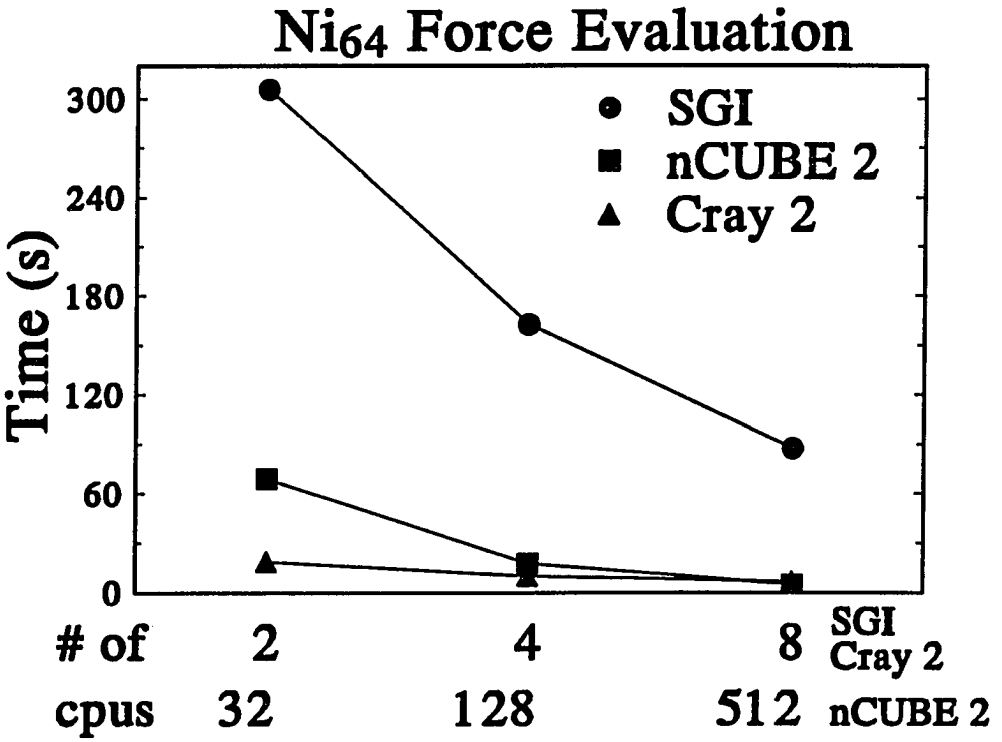

Fig. 4: Time required to evaluate the interatomic forces in a Ni_{64} cluster. Note that the number of Silicon Graphics and Cray processors increase by a factor of two between data points while the nCUBE 2 increases by a factor of four.

V. CONCLUDING REMARKS

Numerical integration of complex integrands can be accomplished efficiently on a hypercube. As presented here, implementation onto the nCUBE 2 hypercube is straightforward. The internode communication overhead is negligibly small even for hypercubes of dimension 9. The large, uniform amount of computational work associated with each quadrature point facilitates a well balanced work load on all nodes. Furthermore, the number of quadrature points is sufficiently large that the problem could be scaled to many more than a thousand processors. As a result, the performance of the hypercube can surpass that of a shared memory supercomputer.

The techniques presented here could be used successfully for other problems. All that is necessary is a data loop with a large number of independent iterations. Two complications do need mentioning. First, if the computational work associated with each iteration is not uniform, close attention needs to be paid to the distribution of iterations to the nodes. Second, if integrand evaluation is fast, many evaluations must be made at each processor to limit interprocessor communication overhead. Neither problem should occur for the integrands in density functional theory.

We end by noting the scientific nature of the present problem. Small metal clusters are models for heterogeneous catalysts, provide critical tests for the comparison of detailed theoretical predictions with experimental data, and require exhaustive calculations to help interpret experimental data. Production computing at Gflops speeds is necessary to investigate these problems even using new theoretical methods. Massively parallel computers have become an indispensable

tool for our work in this area. This success will hopefully encourage additional work on massively parallel processing.

ACKNOWLEDGEMENTS

This work was supported by the Division of Chemical Sciences, Office of Basic Energy Sciences of the U.S. Department of Energy through the Ames Laboratory, which is operated for the U.S. DOE by Iowa State University under Contract No. W-7405-Eng-82. The authors are grateful for considerable computing time on a nCUBE 2 hypercube at two different sites: 1) the Scalable Computing Laboratory, Ames Laboratory; 2) the Massively Parallel Computational Research Laboratory, Sandia National Laboratory. M.S.S. would especially thank Dr. John Gustafson and Michael Carter of the Scalable Computing Laboratory for their aid in implementing code onto the nCUBE 2 hypercube. M.S.S. also acknowledges the support of the Alworth Memorial Foundation.

APPENDIX A

In our implementation on the hypercube, internode communication is accomplished using the *nwrite* and *nread* nCUBE 2 library routines. Their arguments include the starting address and length of the message, the destination or source node process and the message type. The message length is specified in terms of the number of bytes. The destination or source node process is identified by a 4 byte integer. The first 2 bytes identify the node, while the last 2 bytes identify the process. For example, process 1 on node 8 is identified by the integer 65544 expressed in decimal form or 0x00010008 expressed in hexadecimal form. The processor and process identification is necessary when more than one user process is executed concurrently on a node. Such routines are typically part of the software released with distributed memory computers.

As an example of their use, we include the following segment of code from the subroutine that evaluates the analytic derivative of $G(\{A_i\})$. In this case, each node has accumulated values in the arrays *fx*, *fy* and *fz* that when summed across the nodes will be used to determine the force on each atom.

```
c
c Accumulate the partial sum on each node in order to obtain the final result.
c
      call dcopy (natoms, fx, 1, buffer_a(1), 3)
      call dcopy (natoms, fy, 1, buffer_a(2), 3)
      call dcopy (natoms, fz, 1, buffer_a(3), 3)
      nelements = 3 * natoms
      length = 8 * nelements
      msg_type = 2000
      flag = 0
      j = 1
```

```
7000  if (j .eq. nprocessors) go to 7010
      node_proc = iproc .NEQV. j
      nerr = Nwrite (buffer_a, length, node_proc, msg_type, flag)
      nerr = Nread  (buffer_b, length, node_proc, msg_type, flag)
      call Vadd (buffer_a, 1, buffer_b, 1, buffer_a, 1, nelements)
      j = j + j
      go to 7000
7010  continue
```

First, the component force arrays, *fx*, *fy* and *fz*, are all copied into a single array, *buffer_a*, using the BLAS routine *dcopy*. Second, several of the arguments for the communications routines are defined. Third, each node sends its *buffer_a* to one of its neighboring nodes and receives in its *buffer_b* the *buffer_a* from the same neighbor. The elements of the two buffer arrays are then added using the nCUBE Math Library routine *Vadd* to obtain new partial sums stored in *buffer_a* on each node. This final step is repeated until each node has communicated with each of its neighbors. This requires M iterations for a cube of dimension M. Fig. 2 illustrates this process for a hypercube of dimension 2. Each node process is identified by a unique value for the variable *iproc*. The neighboring nodes for a given node are determined by an 'EXCLUSIVE OR' operation between the node process variable, *iproc*, and the loop index, *j*, using a FORTRAN logical operator (i.e., *.NEQV.*). Similar code can also be used to determine the global maximum and minimum of a set of numbers distributed across the nodes.

APPENDIX B

The initial distribution of quadrature points on the hypercube determines the amount of work each node will perform during calculations. It is important to uniformly distribute the computational work in order to minimize the idle time of any node waiting upon other nodes to complete their work. For our application, the work load balance can be optimized by distributing to each node quadrature points that have a range of radial distances to the center of integration. The following segment of code from the primary node program is used to distribute the quadrature points.

```
c
c Pass to each node a subset of the total number of quadrature points & weights.
c
          do 100 iti = 1, ntypes
           nq_tot = nlaguu(iti) * nlege * nphi2
           node = 0
           k1 = ((nq_tot *  node     ) / nprocessors) + 1
           k2 = ((nq_tot * (node + 1)) / nprocessors) + 1
           nquad = k2 - k1
           m = 200 + 10 * iti
           nq = 0
           do 60 k = 1, nlege
            do 50 l = 1, nphi2
             do 40 j = 1, nlaguu(iti)
              nq = nq + 1
              qx(nq) = rv(j, iti) * sinth(k) * cosphi(l)
              qy(nq) = rv(j, iti) * sinth(k) * sinphi(l)
              qz(nq) = rv(j, iti) * costh(k)
              qwght(nq) = rwght(j,iti) * awght(k)
              if (nq .eq. nquad) then
               n = 0
               n = n + nwrite(qx, nbytes, s_prog(node), m, flag)
               n = n + nwrite(qy, nbytes, s_prog(node), m, flag)
```

```
            n = n + nwrite(qz, nbytes, s_prog(node), m, flag)
            if (n .ne. 0) nperror('setup_P')
            k1 = ((nq_tot *  node    ) / nprocessors) + 1
            k2 = ((nq_tot * (node + 1)) / nprocessors) + 1
            nquad = k2 - k1
            m = 200 + 10 * iti
            nq = 0
          end if
 40      continue
 50    continue
 60  continue
100 continue
```

Within CEM a Gauss-Laguerre quadrature is used for the radial integration along with Gauss-Legendre and Gauss-Chebyshev quadratures for the angular integration. For each type of atom, *iti*, the primary program on node 0 distributes a set of quadrature points to the secondary program on every node. The processor/process id for the secondary program is given by the array *s_prog*. The total number of quadrature points per center, *nq_tot*, is a product of the number of Gauss-Laguerre, Gauss-Legendre and Gauss-Chebyshev quadrature points. These numbers are represented by the variables *nlaguu(iti)*, *nlege* and *nphi2*, respectively. The number of points for a given node is determined by the difference between the expressions for the variables *k1* and *k2*. Loops 40, 50 and 60 group the quadrature points into subsets that are passed to individual nodes. Since the radial coordinates are specified by the inner loop, each subset has quadrature points of varying radial distance to the integration center.

REFERENCES

1. J. L. Gustafson, G. R. Montry and R. E. Benner, SIAM J. Sci. Statist. Comput. **9**, 609 (1988).

2. M. E. Colvin, R. A. Whiteside and H. F. Schaefer III, "Quantum Chemical Methods for Massively Parallel Computers" in *Methods in Computational Chemistry*, Vol. 3, ed. S. Wilson (Plenum Press, New York, 1989).

3. P. J. Denning and W. F. Tichy, Science **250**, 1217 (1990).

4. M. J. Quinn, *Designing Efficient Algorithms for Parallel Computers* (McGraw-Hill, New York, 1987).

5. R. G. Parr and W. Yang, *Density-Functional Theory of Atoms and Molecules*, (Oxford University Press, New York, 1989).

6. A. D. Becke, J. Chem. Phys. **88**, 2547 (1988).

7. B. Delley, J. Chem. Phys. **92**, 508 (1990).

8. R. S. Jones, J. W. Mintmire and B. I. Dunlap, Int. J. Quant. Chem.: Quant. Chem. Symp. **22**, 77 (1988).

9. P. M. Boerrigter, G. Te Velde and E. J. Baerends, Int. J. Quant. Chem. **33**, 87 (1988).

10. A. Kaldor and D. M. Cox, J. Chem. Soc. Faraday Trans. **86**, 2459 (1990).

11. E. K. Parks, B. J. Winter, T. D. Klots and S. J. Riley, J. Chem. Phys. **94**, 1882 (1991).

12. J. D. Kress and A. E. DePristo, J. Chem. Phys. **87**, 4700 (1987).

13. J. D. Kress and A. E. DePristo, J. Chem. Phys. **88**, 2596 (1988).

14. J. D. Kress, M. S. Stave and A. E. DePristo, J. Phys. Chem. **93**, 1556 (1989).

15. T. J. Raeker and A. E. DePristo, Phys. Rev. B **39**, 9967 (1989).

16. M. S. Stave and A. E. DePristo, J. Chem. Phys. (submitted July 1990).

17. T. J. Raeker and A. E. DePristo, Int. Rev. Phys. Chem. **10**, 1 (1991).

18. A. E. DePristo and J. D. Kress, Phys. Rev. A **35**, 438 (1987).

19. A. E. DePristo and J. D. Kress, J. Chem. Phys. **86**, 1425 (1987).

20. The theoretical peak performance rates were determined by the number of clock cycles needed to execute both an addition and an multiplication using 64 bit arithmetic. On the nCUBE 2, for instance, an addition requires 10 cycles and a multiplication requires 7 cycles. Since the clock rate is 20 MHz the theoretical peak flops rate determined by these two floating point operations is 2.3 Mflops. The peak rates cited for the Silicon Graphics and Cray 2 processors were determined similarly.

21. A single node program was implemented on the 1024 hypercube at Sandia National Labs on which there is more than 4 Mbytes of memory on each node. However, its performance was unreliable due to peculiarities in certain nCUBE 2 routines and, therefore, we have not pursued this approach further. nCUBE has since improved the problem with its routine.

PAPER III.

THE STRUCTURE OF NI_N AND PD_N CLUSTERS: $4 \leq N \leq 23$

The structure of Ni_N and Pd_N clusters: $4 \leq N \leq 23$

Mark S. Stave
and
Andrew E. DePristo

Ames Laboratory - USDOE
and
Department of Chemistry
Iowa State University
Ames, Iowa 50011

ABSTRACT

Stable geometrical structures of Ni_N and Pd_N clusters (N = 4-23) are identified using a corrected effective medium (CEM) theory. Structural optimization is accomplished by simulated annealing using analytic derivatives to determine the interatomic forces. Unique structural features of these metal clusters are noted especially in relation to the bulk and surface phases of these metals and to structures commonly associated with rare gas clusters. In regard to the last comparison, the predictions of CEM and pairwise additive potentials are analyzed. We show that the structure of these transition metal clusters generally maximizes the minimum coordination of any atom, whereas the structure for rare gas clusters maximizes the number of interatomic distances close to the optimal distance for interaction between rare gas atoms. The latter can be interpreted as the packing of hard balls. Structural transformations between isomers of similar energy are also examined for selected sizes.

I. INTRODUCTION

The geometrical structure of transition metal clusters is undoubtedly an important factor determining their physical and chemical properties. Due to their increasing scientific and technological importance, considerable effort is currently devoted towards advancing our knowledge of their structure.

Recently, experiments have utilized chemical reactions as probes of various structural features of metal clusters.[1-9] These studies often yield clues about the structure of specific clusters such as the number and types of binding sites. While this approach provides valuable information, it does not conclusively determine the structure of clusters.

Theoretical calculations can complement such experimental investigations. However, interaction potentials must be used that are accurate enough for the properties of interest. For clusters of rare gas atoms the interactions are dominated by dispersion forces and, therefore, pairwise additive potentials provide reasonably accurate potential energy surfaces. As a consequence, rare gas clusters have been extensively modeled in the past two decades using just such pairwise additive potentials.[10-12] This work has provided valuable insight regarding the structure and growth of these clusters.

For transition metal clusters the delocalized nature of the electrons and its effect on the atomic interactions must be accurately described. Pairwise additive potentials are inaccurate for systems in which complex many body interactions are significant. At the same time, rigorous quantum chemical calculations[13-15] of these systems are limited by current computing power.

Philosophically and computationally, it is important to study the structure of metal clusters using a hierarchy of theories. Accurate models of metallic bonding, based on well defined approximations to quantum chemical theory, are necessary to identify directions for more rigorous, and presumably more accurate, approaches. The models used for initial probing must have a level of computational intensity that allows a thorough investigation of the many dimensional potential energy surfaces. Currently, several related methods have demonstrated this capability: the embedded atom method (EAM),[16-19] the effective medium method (EM)[20-22] and the corrected effective medium method (CEM).[23-26] All of these approaches are based upon concepts developed within density-functional theory.[27] An approximation of the CEM method has also been developed with much lower computational intensity,[28,29] and is referred to by the acronym MD/MC-CEM. In addition, the EM method may optionally calculate one-electron energy levels for more accuracy with more computational work.[21]

The accuracy of these methods varies in relation to the size of the system to be studied. The zero'th order model of these approaches does not account for size differences of systems. For small systems of a few tens of atoms the electron density is significantly more inhomogeneous than for a large extended system. Although it has been demonstrated that both MD/MC-CEM and EAM model large systems relatively well, they do not explicitly account for such differences in the electron density between small and large systems of atoms. Hence, the accuracy of these approaches for small systems is questionable. On the other hand, both CEM and EM with the one-electron energy correction are more rigorous in their attempts to

account for the effects of the electron density even for small systems.

The results for clusters of Ni and Pd atoms presented here are based on the CEM method. Derivation of the CEM method,[23-26] its approximate formulation in MD/MC-CEM[28,29] and a review of effective medium type approaches[30] are available elsewhere. In this work, we present and analyze the stable structures of clusters of 4 to 23 Ni or Pd atoms. In the process, we demonstrate the importance of effects due to the more inhomogeneous electron density of these small systems.

An overview of the CEM theory and the optimization methods employed are presented in Sec. II. Results and discussion of the optimized cluster structures are provided in Sec. III A, while isomeric transformations between selected stable structures are examined in Sec. III B. Finally, our concluding remarks are given in Sec. IV.

II. METHODOLOGY

Within effective medium type theories the interaction energy of a set of atoms $\{A_i, i=1,...,N\}$ is initially approximated as a sum of the N interaction energies between each atom and a medium that models the effect of the remaining N-1 atoms. This approximation reduces the problem from determining the interaction energy of an N-body system to determining the interaction energy of N one-body systems. The effective medium interacting with atom A_i is defined as an electron gas of uniform density along with a compensating uniform positive charge density. Usually, this effective medium is referred to as jellium and its interaction energy with an atom as an embedding energy. The intent of this approximation is to capture a significant portion of the interaction between an atom and a delocalized distribution of electrons.

Several corrections are added to this initial approximation to obtain the complete expression of the CEM interaction energy:

$$\Delta E(\{A_i\}) = \sum_{i=1}^{N} \Delta E_J(A_i; n_i) + \Delta V_C + \Delta G(\{A_i\}) \; . \qquad (1)$$

As explained above, the first term is the sum of embedding energies for each atom A_i embedded into a jellium of density n_i, $\Delta E_J(A_i; n_i)$. The second corrects for the difference in Coulomb interaction energies between the N-atom system and the atom-in-jellium systems, ΔV_C. The third corrects for the difference in kinetic, exchange and correlation interaction energies between the N-atom system and the atom-in-jellium systems, ΔG. These energy corrections arise due to differences in the electron and positive charge distributions between the N-atom and the N atom-in-jellium systems.

Within CEM the correction energies are calculated via energy functionals of the total electron density of a system. These electron densities are approximated as a superposition of the spherical electron densities of isolated atoms and the jellium electron density. Under this assumption the Coulomb energy correction is simply the sum of Coulomb integrals between all pairs of atoms. In addition, an approximation to the kinetic-exchange-correlation energy correction is minimized by expressing the jellium density as

$$n_i = \frac{1}{2Z_i}\sum_{j\neq i}^{N} \int n(A_i;\ \vec{r} - \vec{R}_i)\ n(A_j;\ \vec{r} - \vec{R}_j)\ d\vec{r}\ , \qquad (2)$$

where Z_i and $\vec{R}_i$ are the nuclear charge and position and $n(A_i;\ \vec{r} - \vec{R}_i)$ is the spherical electron density of atom A_i.

By far the most computationally intensive part of the CEM interaction energy is the evaluation of the kinetic, exchange and correlation energies of the N-atom system. This entails a multi-center, three-dimensional integral over all space that varies explicitly with any change of the atomic coordinates. Recently, the analytic derivative of this integral with respect to the atomic coordinates has been formulated.[31] Moreover, implementation of a quadrature scheme on a hypercube has greatly reduced the time needed to evaluate the integral.[31] These developments have enabled unconstrained optimization of the cluster geometries using the complete CEM interaction potential.

In addition, cluster geometries have been optimized within the MD/MC-CEM approximation. In this case, ΔG is not explicitly calculated and the interaction energy is expressed as

$$\Delta E(\{A_i\}) = \sum_{i=1}^{N} \Delta F_J(A_i; n_i) + \Delta V_C \,, \tag{3}$$

where $\Delta F_J(A_i; n_i)$ is the MD/MC-CEM "effective" embedding energy for atom A_i.

For an atom embedded in jellium of some density the embedding energy is evaluated via interpolation of a set of tabulated points. In this particular study, the embedding points are determined by forcing the CEM and the MD/MC-CEM interaction energy to agree with the bulk cohesive energy predicted by linear muffin tin orbital calculations.[32] Fig. 1 illustrates the embedding functions for Ni and Pd generated by this procedure. In their bulk equilibrium phases, both Ni and Pd assume a fcc crystal structure. In such cases, a one-to-one correspondence exists between the bulk lattice constant and the jellium density for a bulk atom. Consequently, the embedding functions are determined straightforwardly from a set of cohesive energies over a wide range of the lattice constant.

The reader should note that the use of this embedding function is equivalent to using the bulk metal atom as the reference system (for each atom) at an appropriate lattice constant (i.e., to get the same value of n_i). The corrections, ΔV_c and ΔG, are then interpretable as *differences from this reference system*, under the additive density approximation. The terminology of atom-jellium embedding is retained here.

The contribution of ΔG to the interaction energy of a symmetric bulk system is incorporated within the MD/MC-CEM embedding functions. Consequently, its embedding functions are more repulsive than the CEM functions for nearly all

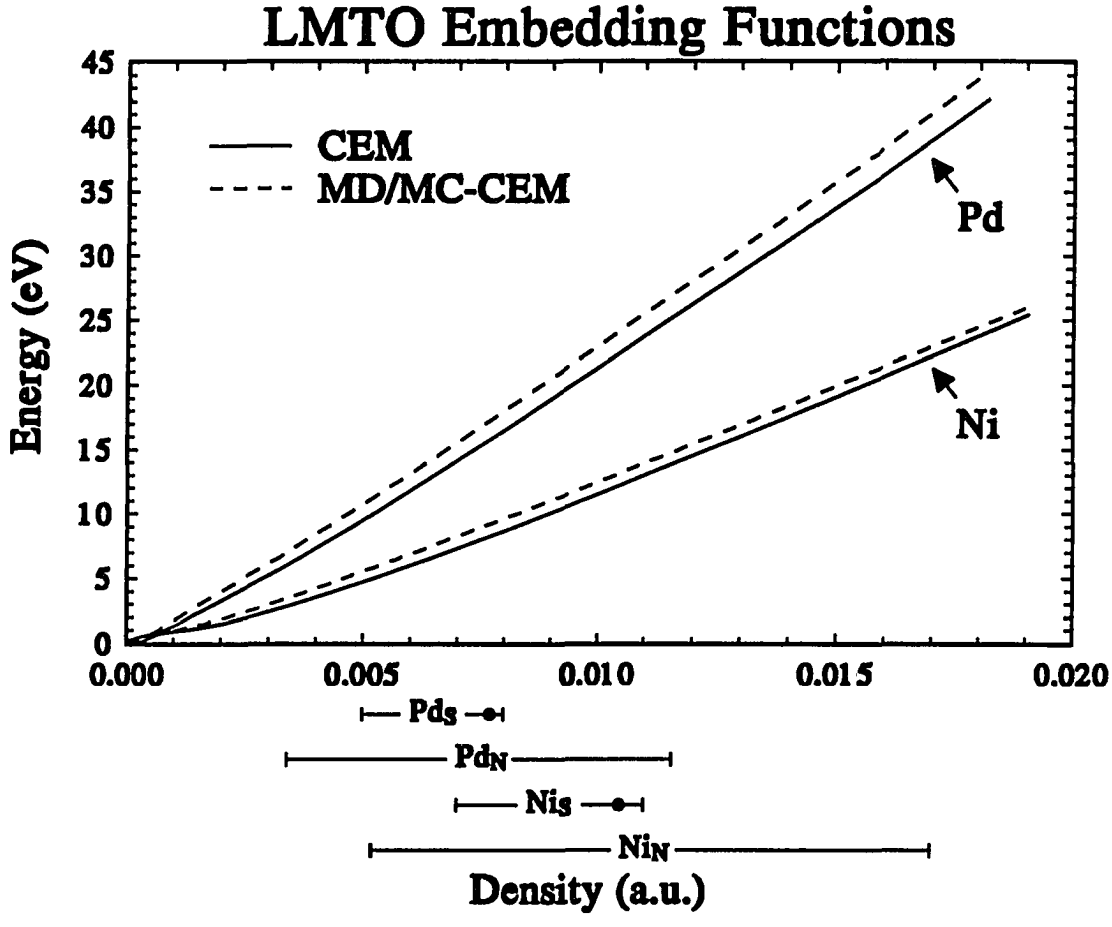

Fig. 1: Ni and Pd embedding functions shown for both CEM and MD/MC-CEM potentials. Also shown are ranges of the jellium density for atoms in Ni_N and Pd_N clusters and for atoms either near or on Ni_S and Pd_S 111, 100 and 110 surfaces. The filled circles on the Ni_S and Pd_S ranges are the respective jellium densities for bulk Ni and Pd.

jellium densities. *In effect, MD/MC-CEM approximates the kinetic-exchange-correlation energy correction associated with an atom in an arbitrary environment by that for an atom in a bulk environment of the same jellium density.* The jellium density of an atom is a weighted average of the electron density about it due to other atoms in the system. It cannot account for all of the effects due to an inhomogeneous electron distribution. The validity of this approximation for small clusters will be examined later.

The structure of the clusters was optimized by simulated melting and annealing using a Langevin molecular dynamics approach.[33-37] For a given number and type of atoms in a cluster the repeated process of melting then annealing leads to a reasonable probability of determining the global minimum. Several structures were discovered during similar simulations of H on Ni clusters. In this case, the H atoms were removed and the structure of the remaining metal atoms was optimized directly using a quasi-Newton algorithm.[38] In all cases, the structures were optimized to the point where the maximum force on any atom was on the order of 1 x 10^{-5} eV/Bohr and 1 x 10^{-2} eV/Bohr within the MD/MC-CEM and the CEM potentials, respectively. The intrinsic accuracy of these potentials is certainly no greater than several meV for binding energies and about 0.1 Bohr for interatomic distances. Therefore, these specified limits are sufficient for the forces to be considered negligible. In addition, the precision of the CEM results is dependent on the numerical integration of ΔG. Sufficient number of quadrature points were used in order to confidently assume a precision of 1 meV per atom.

Recently, Elber *et al.*[39-41] have described a method for polyatomic systems

that determines the minimum energy path through configuration space between two minima. We have modified this approach in order to examine the transformation between isomers of selected clusters. Starting with an initial guess the path is iteratively refined by minimizing the forces perpendicular to the path. An initial guess can be as simple as a set of points in configuration space that lie on a straight line between the two minima. If minimization of these forces is the only criterion, then the points on the path tend to slide downhill to the minima away from the transition state. In order to counteract this tendency, we periodically add points after a given number of minimization steps so that the transition state is bracketed more closely. This modification is motivated by the definition of a transition state as a first order stationary point of the potential energy surface. Our objective is to maximize the energy along the path. The combination of minimizing the force perpendicular to the path and maximizing the energy along the path precisely defines the position of the transition point and the magnitude of the energy barrier to the transformation.

III. RESULTS AND DISCUSSIONS

In the remainder of this paper, we will analyze the structure of stable configurations of Pd and Ni clusters with 4 to 23 atoms. Physical characteristics will be emphasized that distinguish these transition metal clusters from the bulk and surface phases of these metals and from clusters of rare gas atoms whose binding energy is primarily due to dispersion forces. Isomeric transformations between some of the stable structures will also be examined.

A. Stable Structures

The ball and stick diagrams of Fig. 2 illustrate stable structures of transition metal clusters determined in this work. Throughout our discussion the clusters will be identified by their N.M index. For a given number of atoms, N, the structures are listed in order of decreasing stability of the Ni_N clusters, M=1,2,..., as calculated within the CEM potential. The CEM and MD/MC-CEM binding energies for both Ni_N and Pd_N clusters with these geometries are listed in Tables I and II, respectively.

The mean and range of near neighbor distances, the surface area and the volume of selected Ni_N and Pd_N clusters are listed in Tables III and IV. In our analysis of these clusters, we have considered all interatomic distances less than 40% of the CEM interaction range as near neighbor distances (NND). These limits are 18% and 14% larger than the equilibrium bulk NND of Ni and Pd, respectively. Generally, this cutoff distance lies within a large gap between the NND and all other interatomic distances. Therefore, the results of our discussion should not be sensitive to the precise value of this cutoff. The total surface area of a cluster was

Table I. Binding Energy (eV) for Ni_N clusters.

N.M	CEM	MD/MC -CEM	N.M	CEM	MD/MC -CEM	N.M	CEM	MD/MC -CEM
4.1	-7.488	-7.017	11.1	-30.081	-27.890	17.1	-51.615	-47.942
5.1	-10.510	-9.739	11.2	-29.902	-27.588	17.2	-51.462	-47.871
6.1	-13.982	-12.846	11.3	-29.843	-27.593	17.3	-51.381	-47.884
7.1	-17.079	-15.719	11.4	-29.690	-27.353	17.4	-50.817[a]	-47.705
7.2	-16.848	-15.490	12.1	-33.621	-31.374	18.1	-54.872	-51.114
7.3	-16.440	-15.135	13.1	-37.826	-35.432	18.2	-54.825	-50.941
8.1	-20.272	-18.615	13.2	-36.706	-34.165	18.3	-54.778	-51.094
8.2	-19.961	-18.389	13.3	-36.674	-34.125	18.4	-54.325	-51.119
9.1	-23.460	-21.514	14.1	-40.844	-38.104	19.1	-58.385	-55.070
9.2	-23.431	-21.608	14.2	-40.722	-38.130	19.2	-58.216	-54.185
9.3	-23.137	-21.254	15.1	-44.666	-41.592	19.3	-58.142	-54.211
9.4	-23.131	-21.278	15.2	-44.215	-41.371	19.4	-58.065	-54.162[b]
9.5	-23.112	-21.247	16.1	-48.117	-44.728	20.1	-61.847	-58.127
10.1	-26.790	-24.768	16.2	-48.032	-44.632[a]	20.2	-61.843	-58.122
10.2	-26.628	-24.374	16.3	-47.982[a]	-44.678	20.3	-61.777	-58.257
10.3	-26.545	-24.421	16.4	-47.839	-44.517	21.1	-65.597	-61.593
10.4	-26.506	-24.432	16.5	-47.547[a]	-44.572	22.1	-69.374	-65.090
10.5	-26.500	-24.401	16.6	-47.771	-44.524	23.1	-72.383	-68.620

[a]The geometry is not stable within the particular potential since direct minimization of this configuration leads to a different one. The tabulated energy was obtained by uniformly scaling the atomic coordinates until a minimum energy was determined.
[b]This geometry is distorted from C_{2v} to C_2 symmetry in the MD/MC-CEM potential.

Table II. Binding Energy (eV) for Pd_N clusters.

N.M	CEM	MD/MC -CEM	N.M	CEM	MD/MC -CEM	N.M	CEM	MD/MC -CEM
4.1	-5.846	-5.384	11.1	-24.940	-23.322	17.1	-43.200	-40.826
5.1	-8.385	-7.717	11.2	-24.687	-23.071	17.2	-43.102	-40.737
6.1	-11.331	-10.446	11.3	-24.639	-23.047	17.3	-43.068	-40.734
7.1	-13.935	-12.900	11.4	-24.460	-22.830	17.4	-42.822	-40.494
7.2	-13.694	-12.681	12.1	-28.143	-26.380	18.1	-45.960	-43.496
7.3	-13.301	-12.306	13.1	-31.896	-30.052	18.2	-45.878	-43.368
8.1	-16.591	-15.400	13.2	-30.689	-28.800	18.3	-45.901	-43.453
8.2	-16.306	-15.145	13.3	-30.662	-28.761	18.4	-45.833	-43.410
9.1	-19.246	-17.894	14.1	-34.258	-32.284	19.1	-49.533	-46.998
9.2	-19.267	-17.937	14.2	-34.240	-32.299	19.2	-48.726	-46.122
9.3	-18.949	-17.598	15.1	-37.444	-35.339	19.3	-48.735	-46.130
9.4	-18.948	-17.626	15.2	-37.185	-35.094	19.4	-48.661	-46.068[b]
9.5	-18.931	-17.611	16.1	-40.288	-38.047	20.1	-52.308	-49.636
10.1	-22.118	-20.649	16.2	-40.220	-37.963[a]	20.2	-52.302	-49.625
10.2	-21.889	-20.355	16.3	-40.213	-37.987	20.3	-52.331	-49.701
10.3	-21.832	-20.341	16.4	-40.082	-37.831	21.1	-55.393	-52.610
10.4	-21.805	-20.333	16.5	-40.048	-37.838	22.1	-58.508	-55.617
10.5	-21.813	-20.327	16.6	-40.028	-37.811	23.1	-61.599	-58.686

[a]The geometry is not stable within the particular potential since direct minimization of this configuration leads to a different one. The tabulated energy was obtained by uniformly scaling the atomic coordinates until a minimum energy was determined.
[b]This geometry is distorted from C_{2v} to C_2 symmetry in the MD/MC-CEM potential.

Table III. Mean and range of near neighbor distances, surface area and volume for Ni_N clusters in atomic units.

	CEM				MD/MC-CEM			
N.M	Mean[a]	Range[a]	S.A.[b]	Vol.[c]	Mean[a]	Range[a]	S.A.[b]	Vol.[c]
7.1	4.26±.14	4.16-4.77	77.4	47.3	4.52±.11	4.46-4.90	87.6	55.9
8.1	4.36±.39	4.17-5.50	93.1	65.5	4.49±.01	4.48-4.51	104.6	77.5
8.2	4.29±.16	4.14-4.80	94.1	58.0	4.53±.11	4.41-4.90	105.5	67.6
9.1	4.24±.17	4.23-4.27	109.2	87.4	4.48±.02	4.45-4.49	121.8	102.3
9.2	4.32±.17	4.20-4.84	110.5	79.1	4.55±.11	4.49-4.90	123.5	91.0
10.1	4.35±.19	4.18-4.86	127.5	100.7	4.56±.12	4.45-4.86	141.9	114.2
11.1	4.38±.18	4.14-4.78	145.0	121.2	4.58±.11	4.44-4.79	160.9	136.7
12.1	4.40±.13	4.18-4.65	166.8	148.2	4.60±.11	4.39-4.78	183.8	168.4
13.1	4.42±.10	4.26-4.48	174.1	196.7	4.62±.10	4.46-4.69	190.4	224.9
14.1	4.47±.24	4.05-5.16	190.3	221.6	4.64±.20	4.27-4.97	207.4	249.6
14.2	4.43±.15	4.15-4.81	190.7	210.7	4.62±.13	4.41-4.88	207.9	238.0
15.1	4.46±.21	4.11-4.71	203.7	250.0	4.65±.22	4.27-4.89	220.6	281.7
15.2	4.45±.22	4.20-5.45	206.3	236.5	4.62±.14	4.44-5.22	224.9	263.3
16.1	4.48±.24	4.09-4.81	217.8	276.8	4.65±.25	4.25-5.01	235.3	310.4
16.5[d]	4.45±.17	4.28-5.10	223.5	257.4	4.63±.17	4.45-5.30	241.5	289.2
17.1	4.48±.26	4.12-4.90	231.8	304.1	4.66±.27	4.29-5.10	250.1	339.2
17.4[d]	4.46±.17	4.26-5.10	240.5	280.0	4.63±.18	4.42-5.29	259.3	313.4
18.1	4.46±.22	4.16-4.94	247.8	323.2	4.62±.22	4.33-5.10	267.1	356.8
18.4	4.49±.21	4.16-4.86	258.9	314.4	4.64±.15	4.34-4.87	281.9	345.1
19.1	4.48±.14	4.11-4.71	269.6	360.1	4.65±.13	4.22-4.83	290.7	401.1

[a]See text for definition of the near neighbor distances of a cluster.

[b]See text for definition of the surface area of a cluster.

[c]See text for definition of the volume of a cluster.

[d]This geometry is not stable within the CEM potential. The listed data was determined as explained in footnote a of Table I.

Table IV. Mean and range of near neighbor distances, surface area and volume for Pd_N clusters in atomic units.

	CEM				MD/MC-CEM			
N.M	Mean[a]	Range[a]	S.A.[b]	Vol.[c]	Mean[a]	Range[a]	S.A.[b]	Vol.[c]
7.1	4.83±.15	4.72-5.35	99.4	68.4	4.96±.14	4.86-5.46	104.9	74.0
8.1	4.80±.03	4.73-4.84	119.6	95.3	4.92±.02	4.88-4.94	125.7	102.6
8.2	4.85±.15	4.69-5.36	120.5	83.6	4.97±.15	4.85-5.48	127.0	90.0
9.1	4.81±.02	4.79-4.84	140.1	127.0	4.92±.01	4.91-4.93	146.9	136.0
9.2	4.88±.17	4.75-5.40	141.6	113.6	5.00±.16	4.90-5.50	148.7	121.8
10.1	4.91±.17	4.73-5.36	163.0	143.3	5.02±.16	4.87-5.45	170.9	153.1
11.1	4.92±.15	4.72-5.22	185.3	170.7	5.03±.14	4.85-5.32	193.9	182.6
12.1	4.95±.12	4.71-5.11	212.4	209.1	5.05±.12	4.80-5.21	221.3	222.3
13.1	4.98±.11	4.80-5.05	220.9	281.1	5.07±.12	5.07-5.15	229.3	297.3
14.1	5.00±.23	4.60-5.41	241.6	314.3	5.10±.23	4.69-5.47	250.7	332.1
14.2	4.99±.15	4.71-5.32	241.9	299.8	5.08±.14	4.85-5.40	251.2	316.5
15.1	5.03±.24	4.61-5.30	258.1	356.5	5.12±.24	4.69-5.39	267.8	376.7
15.2	5.00±.19	4.76-5.83	261.9	333.9	5.09±.18	4.88-5.89	271.8	351.8
16.1	5.04±.27	4.62-5.44	276.6	395.5	5.13±.28	4.69-5.53	286.6	417.1
16.5	4.98±.15	4.78-5.40	281.2	371.1	5.06±.13	4.89-5.44	291.9	388.8
17.1	5.05±.29	4.66-5.53	294.9	434.9	5.14±.30	4.74-5.64	305.4	457.7
17.4	4.97±.15	4.74-5.49	301.0	405.3	5.09±.21	4.86-5.88	313.2	422.9
18.1	5.02±.25	4.70-5.56	314.7	460.0	5.11±.25	4.79-5.66	325.9	482.9
18.4	5.02±.16	4.67-5.28	329.2	437.7	5.10±.16	4.75-5.36	341.1	460.4
19.1	5.03±.15	4.61-5.26	340.2	509.1	5.12±.15	4.63-5.33	351.2	533.7

[a]See text for definition of the near neighbor distances of a cluster.

[b]See text for definition of the surface area of a cluster.

[c]See text for definition of the volume of a cluster.

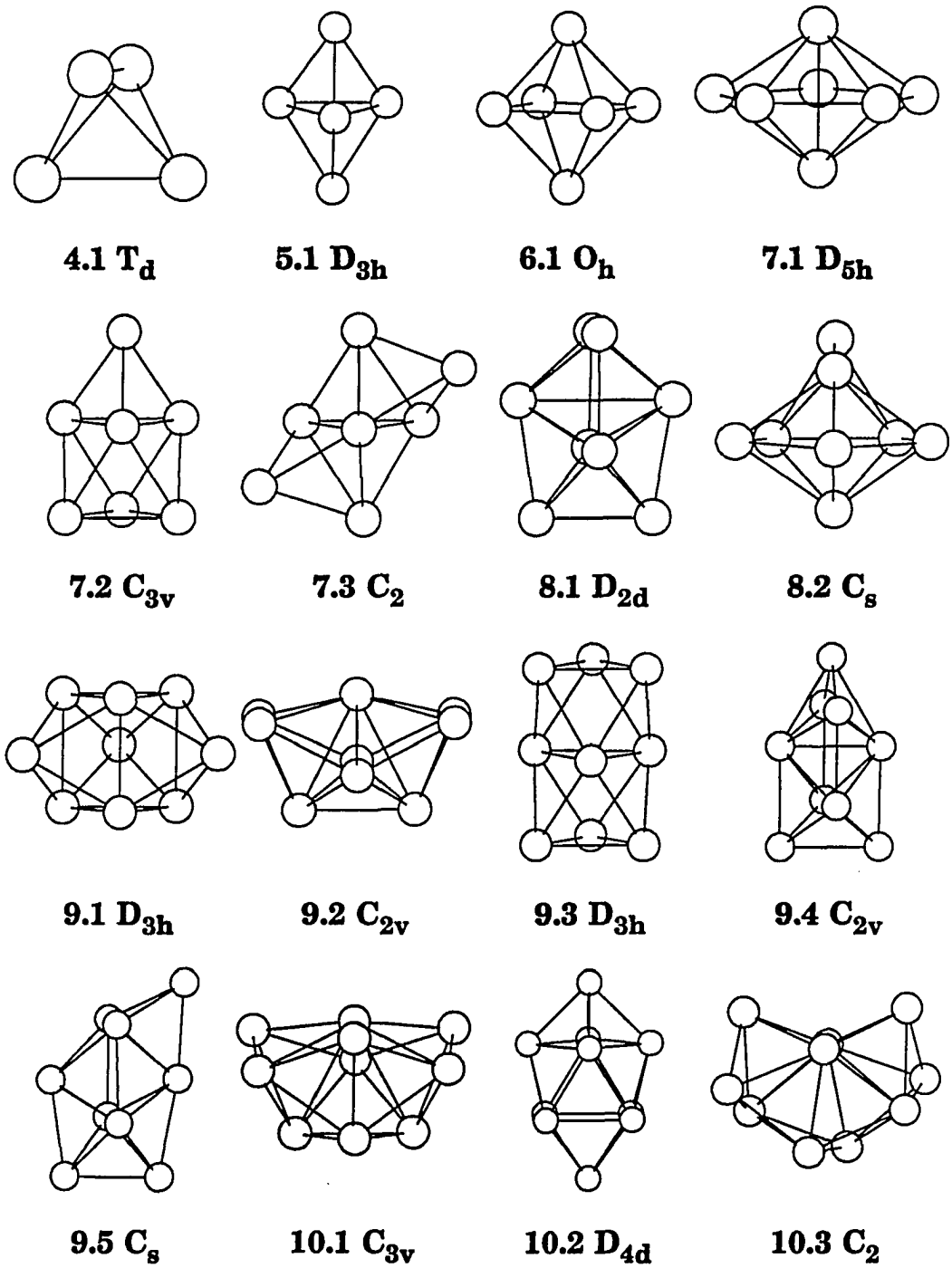

Fig. 2: Ball and stick diagrams for stable geometries of Ni_N and Pd_N clusters. Usually the principal axis of symmetry lies along the length of the page.

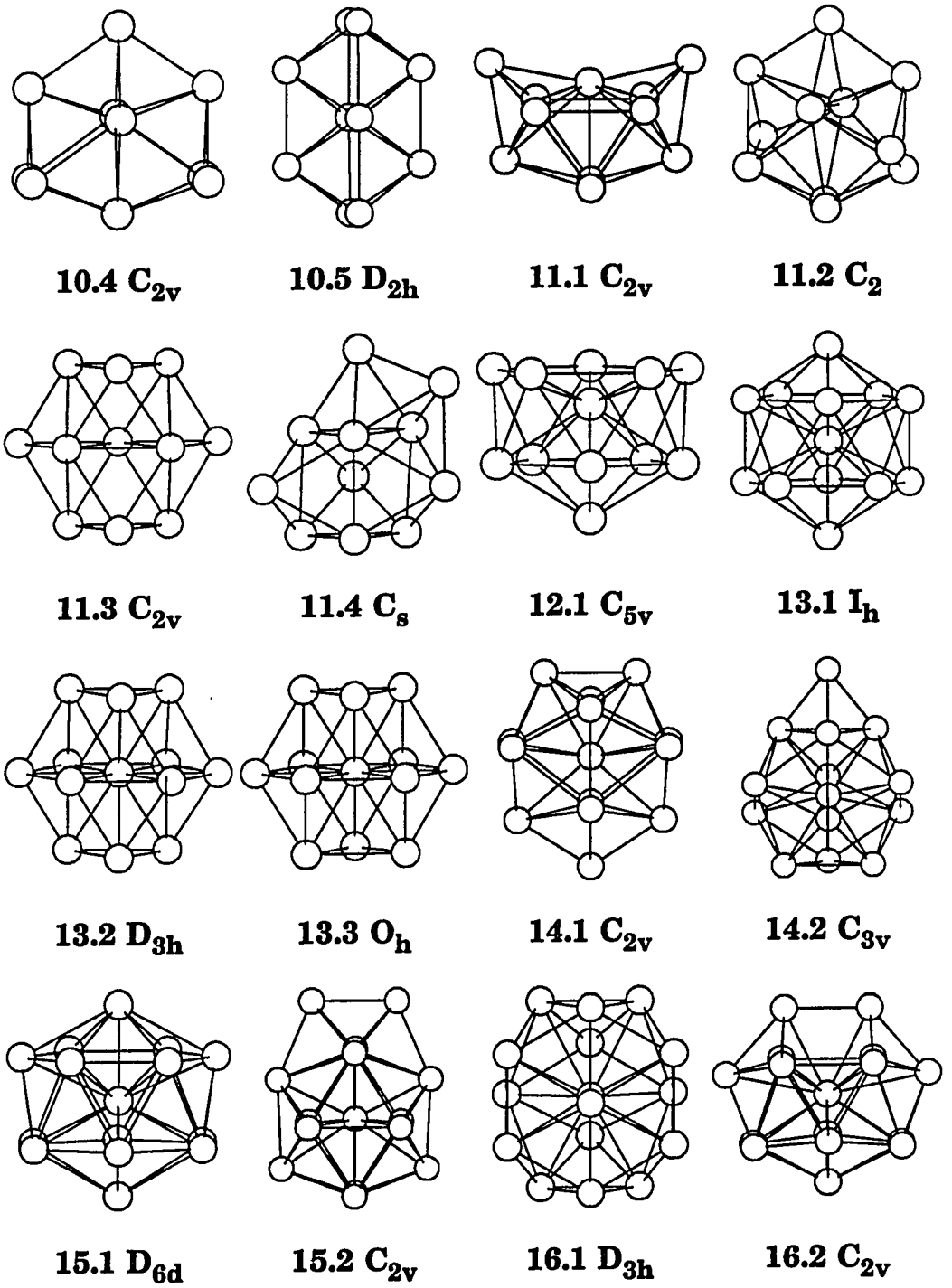

Fig. 2: (continued)

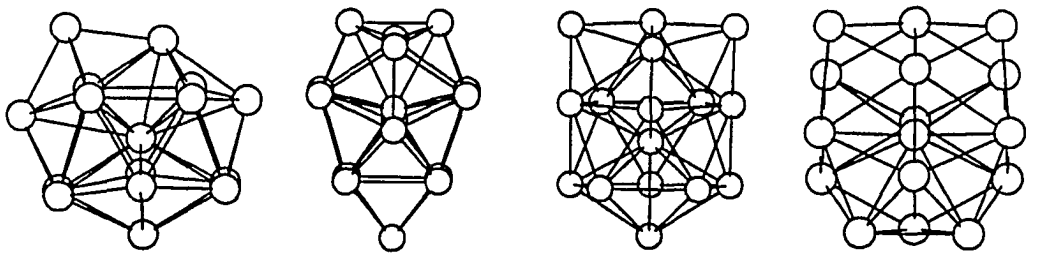

16.3 C_s **16.4 C_{2v}** **16.5 C_s** **16.6 C_s**

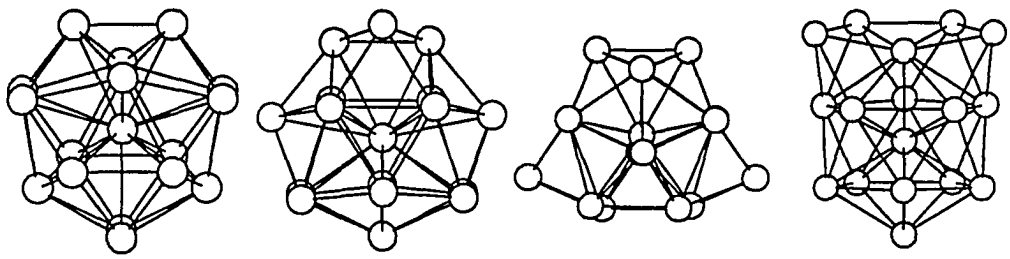

17.1 T_d **17.2 C_s** **17.3 C_2** **17.4 C_s**

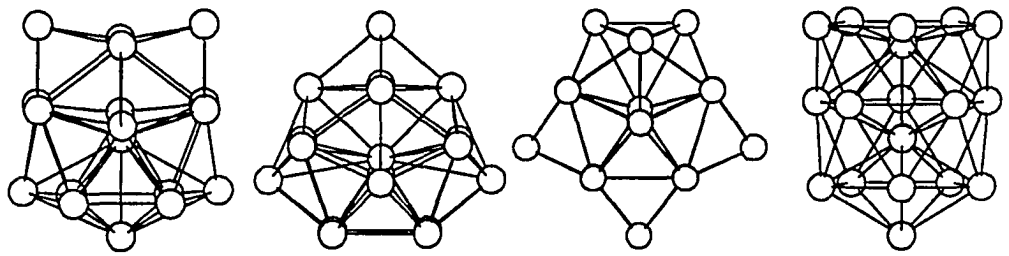

18.1 C_{2v} **18.2 C_{4v}** **18.3 C_{2v}** **18.4 C_{5v}**

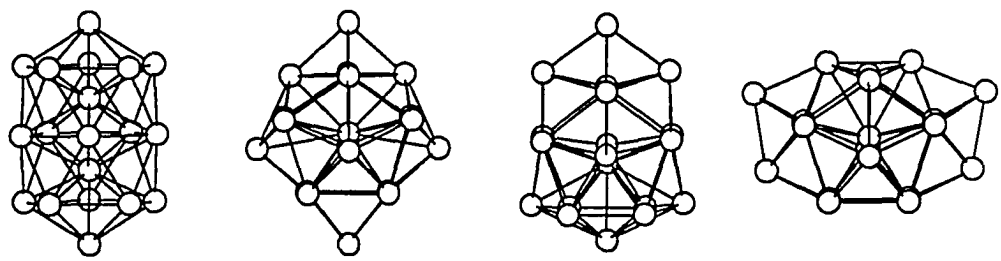

19.1 D_{5h} **19.2 D_{4d}** **19.3 C_{2v}** **19.4 C_{2v}**

Fig. 2: (continued)

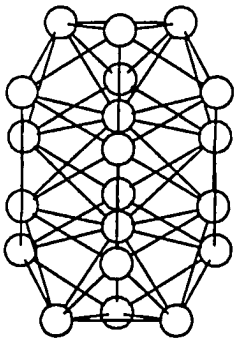

20.1 D_{3d}

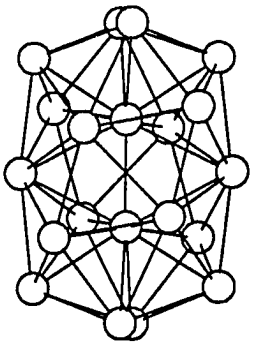

20.2 D_2

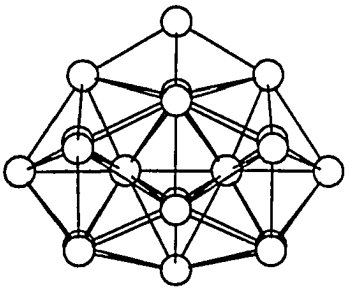

20.3 C_{2v}

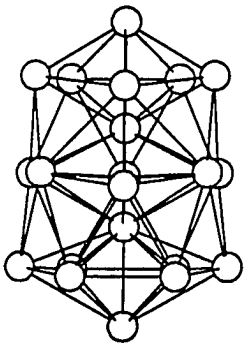

21.1 C_s

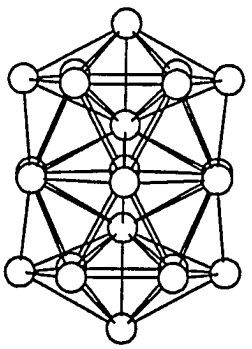

22.1 D_{6h}

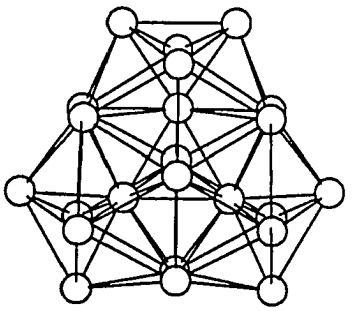

23.1 D_{3h}

Fig. 2: (continued)

calculated by accumulating the area of every face using analytic formulas. The volume of a cluster was determined by enclosing it within a box of known volume and, then, computing the fraction of this volume outside of the cluster surface via Monte Carlo integration.

Except for the 9 and 20 atom clusters, the CEM prediction of the most stable geometries is the same for Ni and Pd. In the case of the exceptions, the isomeric energy differences are small.

Generally, the most stable geometries are spherical or ellipsoidal in shape. The tendency of these geometries to have the smallest surface area, as evident in Tables III and IV, is related to their spherical shape. For a given volume a sphere has the least surface area in comparison to any other shape. Conversely, for a given surface area a sphere has the greatest volume.

In addition, several of these most stable geometries are highly symmetric. For instance, structures 4.1, 6.1, 13.1 and 17.1 have T_d, O_h, I_h and T_d symmetry, respectively. All three principal moments of inertia for each structure are identical. Therefore, each is classified as a spherically symmetric top in terms of its angular momentum properties. Many of the other optimal structures have two of the three moments equal and are classified as either prolate or oblate symmetric tops. In the case of Ni_N clusters, the contracted NND and high symmetry of these structures could significantly alter the magnetic moments of the clusters relative to the bulk phase.[42,43]

The spherical shape and symmetry of many of the most stable geometries suggest that the interatomic forces are balanced. The notion of balanced forces was

first described by Leech in his analysis of the equilibrium distribution of a set of particles confined to the surface of a sphere under any pairwise law of force.[44] The concept of balanced structures was extended by Wales to include arbitrary force laws and more than one set of symmetry related points.[45] Only the components of the forces tangential to the spherical surface are considered in these studies. When these components sum to zero, a structure is considered to be balanced. Since the tangential force vanishes due to symmetry, a balanced structure is a stationary point of some order irrespective of the specific potential determining the forces. (This conclusion assumes that the radial force components directed toward the cluster center allow a bound stationary point to exist at some set of radial distances.) In this context, it is interesting to note that the symmetry of many of the most stable geometries is identical to that for structures shown to minimize the repulsion between a set of particles interacting via a d^{-1} potential, where d is the interparticle distance.[46]

Further structural characterization of these clusters can be accomplished by contrasting them with the bulk and surface environments of extended systems. The high degree of symmetry previously discussed distinguishes these clusters from the bulk and surface phases. Less apparent, however, is the large range of jellium electron densities for atoms at various sites in these clusters. In view of Eq. 2, the jellium density for an atom measures the overlap between its electron density and that of every other atom in the system. Fig. 1 illustrates this range for small Ni and Pd clusters. Also shown are the jellium density for each atom in its equilibrium bulk crystal structure and the jellium densities for atoms in the first few layers of the 111,

100 and 110 relaxed surfaces of these metals.

Starting with the 13 atom clusters, a core atom becomes completely surrounded by atoms on the cluster surface. An additional core atom is gained in structure 19.1 and the 20 through 22 atom clusters. A third core atom is gained in the 23 atom structure. The jellium density for these core atoms is greater than for a bulk atom. For example, the densities for the core atoms of Ni clusters 13.1, 15.1, 17.1, 19.1 and 23.1 correspond to those for a bulk Ni atom with a lattice constant contracted with respect to the equilibrium value by 7%, 5%, 3%, 6% and 6%. Similarly, the Pd clusters require 6%, 4%, 2%, 5% and 5% contractions. For both Ni and Pd contractions greater than 5% decrease the cohesive energy of the bulk system by more than 200 meV. The compression of the bulk crystal structure needed to attain these larger jellium densities would require extremely high pressure. Specifically, a 5% contraction of either the Ni or Pd bulk lattice constant would require a change in pressure on the order of 10^5 atm.[47]

The large densities for these core atoms are due to their large coordination and, in some cases, significant contraction of their near neighbor distances (NND) with respect to the bulk equilibrium value. For instance, the core atoms of structures 13.1, 19.1 and 23.1 have 12 near neighbor atoms just as for a bulk atom. The average NND for each of the core atoms, however, is contracted with respect to the bulk value by 9%, 8% and 7% for the respective Ni clusters and 8%, 7% and 6% for the respective Pd clusters.

NND are not always contracted. For instance, the core atoms of structures 15.1 and 17.1 have 14 and 16 near neighbor surface atoms. Two sets of symmetry

related surface atoms can be formed for each structure. The first set is defined by a set of planes intersecting each cluster. Every plane contains six surface atoms arranged so that they define a hexagon. Structure 15.1 has two of these planes that are parallel to each other. In structure 17.1 there are four such planes, but they are not parallel. Instead, the intersection of any two of these planes defines an edge shared by two of the four hexagons. Both structure 15.1 and 17.1 have a total of 12 surface atoms in these hexagonal arrangements. The second set of surface atoms is defined by capping each hexagon with an atom. These cap atoms lie on the sixfold rotation axis for structure 15.1 and define the vertices of a tetrahedron for structure 17.1. The change in distance to the core atoms relative to the equilibrium bulk NND differs substantially between the two sets of surface atoms. For both Ni_N and Pd_N the distance between the core atom and a cap atom is contracted by more than 10% for structure 15.1 and by more than 7% for structure 17.1. On the other hand, the distance between the core atom and a hexagonal atom is nearly unchanged for structure 15.1 and expanded by more than 4% for structure 17.1. In these structures, the large jellium electron density of the central atom is due to its large coordination.

Generally, the mean NND for Ni_N and Pd_N clusters as predicted by CEM are contracted with respect to the equilibrium bulk NND. From Table III for Ni_N clusters we observe that the mean value increases from 90% of the bulk value for the 7 atom cluster to 95% for the 19 atom cluster. Similarly for Pd_N clusters the mean NND listed in Table IV increase from 93% to 97%. This increase in NND would probably continue smoothly to the bulk value for larger clusters. Hansen *et al.*[22]

found little variation in the mean NND in a study of Cu clusters from 100 - 1000 atoms. Their conclusions were based upon simulations using the effective medium theory but without the one-electron energy corrections. In this regard, note that the predictions of MD/MC-CEM indicate considerably less contraction of the interatomic distances (e.g., 4% and 1% contractions for the same 7 and 19 atom Ni clusters where CEM shows 10% and 5%, respectively). For the size of clusters considered here the explicit corrections for the kinetic, exchange and correlation energies are necessary in order to predict the variation of interatomic distances with the size of the cluster. Moreover, the large range of NND within a single cluster, as noted in the previous paragraph for structures 15.1 and 17.1, is one of the unique aspects of the structure of small Ni_N and Pd_N clusters. We do expect that as the clusters become significantly larger than those studied here, the difference between the bulk and cluster NND would become rather small. Whether this occurs by the 100-1000 atom range, as indicated in ref. 22, will require further simulations of the type presented here.

Atoms on the surfaces of these clusters can have jellium densities ranging from much below to the same as those for metal surface atoms, c.f. Fig. 1. In addition, the coordination of the cluster "surface" atoms can be considerably less than for an atom in the most stable low Miller index 111, 100 or 110 surfaces of these metals. The low coordination and large range of NND would also occur for high Miller index planes, steps and other defect sites on surfaces. While the clusters and these highly reactive sites on surfaces are not identical, we expect that the reactivity of clusters is undoubtedly affected by their structure, much as the types of defects

and steps on surfaces influence reactivity. Thus, both clusters and defective surfaces display the same general types of bonding arrangements that lead to high reactivity, but the particulars will be different on the two.

Many experimental[1-9,48] and theoretical[10,11,19,21,22] studies of atomic clusters have focused on the abrupt and dramatic size dependencies of various physical and chemical properties. The unique properties of these magic number of atoms are often related to the cluster structure and morphology. The concept of magic numbers is aptly illustrated here by the total energy difference between two N atom clusters in the lowest energy configuration and the N - 1 atom cluster plus a N + 1 atom cluster in their respective minimum energy configurations. This energy difference is plotted in Figs. 3 and 4 for Ni_N and Pd_N clusters. A peak in these plots indicates that the stability of the corresponding cluster is enhanced relative to the neighboring cluster sizes. Note the alternating valleys and peaks between the 12 and 20 atom clusters. In this size range, the stability of Ni_N and Pd_N clusters with an odd number of atoms is enhanced relative to the clusters with an even number of atoms.

Peaks in the mass spectra of rare gas clusters suggest that icosahedral geometries are especially stable for these systems. For instance, prominent peaks in the mass spectra of Ar_N clusters at N = 13, 19, 23, ... are associated with the icosahedron (13.1), the doubly nested icosahedron (19.1) and the triply nested icosahedron (23.1).[48,49] The special stability of these structures is rationalized as due to their large number of NND. Furthermore, the growth of these clusters from 7 to 19 atoms is commonly believed to involve the successive capping of faces about a fivefold symmetry axis followed by capping the newly formed pentagon. This series

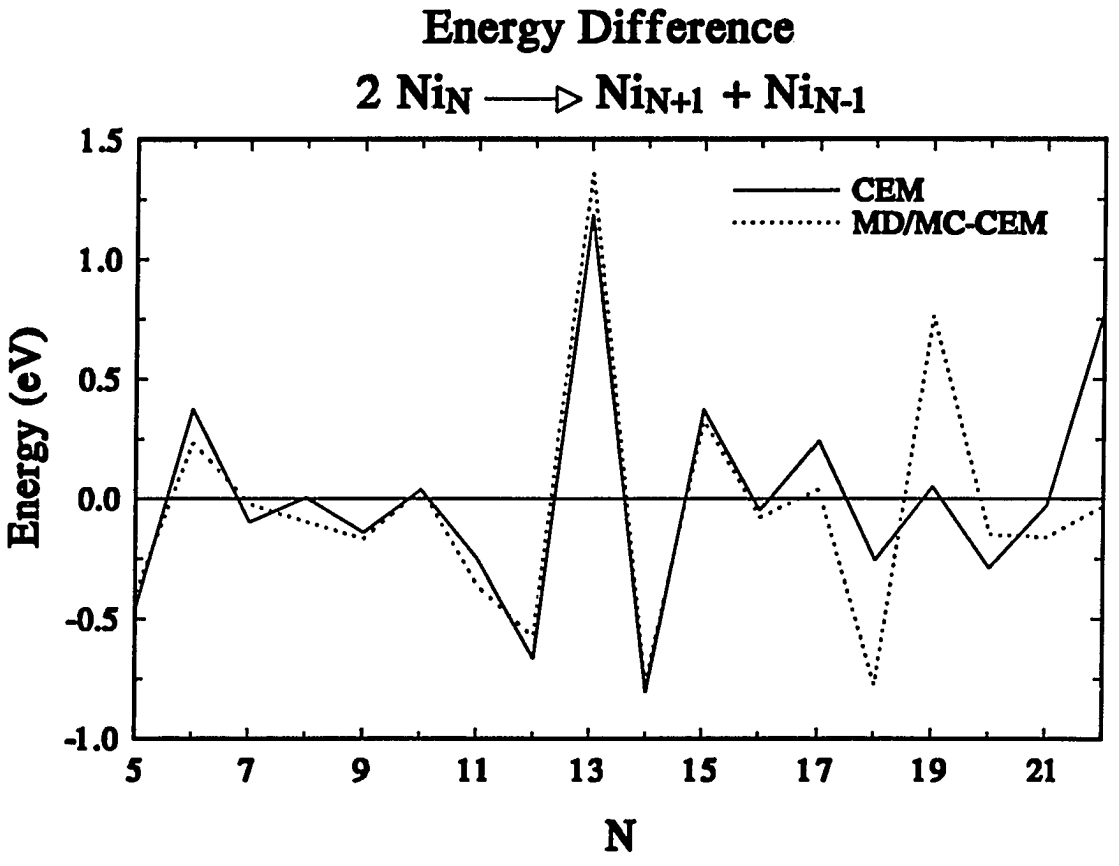

Fig. 3: The total energy difference between the most stable configurations of neighboring Ni_N, Ni_{N+1} and Ni_{N-1} clusters. Results for both CEM and MD/MC-CEM are shown. See text for a complete explanation of this energy difference.

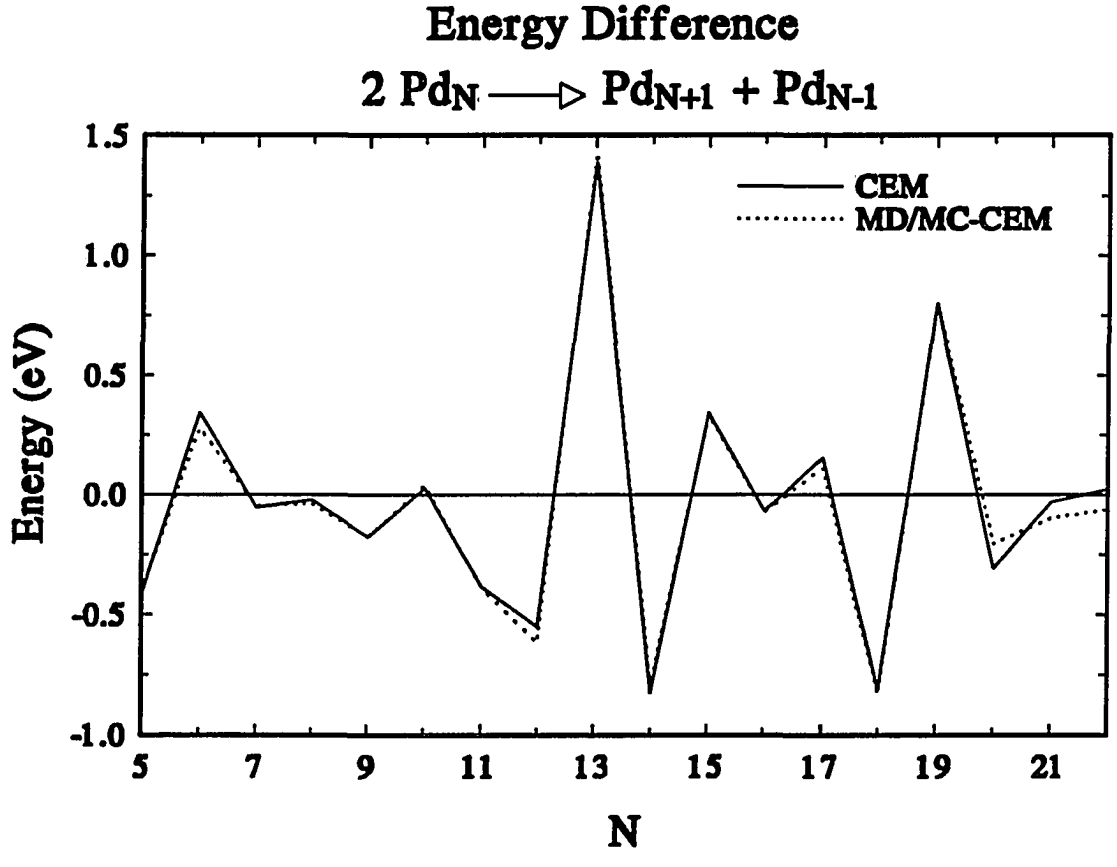

Fig. 4: The total energy difference between the most stable configurations of neighboring Pd_N, Pd_{N+1} and Pd_{N-1} clusters. Results for both CEM and MD/MC-CEM are shown. See text for a complete explanation of this energy difference.

of structures is illustrated in Fig. 5 as the top growth sequence.

Magic numbers have also been observed both experimentally[50] and theoretically[21] for Cu_N ionic and neutral clusters. Currently, no one has reported any indication of magic numbers in the mass spectra of transition metal clusters.[1] However, significant effort has been devoted towards probing the structure of transition metal clusters by examining the size dependence of certain chemical reactions of these clusters.[1-9]

In particular, Parks *et al.* have investigated the structure of Ni clusters in terms of their reactivity with ammonia and water.[1] At lower pressures, they argue convincingly that the adsorbates would preferentially bind to the lower coordinated sites. This binding preference can be used to probe the structure of clusters. For instance, their data on the uptake of ammonia by Ni_8 as a function of ammonia pressure indicates that there are four strong binding sites and four additional weaker sites. This observation is consistent with the D_{2d} structure predicted by CEM as the most stable configuration of Ni_8. In this geometry, four atoms have a coordination of four while the other four atoms have a coordination of six.

Using the saturated product $Ni_{19}(NH_3)_{12}^+$ as evidence, Parks *et al.* also argue that Ni_{19} has the double icosahedral geometry (19.1). The top and bottom pentagonal array of atoms plus the two axial atoms on the cluster surface each have a coordination number of 6. The remaining surface atoms in the middle pentagonal array have a coordination number of 7. Due to their relatively greater exposure on the cluster surface, the sixfold coordinated atoms would preferentially bind the ammonia. Additional binding of ammonia molecules to the middle pentagonal array

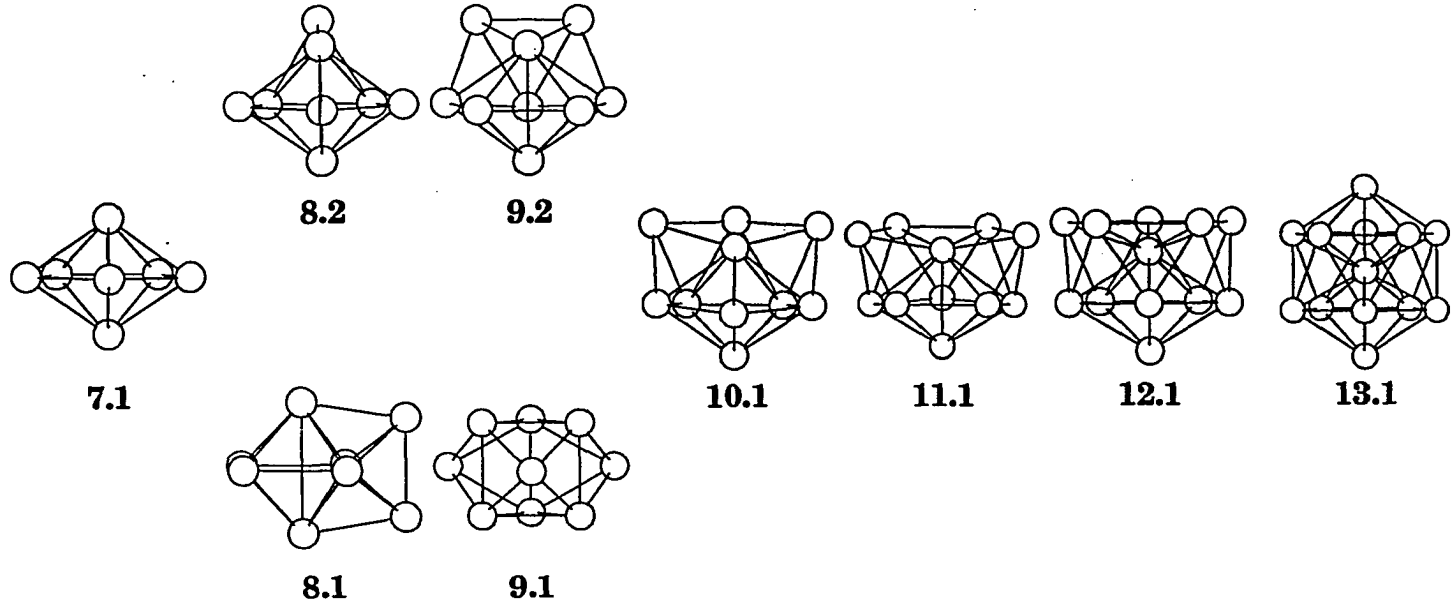

	Ni	Pd	Ni	Pd
CEM	-311	-285	-29	+21
MD/MC-CEM	-226	-255	+94	+43
LJ	+29		+439	

Fig. 5: A comparison of two growth sequences from 7 to 19 cluster atoms. The geometries of the top sequence are commonly believed to be the most stable structures for rare gas clusters. The geometries of the bottom sequence are the most stable structures for Ni and Pd clusters as predicted by CEM (except Pd_9). All structures have been optimized within the CEM, MD/MC-CEM and Lennard-Jones (LJ) potentials. As noted in Table I, structures 16.5 and 17.4 are not stable within the CEM potential. Beneath the structures, the difference in interaction energies (meV) between the bottom and top structure is listed for each of the potentials.

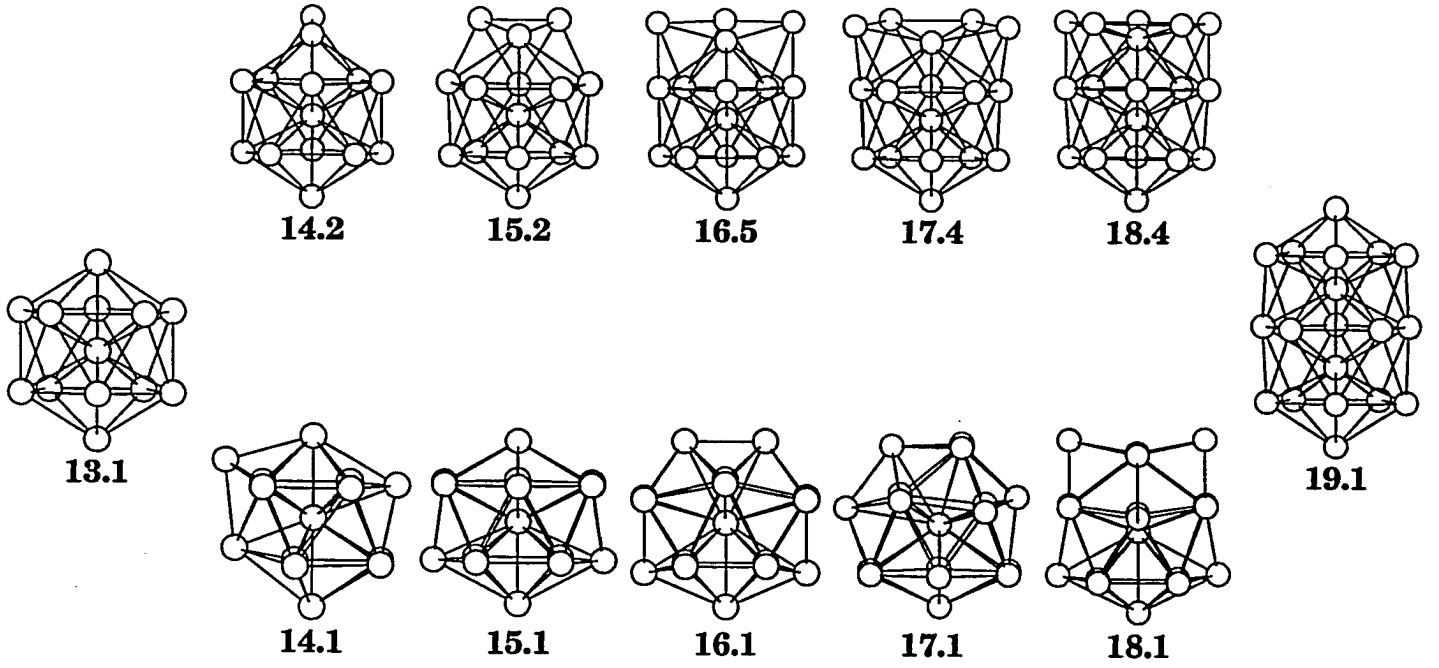

	Ni	Pd	Ni	Pd	Ni	Pd	Ni	Pd	Ni	Pd
CEM	-122	-18	-451	-259	-570	-240	-797	-378	-547	-127
MD/MC-CEM	+26	+15	-221	-245	-156	-209	-237	-332	+5	-86
LJ	+921		+1117		+1521		+1629		+1424	

Fig. 5: (continued)

of Ni atoms would be prohibited due to steric hindrances. Our CEM calculations confirm this geometry as the most stable for both Ni_{19} and Pd_{19}.

Often such experimental data is inconclusive. For example, the mass spectral data shows that the Ni_{18} cluster adsorbs 11 ammonia molecules at saturation. Thus, the 18 atom cluster has one less binding site than the 19 atom cluster. In view of this fact, Parks *et al.* suggest that the structure of Ni_{18} is simply formed by removing one of the axial atoms of the most stable Ni_{19} structure. Although this argument has some consistency, the experimental data can also be rationalized in terms of the binding sites on structure 18.1. In this structure 2 atoms have a coordination of 4, 8 atoms have a coordination of 6, 7 atoms have a coordination of 7 and 1 atom has a coordination of 15. One of the atoms that are sevenfold coordinated has a jellium density that is less than the others in this group. It is on the twofold rotation axis of the structure. This atom plus the other atoms that have a coordination less than 7 comprise 11 binding sites. The predictions of CEM indicate that structure 18.1 is much more stable than 18.4 for both Ni_{18} and Pd_{18}. Experimental data such as produced by Parks *et al.* must be analyzed carefully in view of the different structures these small transition metal clusters can assume and of the possibility of structural changes induced by the chemical reaction itself. The predictions of a theory such as CEM can be invaluable in terms of rationalizing experimental data.

As shown in the bottom sequence of clusters in Fig. 5, the series of most stable structures of Ni_N and Pd_N clusters predicted by CEM can differ significantly from the growth sequence commonly assumed for rare gas clusters. For example, the structure of the 15 through the 18 atom metal clusters is dominated by points of

sixfold symmetry. A detailed comparison of the two growth sequences can clarify the relation between structure and atomic interactions within the different clusters.

In clusters of rare gas atoms the atomic interactions are dominated by dispersion forces. Such systems can be accurately modeled by pairwise additive potentials. The Lennard-Jones and Morse pairwise potentials have been used extensively to study the structure and dynamics of rare gas clusters.[10-12] For a pair of atoms each of these potentials may be formulated as

$$V(r) = \epsilon g(r)[g(r) - 2] , \tag{4}$$

where ϵ is the well depth and r is the interatomic distance. For the Lennard-Jones potential $g(r) = (r_0/r)^6$ while for the Morse potential $g(r) = \exp(-\beta[r - r_0])$. In both potentials, r_0 is the optimal interatomic distance. The width of the potential well is completely determined in the Lennard-Jones potential by the r_0 parameter. In the Morse potential, it is inversely proportional to β. In order to understand the effect of atomic interactions on cluster structure, we have optimized the structure of several clusters shown in Fig. 5 using these pair potentials.

As noted previously, Fig. 5 contrasts the growth of rare gas clusters of 7 to 19 atoms with the most stable structures for Ni_N and Pd_N clusters predicted by CEM. The structures of both sequences have also been optimized within the Lennard-Jones potential. In those cases where the growth sequences differ, CEM, MD/MC-CEM and Lennard-Jones isomer energy differences are listed. The two parameters of the Lennard-Jones potential were determined by forcing it to duplicate the equilibrium cohesive energy and lattice constant of bulk Ni. Since the potential can be completely expressed in units of ϵ and r_0, the particular choice of parameters only

Table V. Mean and range of near neighbor distance (Bohr) and binding energy (eV) for Ni_N clusters optimized using a Lennard-Jones potential[a].

N.M	Mean[b]	Range[b]	B.E.	N.M	Mean[b]	Range[b]	B.E.
7.1	4.83±.04	4.81-4.95	-8.576	14.2	4.83±.11	4.66-4.93	-24.861
8.1	4.81±.02	4.78-4.84	-10.270	15.1	4.91±.24	4.54-5.22	-26.070
8.2	4.83±.03	4.79-4.94	-10.299	15.2	4.83±.11	4.65-5.08	-27.187
9.1	4.80±.01	4.77-4.81	-12.091	16.1	4.93±.27	4.55-5.30	-28.001
9.2	4.82±.05	4.76-4.92	-12.530	16.5	4.83±.11	4.63-5.06	-29.522
10.1	4.83±.07	4.73-4.92	-14.769	17.1	4.93±.29	4.58-5.43	-30.227
11.1	4.83±.08	4.70-4.98	-17.026	17.4	4.83±.12	4.60-5.02	-31.856
12.1	4.84±.11	4.66-5.00	-19.728	18.1	4.87±.24	4.62-5.49	-33.146
13.1	4.84±.11	4.67-4.91	-23.033	18.4	4.84±.13	4.54-5.09	-34.570
14.1[c]	4.89±.22	4.50-5.24	-23.940	19.1	4.84±.13	4.46-4.97	-37.755

[a]Lennard-Jones parameters: $\varepsilon = 0.520$ eV, $r_0 = 4.84$ Bohr.
[b]See text for definition of the near neighbor distances of a cluster.
[c]Structure 14.1 relaxes to 14.2 if the forces are minimized. The listed data was obtained by uniformly scaling the atomic coordinates until a minimum energy was determined.

scales the results and the predicted behavior is independent of any particular parametrization. Our choice is convenient for comparison with Ni clusters. Table V lists the binding energies and the mean and range of NND for clusters optimized using the Lennard-Jones potential. Additional data, relevant for the analysis of cluster stability in terms of NND, is listed in Table VI. The data in this table is applicable for structures optimized in either the CEM or the Lennard-Jones potential.

As evident in Table VI, atoms in the most stable CEM structures are usually

Table VI. Number of near neighbor distances, range and mean of the number of neighbors for a given atom.

N.M	No.	Range	Mean	N.M	No.	Range	Mean
7.1	16	4 - 6	4.57	14.2	45	3 - 12	6.43
8.1	20	4 - 6	5.00	15.1	50	6 - 14	6.66
8.2	19	3 - 7	4.75	15.2	49	4 - 12	6.53
9.1	21	4 - 5	4.66	16.1	54	6 - 15	6.75
9.2	23	4 - 8	5.11	16.5	53	4 - 12	6.63
10.1	27	4 - 9	5.40	17.1	58	6 - 16	6.82
11.1	31	4 - 10	5.63	17.4	57	4 - 12	6.71
12.1	36	5 - 11	6.00	18.1	60	4 - 15	6.66
13.1	42	6 - 12	6.46	18.4	62	5 - 12	6.88
14.1	46	5 - 13	6.57	19.1	68	6 - 12	7.16

more coordinated than atoms in the most stable Lennard-Jones structures. If our focus is restricted to optimization within the Lennard-Jones potential, we observe from Table V that the mean NND of the most stable Lennard-Jones clusters nearly equals the optimal interatomic distance, r_0 = 4.84 Bohr. On the other hand, the mean NND of those structures corresponding to the most stable CEM clusters is usually larger than r_0. The variance or range of the NND is also much smaller for the rare gas optimal structures. Clearly, structural optimization within the Lennard-Jones potential is accomplished by maximizing the number of NND close to r_0.

At this point, it should be noted that structures optimized within the Lennard-Jones potential are expanded relative to the bulk. This is a universal behavior for any Lennard-Jones potential without a radial cutoff. The infinite number of shells of atoms about a bulk atom forces r_0 to be larger than the bulk

NND. When there is no longer an infinite number of atoms as in the clusters, the interatomic distances expand in order to be closer to r_0. This behavior is opposite to the significant contraction of the mean NND predicted by CEM for Ni_N and Pd_N clusters. The LJ predicted expansion is less in error for Ar_N clusters where the observed NND is 7.10 Bohr for both diatomic[55] and bulk.[47] The important point is that maximizing the number of interatomic distances close to r_0 leads to very stable geometries within the Lennard-Jones potential.

In view of this fact, it is also apparent that the stability of rare gas clusters is determined by the short ranged nature of the atomic interactions. The special stability of the icosahedral geometries 13.1, 19.1 and 23.1 is due to the large number of NND of approximately *equal* length. The fivefold symmetry of these structures maximizes the number of interatomic distances that are approximately equal. For rare gas clusters, moreover, the structure of the fivefold symmetric clusters is likely not disturbed as the clusters grow from 7 to 19 atoms. Since the interactions are short ranged, it should be energetically unfavorable for these clusters to rearrange and destroy the local sites of fivefold symmetry. This is reasonable in spite of the fact that simply capping the fivefold symmetric structures results in a very low coordination of the newly added atoms.

In contrast, the transition metal clusters gain additional energy by restructuring so that the degree of coordination is more uniform among the atoms exposed at the cluster surface. As a result, the clusters are nearly spherical in shape. In order for the Ni_N and Pd_N clusters to adopt their most stable geometries the NND distances must vary significantly. This does not introduce any significant

Table VII. Morse potential parameters for diatomic[a] and bulk[b] Ni.

	ε (eV)	r_0 (Bohr)	β (Bohr^{-1})	ρ_0
Ni_2	2.0920	4.157	1.017	4.228
Ni bulk	0.4205	5.253	0.751	3.957

[a]See ref. 15.
[b]See ref. 54.

strain as it would for the rare gas clusters. Instead, the stability of Ni_N and Pd_N clusters is usually enhanced by *maximizing the minimum coordination* of any atom.

Braier *et al.*[51] have examined the interaction range of the Morse potential and its effect on stationary points of the potential energy surface for six and seven atom clusters. In their work this interaction range is quantified as $\rho_0 = r_0\beta$, where r_0 and β are the parameters in Eq. (4). As they noted, physically relevant values of ρ_0 lie between 1.5 and 7. For large values of ρ_0 the interaction range is short and the binding energy is largely due to pairs of near neighbor atoms. As the value of ρ_0 decreases, the interaction range increases and all pairs of atoms contribute to the binding energy. When $\rho_0 = 6$ the curvature at the bottom of the potential well equals that for the Lennard-Jones potential.

In order to more closely examine the effect of the potential interaction range on structural stability, we have optimized the 13, 15 and 17 atom clusters shown in Fig. 5 within the Morse potential for a range of ρ_0 values. The parametrization necessary to duplicate the equilibrium diatomic or bulk Ni systems, along with the consequent values of ρ_0, are listed in Table VII.

For various potentials, Fig. 6 illustrates the relative change in the binding

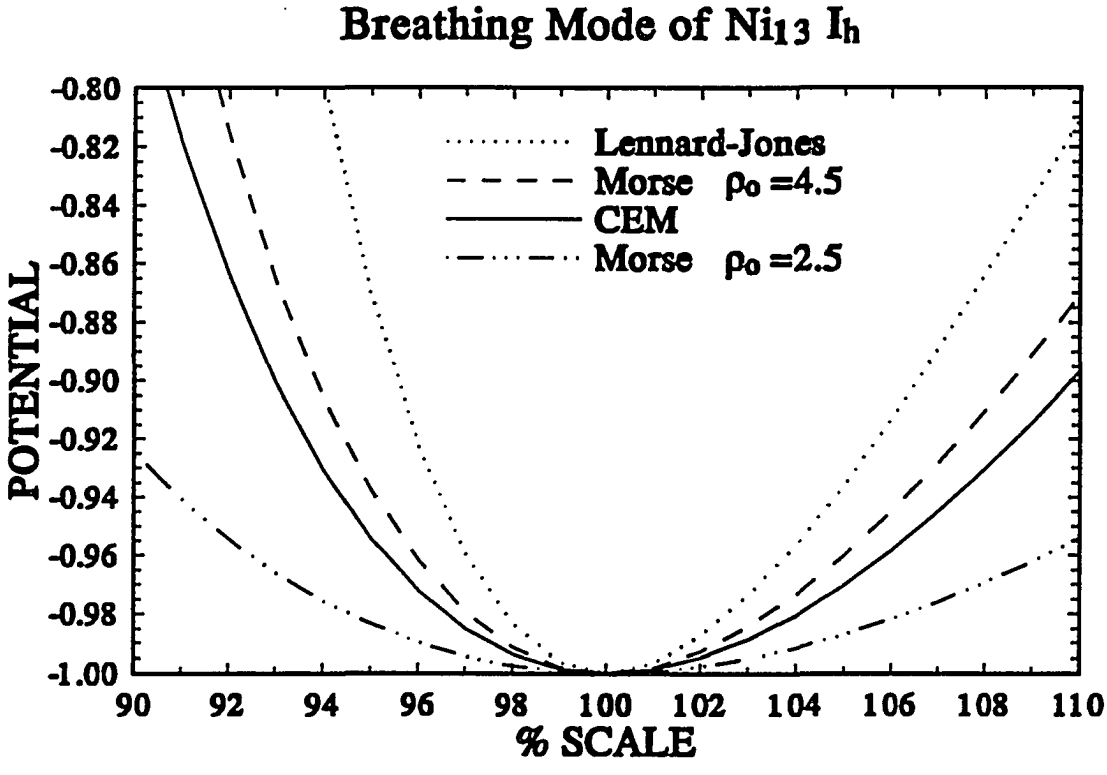

Fig. 6: The change in potential energy of icosahedral Ni_{13} (13.1) plotted as the radial NND is uniformly scaled from 90% to 110% of the optimal distance for various potentials. The change in potential energy and the radial distance are relative to the same quantities in the optimized cluster of each respective potential.

energy of Ni_{13} as the radial NND are uniformly contracted and expanded. The widths of the potential wells are indicative of the length of the interaction range within each potential. Consistent with our previous assessment, the Lennard Jones potential has a very narrow range of interaction in comparison to the CEM potential. The width of the Morse potential well varies with ρ_0. As shown this width can be adjusted so that it is either less than or greater than the width of the CEM potential. If the binding energy of Ni_{13} was plotted using the bulk parametrization of the Morse potential, it would lie nearly on top of the CEM curve. The Morse potential parametrized by the diatomic data would increase more steeply since it has a somewhat larger value for ρ_0.

As for the Lennard-Jones potential, the Morse potential with the bulk parametrization predicts structure 15.2 as more stable than 15.1 and structure 17.4 as more stable than 17.1. Again, this is because structures 15.2 and 17.4 have more NND that are close to the optimal interaction distance. Fig. 7 illustrates the energy change of the 15 and 17 atom isomers as ρ_0 is adjusted. As the potential flattens with decreasing ρ_0, the isomer energy difference decreases. Eventually, the Pd and Ni optimal structures become more stable than the optimal rare gas structures but only at very small values of ρ_0. At small values of ρ_0 the potential is rather insensitive to small differences in the interatomic distances. Therefore, although their range of NND is larger, structures 15.1 and 17.1 are more stable than 15.2 and 17.4 since they have one additional NND (c.f. Table VI).

The stability of Ni_N and Pd_N is determined by more than just the range ofatomic interactions. Clearly, the electron density of the system is a significant

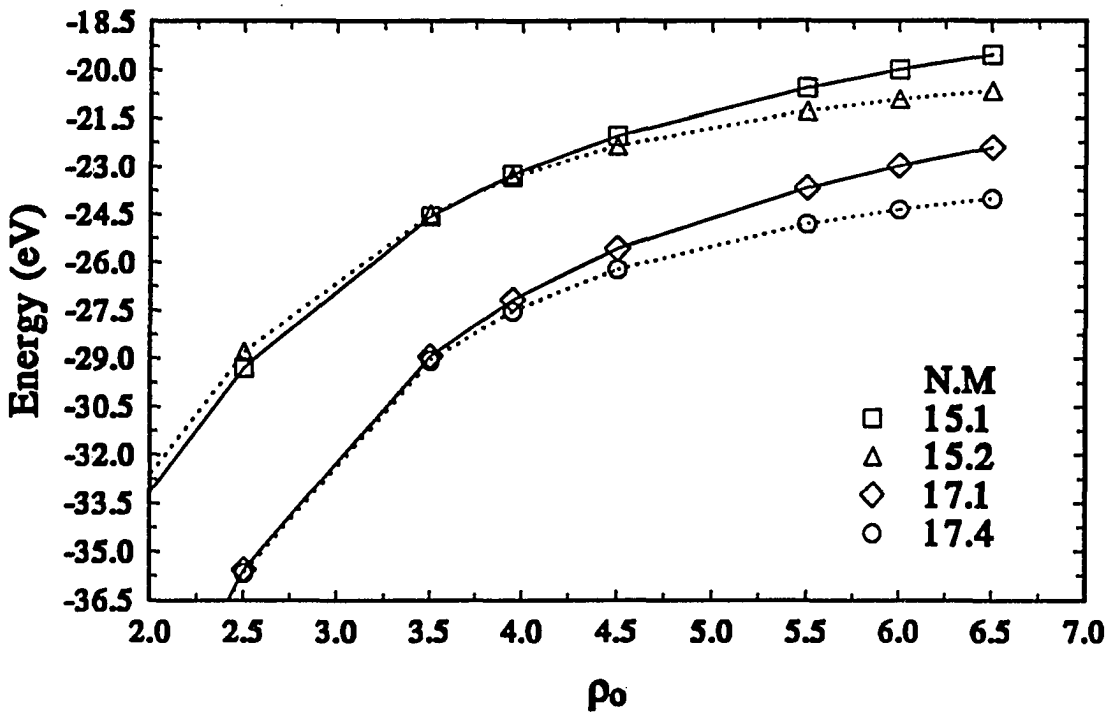

Fig. 7: The interaction energy for 15 and 17 atom isomers plotted as a function of the range of interaction within the Morse potential.

factor. This is especially evident for the 18 atom clusters. In this case, the most stable geometry for the metal clusters (18.1) has fewer NND than the geometry probably assumed by rare gas clusters (18.4). Perhaps the greater stability of 18.1 relative to 18.4 is attributable to the fact that structure 18.4 has nearly two core atoms whereas 18.1 has only one. The jellium electron density for either of these two atoms is greater than that for the core atom of structure 18.1. In fact, the jellium electron density is larger for each core atom of the structures in the top growth sequence shown in Fig. 5 than for those of the bottom growth sequence. In comparison to the optimal structures for rare gas clusters, the most stable structures for Ni_N and Pd_Nnot only more uniformly coordinate the atoms on the cluster surface but also decrease the electron density about the atom(s) in the cluster core.

Throughout the previous discussion our emphasis has focused on the predictions of CEM while the MD/MC-CEM results have been included in the various tables and figures. Since MD/MC-CEM models delocalized, many body interactions expressed in terms of the embedding functions, it is inherently more accurate for transition metal systems than the pairwise potentials. Nevertheless, the predictions of MD/MC-CEM differ from those of CEM in several respects. First, the binding energies decrease by 5% to 8% as shown in Tables I and II. Second, the interatomic distances expand by 3% to 5% as evident in the structural data in Tables III and IV. Third, the order of stability for isomers of a given number of atoms changes in several instances.

In particular, the MD/MC-CEM prediction for the most stable isomer of 9, 14, 18 and 20 Ni atoms and 14 Pd atoms differs from the CEM prediction. These

discrepancies occur since ΔG, the correction for the kinetic, exchange, and correlation energies, is smaller in the optimized clusters than the sum of this correction for bulk atoms at jellium densities equal to those for the cluster atoms. For example, the most stable isomer of Ni_{18} is structure 18.1 within CEM and structure 18.4 within MD/MC-CEM. The CEM energy difference of these isomers is -547 meV while it is +5 meV for MD/MC-CEM. ΔG for the optimized CEM structures 18.1 and 18.4 is +11.588 eV and +11.595 eV, respectively. For each structure kinetic-exchange-correlation energy corrections for a bulk atom at the same jellium densities as those for the cluster atoms can be accumulated. These sums are +16.571 eV and +16.102 eV for structures 18.1 and 18.4, respectively. Calculating the MD/MC-CEM binding energies of these clusters is equivalent to replacing the actual values of ΔG with the accumulated bulk values. For both structures this replacement introduces considerably more repulsion in the potential. As a result, the clusters expand and the binding energy decreases. Furthermore, the MD/MC-CEM approximation for structure 18.1 errs by roughly 500 meV more than for structure 18.4. Consequently, MD/MC-CEM predicts that the two isomers are nearly isoenergetic with structure 18.4 being slightly more stable than 18.1. The explicit evaluation of ΔG within CEM strongly favors structure 18.1 over 18.4. The other discrepancies in the predicted order of isomer stability can be accounted for similarly.

The validity of the MD/MC-CEM approximation is critically dependent on whether the kinetic-exchange-correlation energy correction associated with each atom in a system can be replaced with uniform accuracy by this correction for a bulk atom at the same jellium density. The varying degree of accuracy for the MD/MC-CEM

approximation can lead to significant errors as discussed for Ni_{18} in the preceding paragraph. Interestingly, MD/MC-CEM correctly predicts the most stable structure for Pd_{18} as 18.1. The main disadvantage of MD/MC-CEM lies in the difficulty of knowing when its approximation of the kinetic-exchange-correlation energy correction will be uniformly valid.

B. Isomeric Transformations

Transformations between isomers of similar binding energy likely play a significant role in the physical and chemical properties of these clusters. For instance, Kaldor *et al.*[4-6] have studied the hydrogen steady-state saturation coverage of gas-phase transition metal clusters and have reported significant size dependencies. In the case of Ni_N clusters, the 14, 16 and especially the 18 atom clusters display enhanced hydrogen uptake levels relative to the neighboring clusters of odd numbers of Ni atoms. Recall from Fig. 3 that Ni_{14}, Ni_{16} and Ni_{18} are not very stable in comparison to Ni_{13}, Ni_{15}, Ni_{17} and Ni_{19}. In addition, the Ni_{14}, Ni_{16} and Ni_{18} clusters each have stable isomers within approximately 100 meV of their most stable geometries. These low energy isomers often are not as compact as the most stable structures. Structural features such as these may account for the size dependence of hydrogen uptake by Ni_N clusters. A future paper[52] will examine closely the correlation between cluster structure and the ability to adsorb hydrogen. In this work we will only illustrate some of the transformations between Ni isomers of similar energy.

Table VIII lists the binding energy differences, ΔE_I, and energy barriers, ΔE_B, for the isomeric transformations considered here. For the sake of time some of this tabulated data was not calculated with as many quadrature points as for the binding energies in Tables I and II. We have, however, noted the uncertainties that should be associated with the energy differences. Note, the conversions proceed from the less stable to the more stable structure as calculated within CEM. The energy barrier within CEM for the transformation of the opposite direction is simply the

Table VIII. Energy barriers (meV) for isomeric transformations of Ni_N clusters.

	CEM		MD/MC-CEM	
Conversion	ΔE_I[a]	ΔE_B[b]	ΔE_I[a]	ΔE_B[b]
9.2 --> 9.1	-31±2	+170±2	+94	+243
14.2 --> 14.1	-121±2	+23±2	+26	+92
16.2 --> 16.1	-88±4	(+3)	-97	---[c]
18.2 --> 18.1	-43±4	+94±4	-172	+266
18.3 --> 18.1	-94±4	+11±4	-20	+74

[a]ΔE_I is the binding energy difference between the listed isomers.
[b]ΔE_B is the energy barrier for the transformation of the first structure to the second.
[c]Structure 16.2 is not stable within the MD/MC-CEM potential.

sum of the absolute values of ΔE_I and ΔE_B.

Our first example is the conversion of structure 9.1 to 9.2 as shown in Fig. 8. Recent experimental measurements of the rate constant for D_2 dissociation on Ni_9 have disagreed.[8,9] This could be due to different proportions of these two stable isomers of Ni_9 in the experiments. In fact, classical trajectory calculations of the dissociation cross sections of these two isomers of Ni_9 indicate that their reactivity differs substantially. Details of the calculation and a thorough analysis of the questions posed by this experimental disagreement are presented elsewhere.[53] Our emphasis here is on the structural transformation itself.

In structure 9.2 the lines between atom pairs (2, 6), (3, 5) and (8, 9) are perpendicular to the plane determined by atoms 1, 4 and 7. As the conversion to structure 9.1 progresses, these lines reorient so that atoms 3 and 6 approach each other while atom pairs (8, 9), (1, 7) and (1, 4) become farther apart. This results in a

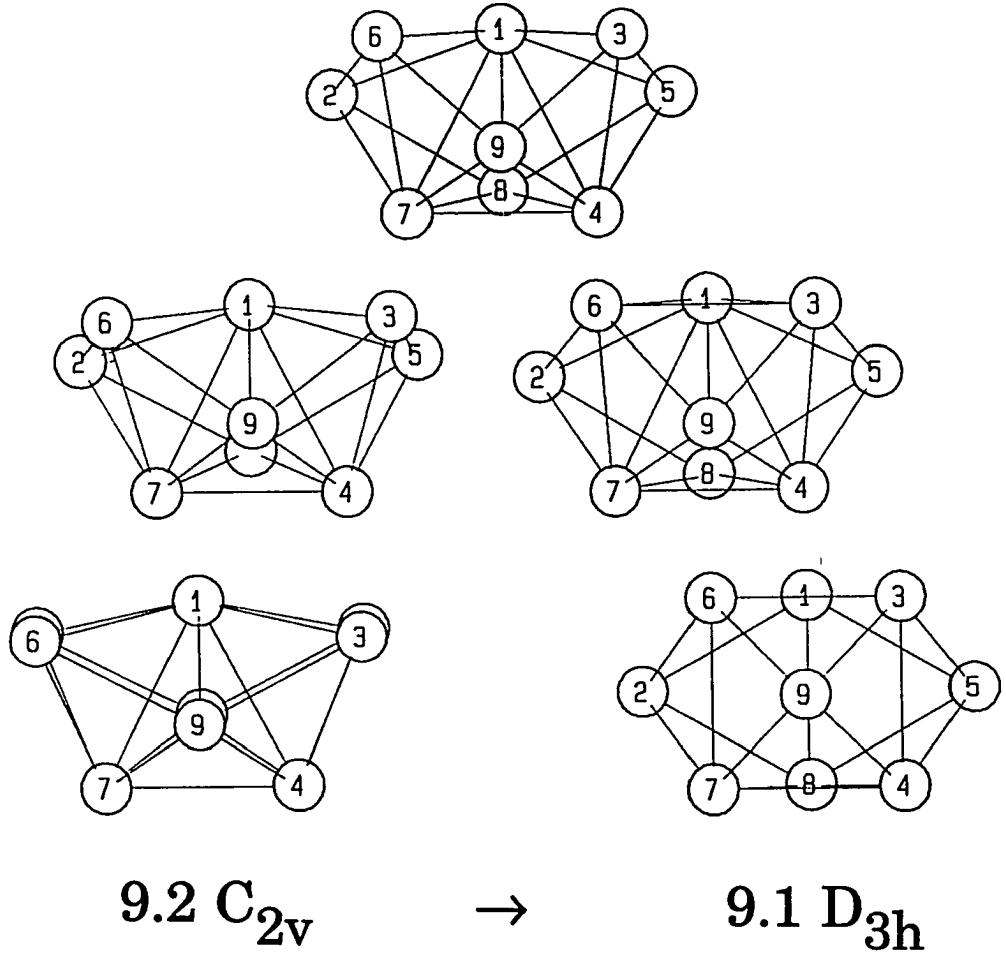

Fig. 8: Transformation of structure 9.2 (C_{2v}) to 9.1 (D_{3h}).

net loss of 2 NND for structure 9.1 in comparison to 9.2.

The structural symmetry allows six equivalent transformations from the 9.1 geometry to the 9.2 geometry--two for each diagonal mirror plane of the D_{3h} structure. As a result, the atoms are not restricted to stay within a set of symmetry related sites. For instance, multiple transformations can move an atom from a site capping a face of the trigonal prism in 9.1 to a site forming a vertex of the prism.

As illustrated in Fig. 9 the transformation of structure 14.2 to 14.1 is straightforward. Structure 14.2 is formed by capping a threefold face of an icosahedron. As this cap atom is moved across an icosahedral edge, the atoms forming the edge move apart while the cap atom sinks deeper into the surface and closer to the core atom. As noted in the previous section, the atomic interactions in Ni_N clusters allow this deformation of the icosahedral geometry in order to better coordinate the atom on the surface of the icosahedron.

The energy barrier for the transformation from 16.2 to 16.1 was difficult to calculate precisely. It appears to be only several meV. As shown in Fig. 2 structure 16.2 has two rectangular faces. Generally, geometries with fourfold faces are not as stable for Ni_N or Pd_N clusters as those with only threefold faces. The reactivity of a cluster, however, may be enhanced by these fourfold faces. Structure 16.2 may be stabilized by the addition of hydrogen. Fig. 10 shows the transformation from structure 16.2 to 16.1. The perspective in this figure of structure 16.2 looks down at the fourfold faces along the C_{2v} symmetry axis. These faces are defined by atoms (3, 4, 6, 16) and (3, 4, 7, 13). The threefold rotation axis of structure 16.1 is in the plane containing atoms 1, 3, 4, 8 and 14. For the most part, the conversion from structure

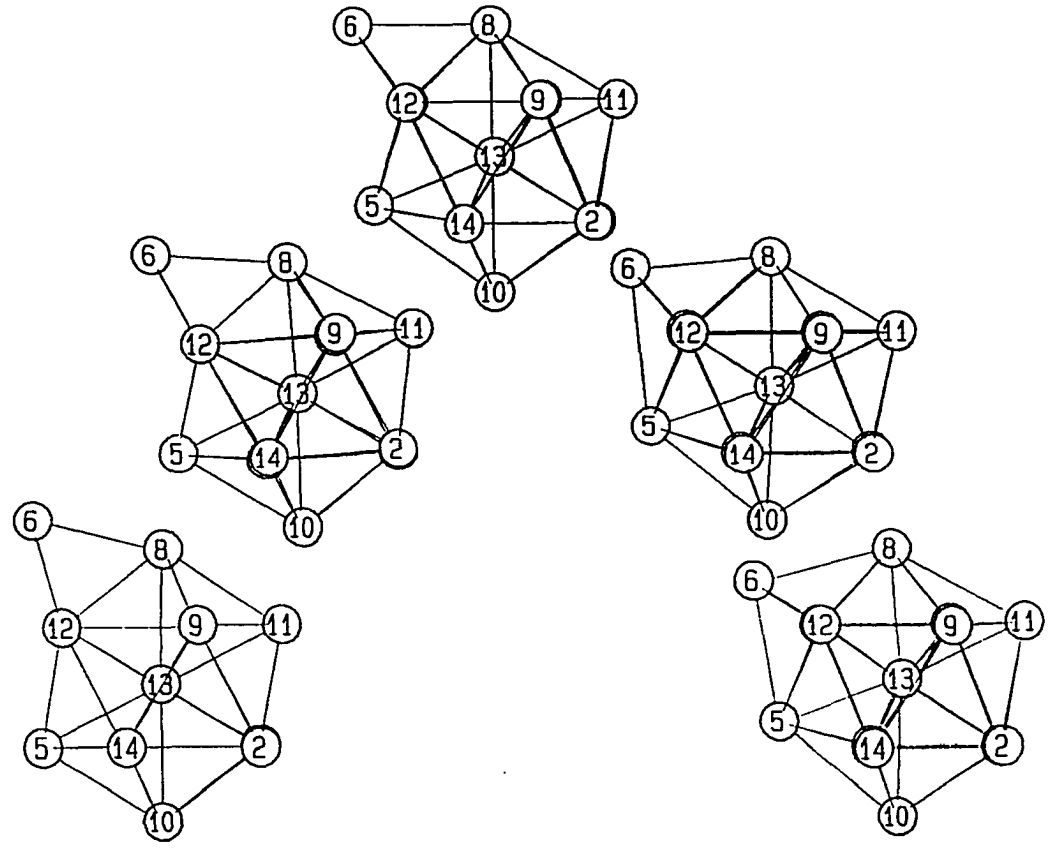

Fig. 9: Transformation of structure 14.2 (C_{3v}) to 14.1 (C_{2v}).

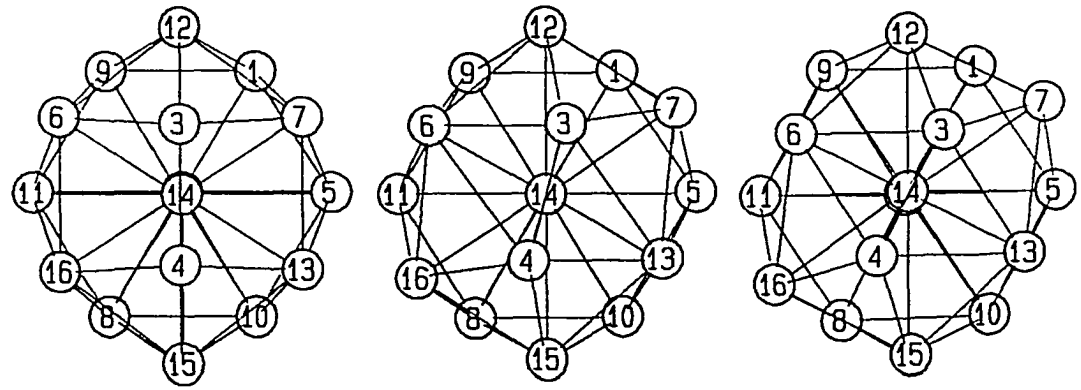

Fig. 10: Transformation of structure 16.2 (C_{2v}) to 16.1 (D_{3h}).

16.2 to 16.1 can be characterized as a small rotation of the NND between atoms 3 and 4. The positions of several other atoms adjust to this rotation, notably atoms 6, 7, 13 and 16. This conversion transforms the fourfold faces into threefold faces. Also, note that the threefold rotation axis of structure 16.1 makes the atom pair (3, 4) equivalent with the pairs (9, 11) and (5, 10). These additional pairs can also be rotated to convert the D_{3h} geometry to structures equivalent to the C2v structure show in Fig. 10.

The 18 atom Ni cluster has three low lying isomers. As shown in Figs. 11 and 12 all three structures appear to have a pentagonal prism arrangement of atoms. The pentagons are actually distorted, but the characterization is still useful. The isomers differ in how the faces of the prism are capped. Interconversion between the geometries primarily involves adjusting the position of the cap atoms.

Fig. 11 shows the conversion of structure 18.2 to 18.1. In this case, the five atoms of the pentagonal prism visible in the figure are 1, 5, 6, 8 and 12. Atoms 2, 15, 16, 17 and 18 cap the fourfold faces of the prism while atom 9 caps one of the fivefold faces. In Figs. 2 and 11 structure 18.2 lays on its square face. As mentioned for structure 16.2, this fourfold face may make it especially reactive with hydrogen.

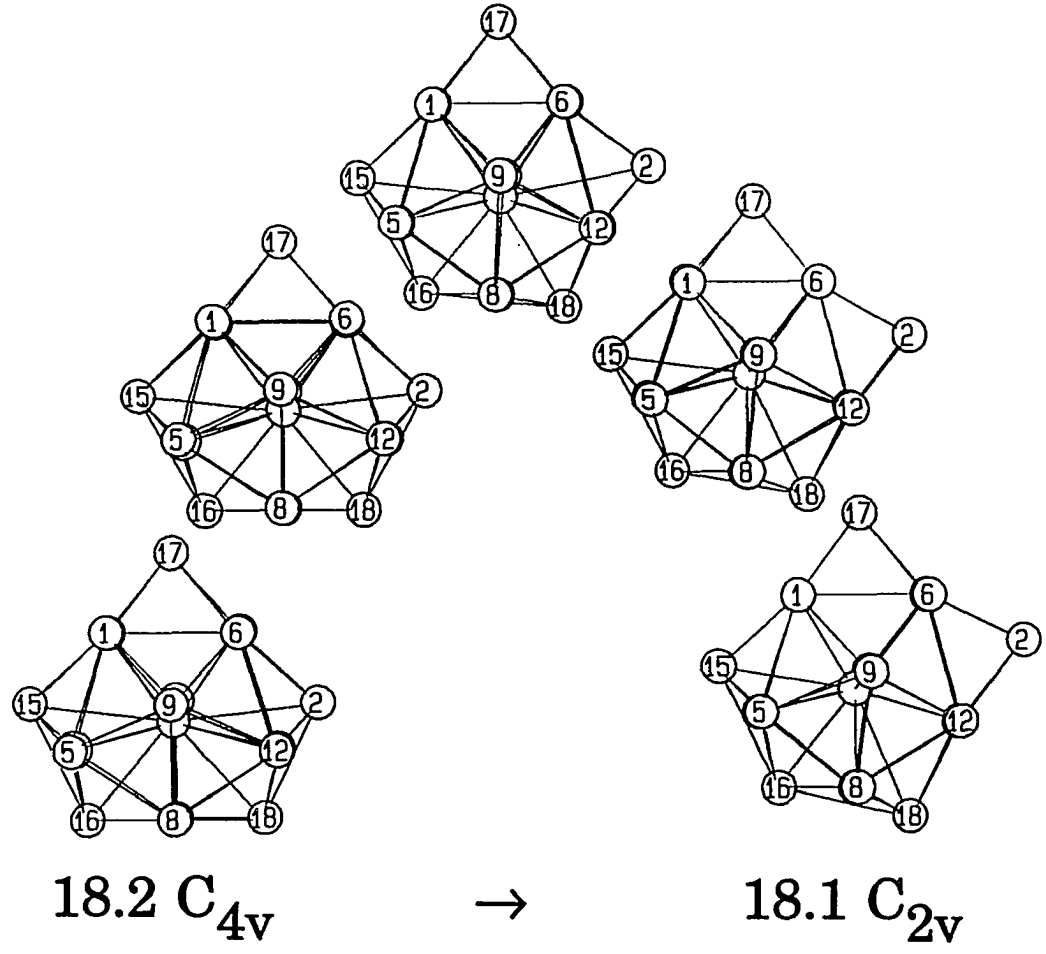

Fig. 11: Transformation of structure 18.2 (C_{4v}) to 18.1 (C_{2v}).

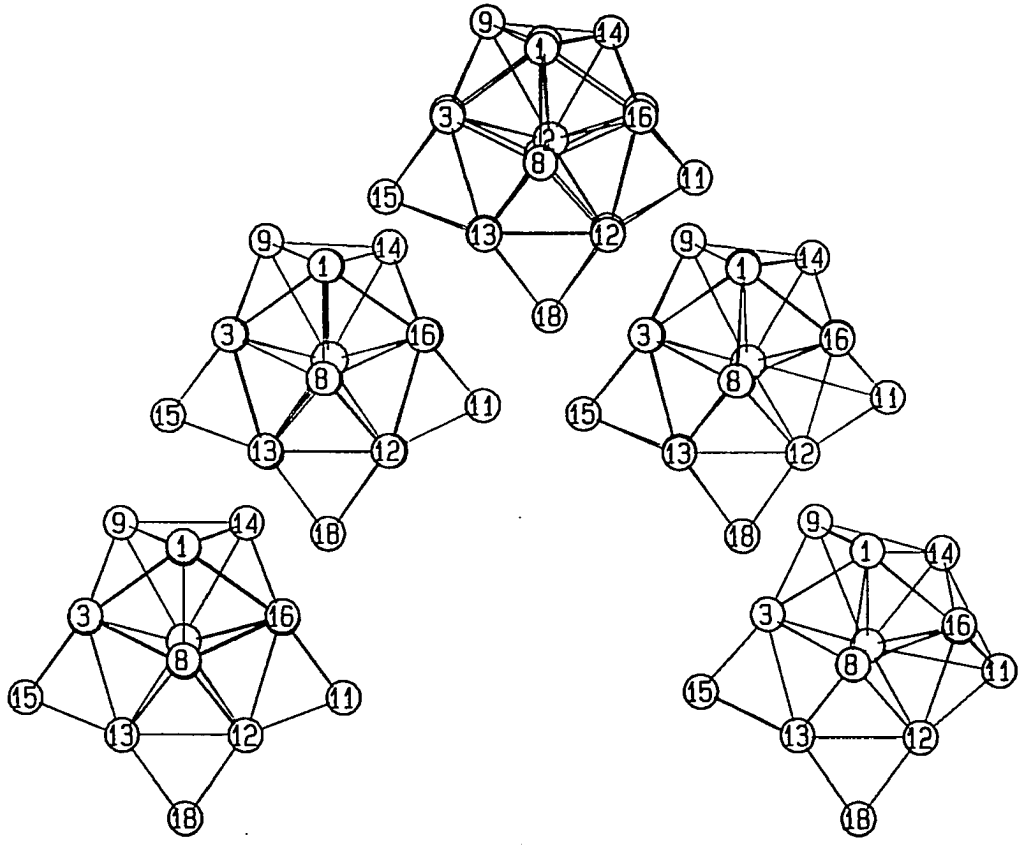

Fig. 12: Transformation of structure 18.3 (C_{2v}) to 18.1 (C_{2v}).

IV. CONCLUDING REMARKS

Our discussion of the Ni_N and Pd_N clusters has demonstrated their unique structural properties. Without the predictions of a theory such as CEM, one might surmise that the 13 and 19 atom clusters assume structures similar to fragments of the FCC crystal structure corresponding to the 1st and 2nd completed coordination shells about a bulk atom. Alternatively, one might rationalize that the structure of transition metal clusters resembles that of rare gas clusters since both are strongly influenced by their finite size. As a result of the CEM calculations discussed in this paper, we assert that neither of these rationalizations is correct. *The structure of these transition metal clusters cannot be characterized as similar to fragments of the bulk crystal structure or as similar to structures assumed for rare gas clusters.* Their finite size and atomic interactions, determined by the delocalized electron density of these clusters, distinguishes the Ni_N and Pd_N from either the bulk phases of these metals or rare gas clusters. (In retrospect, this is perhaps not surprising as a general conclusion, but the implications for the particular structures of various clusters are not as easily rationalized.)

Our results have also demonstrated the structural diversity of these clusters. For some cases several isomers of similar binding energy have been predicted. In the size range from 7 to 23 atoms, the structure of these clusters is dominated alternately by points of fivefold and sixfold symmetries. In most cases, the driving force can be characterized as *maximizing the minimum coordination of any atom on the surface of the cluster.* This leads to the nearly spherical shape of the clusters, their large range of NND and the very high coordination and large electron density

about the core atoms of the clusters. In contrast, the stability of rare gas clusters is enhanced by structures that have a large number of NND of approximately the same distance. As a result, certain atoms on the surface of these clusters have very low coordination and the dominance of fivefold symmetry is observed in all clusters from 7 to 19 atoms. Since there is little physical relationship between the rare gas and metal clusters, one should display caution in using structures and properties of the former in analysis of the latter. For example, the transformation from icosahedral to close packed structures occurs at many thousands of atoms in LJ clusters, but this may not be the case in metallic clusters.

Theoretical calculations are necessary in order to accurately interpret the results of experimental investigations of these clusters. Accurate computational modeling of these clusters provides structural predictions that can be correlated with experimental reactivity data. In addition, some of the present studies using the CEM model need to be supplemented with more accurate, more computationally intensive calculations in order to make more definite conclusions. For instance, the 9 atom cluster has two isomers of nearly the same energy for both Ni and Pd. The order of stability of these structures differs between the Ni and Pd clusters. A more accurate determination of the order of stability and the energy barrier to the transformation between the two isomers is important in order to interpret the behavior of these clusters. A hierarchy of theoretical models will be necessary for continued progress in the investigations of metal clusters.

ACKNOWLEDGEMENTS

This work was supported by the Division of Chemical Sciences, Office of Basic Energy Sciences of the U.S. Department of Energy through the Ames Laboratory, which is operated for the U.S. DOE by Iowa State University under Contract No. W-7405-Eng-82. The authors are grateful for considerable computing time on a nCUBE 2 hypercube at two different sites: 1) the Scalable Computing Laboratory, Ames Laboratory; 2) the Massively Parallel Computational Research Laboratory, Sandia National Laboratory. M.S.S. would especially thank Dr. John Gustafson and Michael Carter of the Scalable Computing Laboratory for their aid in implementing code onto the nCUBE 2 hypercube. M.S.S. also acknowledges the support of the Alworth Memorial Foundation.

REFERENCES

1. E. K. Parks, B. J. Winter, T. D. Klots and S. J. Riley, J. Chem. Phys. **94**, 1882 (1991).

2. T. D. Klots, B. J. Winter, E. K. Parks and S. J. Riley, J. Chem. Phys. **92**, 2110 (1990).

3. E. K. Parks, T. D. Klots and S. J. Riley, J. Chem. Phys. **92**, 3813 (1990).

4. P. Fayet, A. Kaldor and D. M. Cox, J. Chem. Phys. **92**, 254 (1990).

5. A. Kaldor and D. M. Cox, J. Chem. Soc. Faraday Trans. **86**, 2459 (1990).

6. D. M. Cox, P. Fayet, R. Brickman, M. Y. Hahn and A. Kaldor, Catal. Lett. **4**, 271 (1990).

7. S. Nonose, Y. Sone, K. Onodera, S. Sudo and K. Kaya, J. Phys. Chem. **94**, 2744 (1990).

8. W. F. Hoffman III, E. K. Parks, B. C. Nieman, L. G. Pobo and S. J. Riley, Z. Phys. D **7**, 83 (1987).

9. M. D. Morse, M. E. Geusic, J. R. Heath and R. E. Smalley, J. Chem. Phys. **83**, 2293 (1985).

10. B. Raoult, J. Farges, M. F. de Feraudy and G. Torchet, Philos. Mag. B **60**, 881 (1989); see also references therein.

11. J. A. Northby, J. Chem. Phys. **87**, 6166 (1987); see also references therein.

12. M. R. Hoare, Adv. Phys. **40**, 49 (1979).

13. D. R. Salahub, Adv. Chem. Phys. **69**, 447 (1987).

14. J. Koutecky and P. Fantucci, Chem. Rev. **86**, 539 (1986).

15. M. D. Morse, Chem. Rev. **86**, 1049 (1986).

16. M. S. Daw, Phys. Rev. B **39**, 7441 (1989).

17. S. M. Foiles, M. I. Baskes and M. S. Daw, Phys. Rev. B **33**, 7983 (1986).

18. M. S. Daw and M. I. Baskes, Phys. Rev. B **29**, 6443 (1984).

19. C. L. Cleveland and U. Landman, J. Chem. Phys. **94**, 7376 (1991).

20. K. W. Jacobsen, J. K. Norskov and M. J. Puska, Phys. Rev. B **35**, 7423 (1987).

21. O. B. Christensen, K. W. Jacobsen, J. K. Norskov and M. Manninen, Phys. Rev. Let. **66**, 2219 (1991);

22. L. B. Hansen, P. Stoltze, J. K. Norskov, B. S. Clausen and W. Niemann, Phys. Rev. Let. **64**, 3155 (1990).

23. J. D. Kress and A. E. DePristo, J. Chem. Phys. **87**, 4700 (1987).

24. J. D. Kress and A. E. DePristo, J. Chem. Phys. **88**, 2596 (1988).

25. J. D. Kress, M. S. Stave and A. E. DePristo, J. Phys. Chem. **93**, 1556 (1989).

26. T. J. Raeker and A. E. DePristo, Phys. Rev. B **39**, 9967 (1989).

27. R. G. Parr and W. Yang, *Density-Functional Theory of Atoms and Molecules*, (Oxford University Press, New York, 1989).

28. M. S. Stave, D. E. Sanders, T. J. Raeker and A. E. DePristo, J. Chem. Phys. **93**, 4413 (1990).

29. D. E. Sanders, M. S. Stave and A. E. DePristo, Comp. Phys. Comm. (in press).

30. T. J. Raeker and A. E. DePristo, Int. Rev. Phys. Chem. **10**, 1 (1991).

31. M. S. Stave and A. E. DePristo, J. Comp. Phys. (submitted July 1991).

32. S. B. Sinnott, M. S. Stave, T. J. Raeker and A. E. DePristo, Phys. Rev. B (submitted April 1991).

33. A. E. DePristo and H. Metiu, J. Chem. Phys. **90**, 1229 (1989).

34. M. Berkowitz and J. A. McCammon, Chem. Phys. Lett. **90**, 215 (1982).

35. C. L. Brooks III and M. Karplus, J. Chem. Phys. **79**, 6312 (1983).

36. R. Lucchese and J. C. Tully, J. Chem. Phys. **80**, 3451 (1984).

37. R. Biswas and D. R. Hamann, Phys. Rev. B **34**, 895 (1986).

38. Routine UMING in the *IMSL Math/Library: FORTRAN Subroutines for Mathematical Applications*, edition 1.1 (IMSL, Inc. Houston, 1989).

39. C. Choi and R. Elber, J. Chem. Phys. **94**, 751 (1991).

40. R. Czerminski and R. Elber, J. Chem. Phys. **92**, 5580 (1990).

41. A. Ulitsky and R. Elber, J. Chem. Phys. **92**, 1510 (1990).

42. B. I. Dunlap, Phys. Rev. A **41**, 5691 (1990).

43. R. Fournier and D. R. Salahub, Int. J. Quantum Chem. **29**, 1077 (1986).

44. J. Leech, Math. Gazette **41**, 81 (1957).

45. D. J. Wales, J. Am. Chem. Soc. **112**, 7908 (1990).

46. J. B. Weinrach, K. L. Carter, D. W. Bennett and H. K. McDowell, J. Chem. Ed. **67**, 995 (1990).

47. C. Kittel, *Introduction to Solid State Physics*, 6th ed. (Wiley, New York, 1971). Both Ni and Pd have a bulk modulus, B, of ~2 x 10^{11} N m^{-2} (~2 x 10^6 atm). The change in pressure required to effect a change in volume from V_1 to V_2 is given by $\Delta P = B \ln(V_1/V_2)$.

48. I. A. Harris, R. S. Kidwell and J. A. Northby, Phys. Rev. Lett. **53**, 2390 (1984).

49. J. Farges, M. F. de Feraudy, B. Raoult and G. Torchet, Adv. Chem. Phys. **70**, 45 (1988).

50. I. Katakuse, I. Ichihara, Y. Fujita, T. Matsuo, T. Sakurai and H. Matsuda, Int. J. Mass Spectrom. Ion Proc. **67**, 229 (1985).

51. P. A. Braier, R. S. Berry and D. J. Wales, J. Chem. Phys. **93**, 8745 (1990).

52. M. S. Stave and A. E. DePristo (to be submitted).

53. R. Fournier, M. S. Stave and A. E. DePristo, J. Chem. Phys. (submitted June 1991).

54. L. A. Girifalco and V. G. Weizer, Phys. Rev. **114**, 687 (1959).

55. K. P. Huber and G. Herzberg, *Molecular Spectra and Molecular Structure. IV. Constants of Diatomic Molecules* (Van Nostrand Reinhold, New York, 1979).

GENERAL SUMMARY

In this dissertation, the structure and energetics of Ni_N and Pd_N clusters ($4 \leq N \leq 23$) were investigated. Computational developments necessary for this research were also discussed--including the formulation of the analytic derivative of the kinetic, exchange and correlation energy functionals within the additive density approximation of the CEM theory and the implementation of the CEM code onto a hypercube computer.

In addition to the significant technological applications, the physical and chemical properties of transition metal clusters are important to study in their own right. As a consequence of their finite size, the geometric structure of small metal clusters does not resemble that of the bulk metal. In combination with the probable alteration of their electronic structure, the unique geometric arrangements and low coordination of their atoms contribute to their notable reactivity. In addition, the structure and energetics of transition metal clusters differ distinctly from clusters of rare gas atoms. The atomic interactions within Ni_N and Pd_N clusters, determined by their delocalized valence electron density, allow their structures to relax from geometries dominated by points of fivefold symmetry to geometries that more uniformly coordinate the atoms on the surface of the cluster. Future research using the CEM method will continue to add to our knowledge of the evolution of the structural properties of transition metal clusters with increasing size, the variation of these properties with different cluster atoms and clusters comprising more than one type atom and the structure-reactivity relationships between these clusters and various adsorbates.

As demonstrated by the results presented herein, the predictions of the corrected effective medium (CEM) theory are extremely valuable in attempts to understand the structure and energetics of transition metal clusters. Nonetheless, it is important to realize the limitations of such an approach. Fundamentally, it approximates the electron density of a system using a superposition of atomic spherical electron densities. This assumption is reasonably accurate for systems whose electron density is delocalized. Even in these systems, however, there are instances when the structure and energetics need to be more accurately determined. For example, the order of stability and the barrier to isomeric transformation of the two nine atom isomers examined in Paper III require additional investigation. When the atomic interactions are determined by an electron distribution that is localized between atoms (i.e., directional bonding dominates the interactions), the additive density approximation is no longer valid. Future theoretical development of the CEM method may enhance its predictive ability. Currently, the CEM method is an accurate model for transition metal systems whose predictions of structure and energetics can direct subsequent research using more rigorously accurate quantum chemical methods.

Massively parallel computations will certainly assume a significant role in future scientific calculations. As demonstrated by Paper II, significant advances in computational modeling of complex systems should follow the nearly revolutionary advances now emerging with the appearance of multicomputers.

REFERENCES

1. (a) J. H. Sinfelt, Acc. Chem. Res. **20**, 134 (1987);
(b) V. Ponec, Adv. Catal. **32**, 149 (1983).

2. (a) A. Kaldor and D. M. Cox, J. Chem. Soc. Faraday Trans. **86**, 2459 (1990);
(b) E. K. Parks, B. J. Winter, T. D. Klots and S. J. Riley, J. Chem. Phys. **94**, 1882 (1991).

3. (a) J. D. Kress and A. E. DePristo, J. Chem. Phys. **88**, 2596 (1988);
(b) J. D. Kress, M. S. Stave and A. E. DePristo, J. Phys. Chem. **93**, 1556 (1989);
(c) T. J. Raeker and A. E. DePristo, Phys. Rev B **39**, 9967 (1989);
(d) T. J. Raeker and A. E. DePristo, Surf. Sci. **235**, 84 (1990).
(e) T. J. Raeker and A. E. DePristo, Int. Rev. Phys. Chem. **10**, 1 (1991).

ACKNOWLEDGEMENTS

First, I would like to thank my research director, Professor Andrew E. DePristo, for providing a stimulating research environment. During the course of my graduate research, he has allowed me the freedom to explore several research projects and has given valuable direction and criticism of my work. In addition, I would like to thank various members of the Theoretical Chemistry Group of Ames Laboratory. Among others, I have benefited from interaction and collaboration with Leslie Perkins and Susan Sinnott and Drs. Steve Elbert, René Fournier, Todd Raeker and Dave Sanders.

I am especially grateful for the opportunity to work with Dr. John Gustafson, Mike Carter and other members of the Ames Lab Scalable Computing Laboratory, Ames Laboratory. Their assistance was indispensable in my work on the nCUBE 2 hypercube computer. I also appreciate the large amount of nCUBE 2 computer time provided by the Massively Parallel Computing Research Laboratory, Sandia National Laboratories. The work on the hypercube provided me with a research opportunity at the forefront of massively parallel computing technology and gained me a certain amount of notoriety (especially at Sandia where they have written a special program for me, named *kill_stave*).

The Marshall H. and Nellie Alworth Memorial Scholarship Fund provided significant financial support during my undergraduate and graduate education. I am grateful for the thoughtful encouragement of the directors of this foundation.

Finally, I would like to thank my wife, Deborah, my children, Lindsey, Michael and Ryan and our parents for their support. Many difficulties were

experienced during the course of my education and I am grateful for the sacrifices made by my wife and children.

This work was supported by the Division of Chemical Sciences, Office of Basic Energy Sciences of the U.S. Department of Energy through the Ames Laboratory, which is operated for the U.S. DOE by Iowa State University under Contract No. W-7405-Eng-82.